港湾技術研究所報告 (REPORT OF P.H.R.I.)

第27巻　第3号 (Vol. 27, No. 3), 1988年9月 (Sept. 1988)

目　　次 (CONTENTS)

2. Large Scale Model Tests and Analyses of Gravel Drains

Susumu IAI*

Synopsis

Performance of gravel drains, installed as one of remedial measures against liquefaction, is studied by conducting large scale model tests. The tests are conducted with a container, set up on the shaking table, made of a stack of 64 aluminum rings; the rings of about two meters in diameter being stacked to the height of about two meters. The tests have been conducted under sinusoidal as well as earthquake input motions. The results of the tests are analysed by using a model of consolidation with an additional term for generating excess pore water pressures.

The following conclusions are obtained: (1) the effect of the gravel drain is to reduce the rate of increase in pore water pressures and to increase the rate of dissipation in pore water pressures; (2) the maximum excess pore water pressures can be reduced by the gravel drain but they are very sensitive to the slight variations in the properties of the sand deposit and the intensity level and other properties of the input motions; (3) the simple model used for the analyses provides a resonable approximation on the performance of the gravel drain within the range of the safety factor of two.

Key Words: Earthquake, Gravel Drain, Liquefaction, Shaking Table Tests

---

* Senior Research Engineer, Structural Engineering Division

2. グラベルドレーンの大型模型振動実験と解析

井合　進*

要　旨

　液状化対策としてのグラベルドレーンの挙動に関して大型模型振動実験を実施した。この実験には，64段のアルミ製リングからなるせん断土槽を振動台の上に載せたものを用いた。土槽の直径・高さともおおむね2mである。入力振動波形としては，正弦波及び地震波を用いた。これらの条件により得た実験結果を，圧密の式に過剰間隙水圧の発生項を付加したモデルにより解析した。

　これら実験及び解析の結果，以下の結論が得られた。(1)グラベルドレーンの効果は，過剰間隙水圧の上昇速度を低下させるとともに，その消散速度を高めるものである。(2)グラベルドレーンにより，最大過剰間隙水圧の値を低下させることはできるが，この値は，砂地盤の密度や入力地震動のレベル等のわずかな変化に対応して，変化する。(3)解析に用いた単純なモデルにより，グラベルドレーンの挙動は，安全率2程度の誤差を許容すれば，シミュレートできる。

キーワード：液状化，グラベルドレーン，地震，振動台試験

---

* 構造部主任研究官（地震動解析担当）

CONTENTS

1. Introduction

Liquefaction of sandy grounds during earthquakes often causes extensive damages to the structures. The examples of the damages are failures of retaining walls, slopes, and foundations. Obviously these damages could be caused without the liquefaction but significant damages are generally caused by the liquefaction. The case histories of such damages are abundant in the seismically active areas in the world, especially in Japan.[1][2]

If the sandy grounds are potentially liquefiable and the liquefaction will be likely to cause damages to the structures, a measure is usually taken to mitigate the potential damages. The most popular measure has been the ground compaction. The grounds improved by the compaction method have actually shown their sound performances against liquefaction during the past earthquakes.[3] The ground compactions have sound technical backgrounds for designing the degree[4] and the area of compaction.[5] The ground compactions thus deserve the popularity but they are not applicable on some occasions. For example, if there is a potentially liquefiable backfilling just behind the steel sheet pile retaining walls, the ground compactions are not applicable. The same is true if there is a potentially liquefiable ground just around an existing building. In these occasions, the grounds have to be treated with remedial measures other than the ground compactions. One of the promising measures is the installment of gravel drains.

As a remedial measure against liquefaction, the gravel drains are installed so as to increase the average permeability of the ground with the effect of drainage and thus to reduce the liquefaction potential. Various forms of gravel drains are currently used or proposed; i.e., a columnar form as shown in **Fig. 1**, a wall-like form, and a form of drain zone beneath and around the bases of the structures. Moreover, rubble backing and gravel filling used for bulkheads and quaywalls are, if installed with permeable filtering sheets, also regarded as one form of the gravel drains. Apart from the forms of the gravel drains, various materials of the drains are currently used or proposed; i.e., gravels, crushed stones. Geomembranes and geotextiles, if formed as very permeable drains such as pipes made of a plastic net, can be regarded as variations of the gravel drains. Thus, various types of gravel drains are used or proposed. Among the various types of gravel drains, the most frequently used type of gravel drains is, at present, the one made of gravels or crushed stones as shown in **Fig. 1**. Hereafter this type of the gravel drains will be exclusively considered in this report and simply called as the gravel drains.

The history of the gravel drains is rather new as compared with the history of the ground compactions. Indeed, 1977 is the first year when a research paper on the gravel drains appeared. In that paper, Seed and Booker (1977) analysed the performance of the gravel drain under several assumptions using finite element method and offered the results of the analysis in several figures which could be used as a basis for designing the gravel drains[6]. Tokimatsu and Yoshimi (1980) conducted small scale shaking tests on the performance of the gravel drains installed around a structure and offered the results of the analyses in a original figure which could be used as a basis for designing the gravel drains[7]. Tanaka et al. (1984) conducted small scale tests on the performance of the gravel drains and obtained simplified equations which could be used as a basis for designing the gravel drain[8].
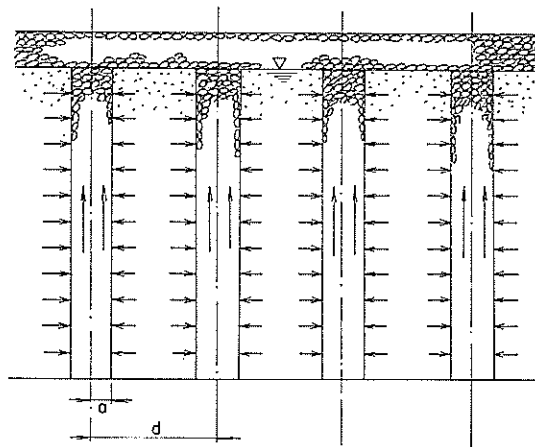
Apart from those studies based on the small scale model tests, Ishihara et al. (1980) conducted in-situ tests by generating excess pore water pressures in the
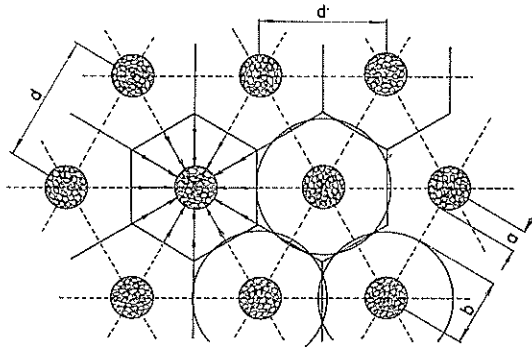
(a) Plan of the gravel drains in equilateral triangular pattern
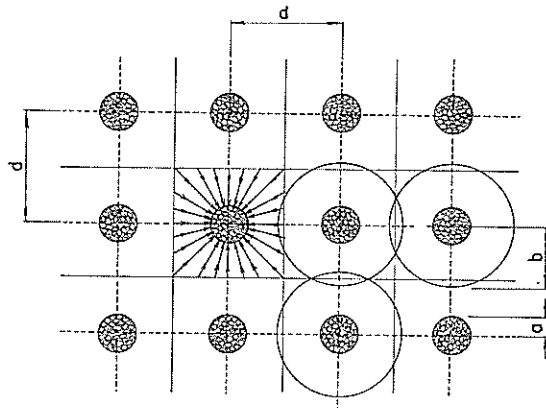
(b) Plan of the gravel drains in square grid pattern

(c) Cross section of the gravel drains

Fig. 1 Gravel drains in plan and cross section

ground using steel rods, which were inserted into the ground while they were vertically vibrated, and presented an analytical method on the improved rate of pore water pressure dissipation[9]. Miyame et al. at Hokkaido Electric Power Co. (1985) conducted in-situ tests by generating excess pore water pressures with vertically vibrating steel pipe, which had been driven into the ground and within which a gravel drain had been installed[10], and Onoue et al. (1987) and Tanaka and Takano (1987) analysed the results, comfirming the applicability of each method presented at each paper[11][12].

Other than the laboratory or in-situ tests of the gravel drains stated above, no case history has been available for confirming the performance of the gravel drains during earthquakes. Therefore, some of the studies are still going on for better and more reliable understandings on the performance of the gravel drains; the author's present work as one of them. In contrast to the previous small scale model tests, the author conducted large scale model tests by using models of which dimensions are about two meters in diameter and about two meters in height. In contrast to the previous in-situ tests, the author conducted the model tests under the horizontal shaking of sinusoidal and earthquake motions. These types of excitations are considered more suitable for simulating the performance of the gravel drains during earthquakes.

The performance of the gravel drains is characterized by the two kinds of quantities; excess pore water pressures and settlements. These quantities are affected by many factors; i.e., 1) intensity and characteristics of earthquake ground motions, 2) density, permeability, and compressibility of the ground, 3) permeability and compressibility of gravel drains, and 4) diameters and spacings of gravel drains. Some of these factors may significantly affect the performance of the gravel drains while others may scarcely do. The purpose of the present study is to understand how those factors affect the excess pore water pressures and the settlements of the ground at which the gravel drains have been installed.

Obviously a good understanding on the effect of above-mentioned factors provides an important basis for designing the gravel drains. However, understanding the performance of the gravel drains is not the same as designing the gravel drains. Additional considerations are necessary for designing the gravel drains upon the following items; the systematic and simplified procedures for the design, the required stability of the ground, the reliability of the design procedure, and the areas to be drained. In this context, the scope of the present report is limited within the understanding of the performance of the gravel drains during earthquakes. The considerations necessary for designing the gravel drains will be presented in a separate report. For those who have the urgent need for designing the gravel drains, some of the considerations are found in the papers[13][14]. Other considerations which become necessary when the gravel drains are used around the compacted area are found in the paper on the ground compaction[5].

2. Large scale model tests

2.1 Outline of model tests

The gravel drains are usually installed in equilateral triangular pattern or square grid pattern as shown in **Fig. 1**. The ground shown in this figure can be regarded as a composite ground made of two parts; i.e., one part is the sand deposits, the other the gravel drains. When the composite ground undergoes a strong earthquake motion, the part of the sand deposits tends to liquefy or at least tends to
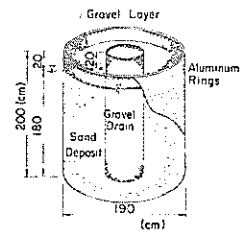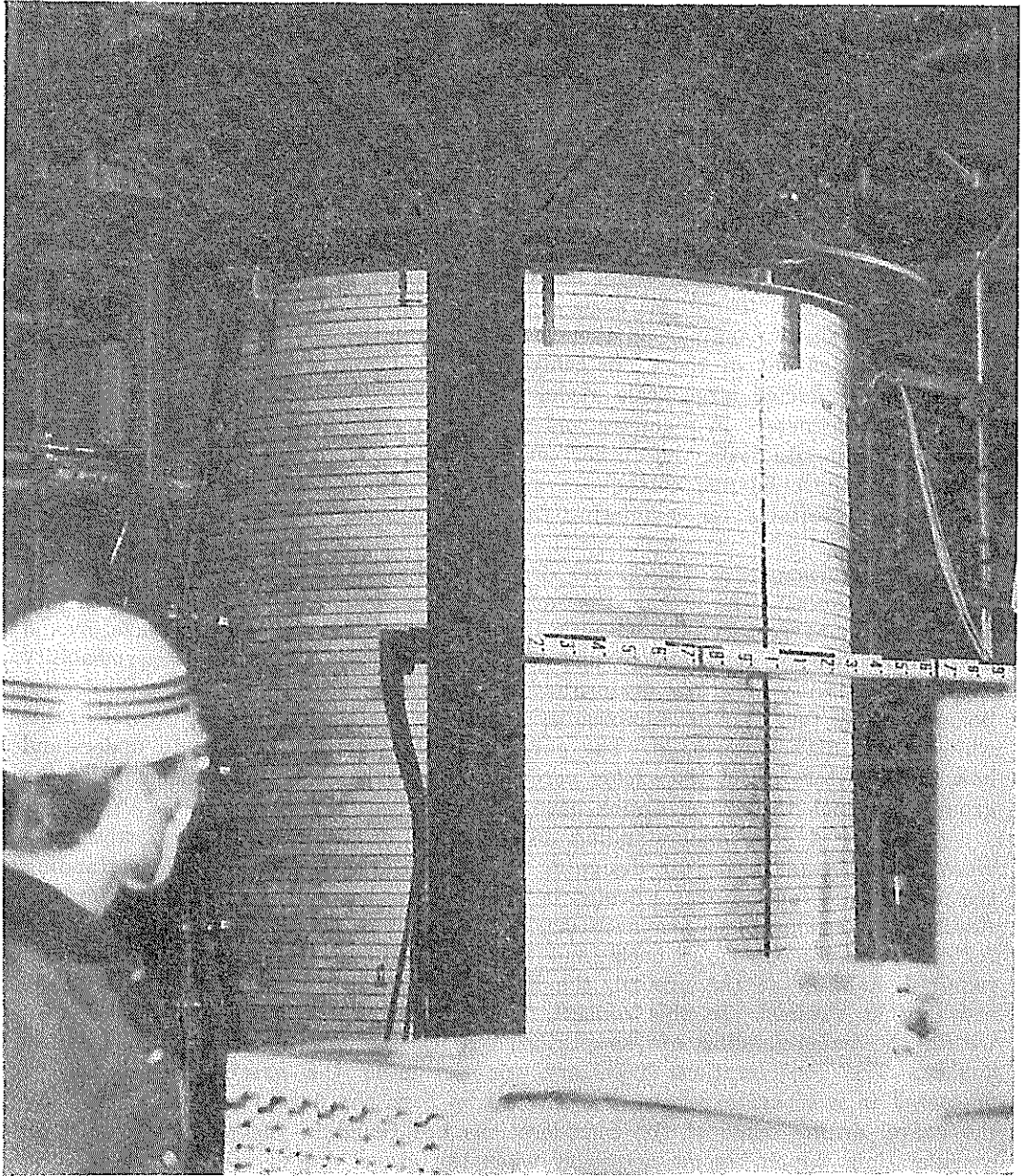
Photo 1 A stack of 64 aluminum rings on the shaking table

generate excess pore water pressures. The excess pore water pressures in the sand deposits, then, lead seepage towards the gravel drains as shown by the arrows in **Fig. 1.** In plan view, the seepage from any part of the sand deposits is directed towards the center of the nearest gravel drain. Therefore, the performance of the whole composite ground can be represented by that of a single area bounded by the hexagonal or the square mesh in **Fig. 1** (a) or (b). Furthermore, the performance of this single area can well be approximated by that of the area bounded by the equivalent circle shown in the same figure. Consequently, for studying the performance of the whole area of the composite ground such as shown in **Fig. 1,** it is enough to study the performance of the single area of the composite ground bounded by the equivalent circle. With these facts in mind, shaking table tests were conducted on the models of the single area of the composite ground bounded by the equivalent circle.

When the ground is shaken by earthquakes, the ground undergoes a deformation which can be represented by a pure horizontal shearing mode due to vertically propagating seismic shear waves. Therefore, the model of the composite ground was made in a special container designed for enforcing a pure horizontal cyclic shearing. The container, as shown in **Photo 1,** was made of a stack of 64 aluminum rings of about two meters in diameter. The height of the stack amounted to about two meters, too. This container was put on the shaking table and the model tests were conducted under the horizontal shaking motions.

Nine series of shaking table tests were conducted under the conditions shown in **Fig. 2.** There were basically two groupes of tests; one groupe, i.e. R-100, R-400, R-500, R-700, and R-900 series, was the tests of the model ground with a gravel
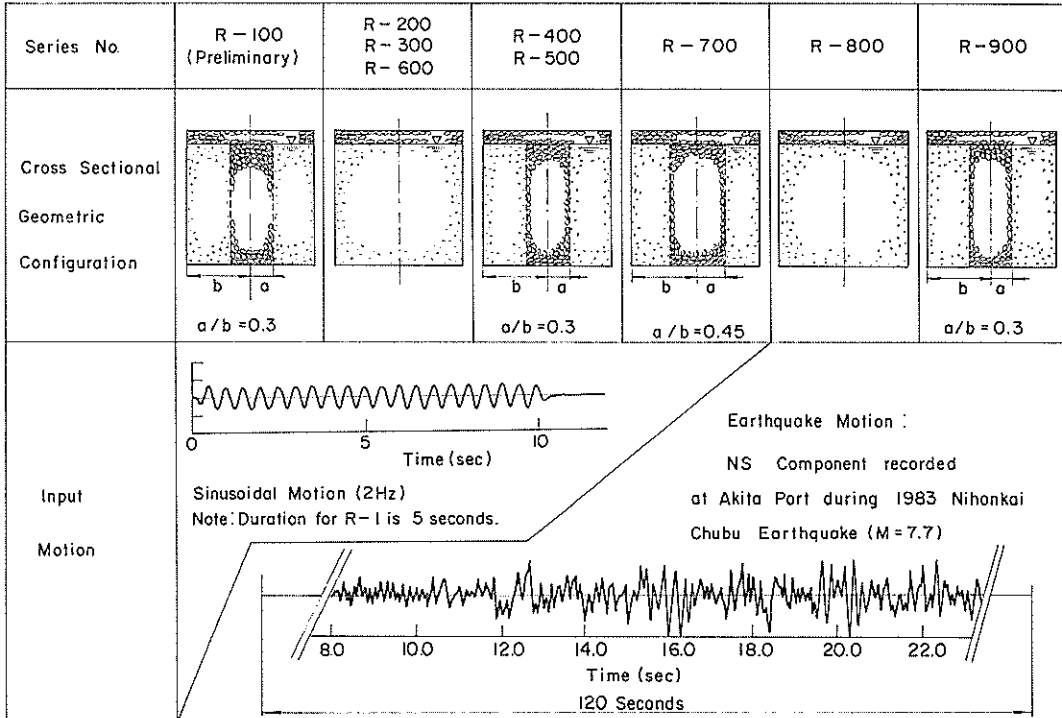

Fig. 2 Conditions on the nine series of the model tests

Table 1 Specifications on the shaking table

Items	Specifications
Freedom of shaking	One horizontal direction
Maximum amplitude of displacement	18 tonf G
Maximam total load (including dead load)	40 tonf
Dead load	15 tonf
Dimensions of the table	4 m (in the direction of vibration)×3.5m
Maximum amplitude of displacement	10 cm
Maximum amplitude of velocity	25 cm/s
Maximum amplitude of acceleration when the maximum load is shaken	0.45G
Shaking motion	Arbitrary motions controlled by input data
Effective frequency range	from 1 to 100 Hz

drain, the other, i.e. R-200, R-300, R-600, and R-800 series, was the tests without a gravel drain. By comparing the results of these groupes with each other, effects of the gravel drain could well be understood. Some of the series of the tests, i.e. R-100 through R-700 series, were conducted under sinusoidal input motions, others, i.e. R-800 and R-900 series, under earthquake motions. By using these input motions, influence of wave forms of the input motions were studied. Most of the series of the tests, except for R-100 and R-500 series, were conducted with filters against migrating sand into the gravel drain; the filters were made of a thin cloth and put around the gravel drain. Each series of tests was conducted in several stages, in which the amplitude of the input motions was varied in step-by-step wise. More specific conditions for the model tests will be presented later. Measured items during the shaking table tests were accelerations, displacements, pore water pressures, settlements, and amounts of drained water by the gravel drain.

2.2 Shaking table

The shaking table used for the present study is of electromagnetic type. This type of shaking tables is known to achieve the best accuracy in reproducing input motions among various types of shaking tables. Degree-of-freedom of the motion of the shaking table is one horizontal direction. Dimensions of the table are four meters in length and 3.5 meters in width. More specific details on the shaking table are shown in Table 1.

2.3 Container made of a stack of rings

Upon this shaking table, the container was set up for conducting the shaking tests. The container was, as mentioned earlier, made of a stack of 64 aluminum rings; each ring had the inside diameter of 190 cm, the outside diameter of 194 cm, and the vertical thickness of 3 cm. The total height of the stack amounted to 206 cm. In order to reduce the friction between the rings, roller bearings of 0.245 cm in diameter were inserted. On the top of the container, a load of 2.5 tf in weight was placed for preventing rocking motion of the container during the shaking. Ball bearings of 3.8 cm in diameter were inserted between the load and the top of the container in order to reduce the friction between them. As an inner cell for the container, a rubber membrane of 0.13 cm in thickness was used for keeping the model ground saturated with water.

After setting up the aluminum rings and the rubber membrane, the exact inside diameter, including the thickness of the rubber membrane, was measured by filling

Plan

⊖X ← → ⊕X

Flexible Pipes
for Collecting
Drained Water

Casing for Guiding Drained Water
from the Gravel Drain

SS4

SS3
P30
P12 P22 P32 P42
P15 P25 P35 P45
HII–HI5 AV
A11–A15 A22–A25
AO AHI

P62
P62
P65
SS0
P53
P55
E3 E4
A31
A32

SS5

P70

SI–S3

E1

AV2

AH2

SS2

SS6

SS1

Direction of
Vibration

▽ Gauge for
Drained Water   (L)

△ Accelerometer
(Horizontal)   (A)

▲ Accelerometer
(Vertical)   (A)

● Pore Water
Pressure Gauge (P)

□ Earth Pressure
Gauge   (E)

◆◇ Settlement
Gauge   (S)(SS)

▭ Displacement
Transducer   (H)

Cross Section

Casing for Guiding Drained Water

SS2
SS3

SS0

SS5
SS6

AVI
AHI

P30

A11

A31

P70

▽

AV2
AH2

HII

HI2

P12 P22 P32 P42
A12   A22

P62
P62

SI

HI3

P13 P23 P33 P43 P53
A13   A23   A32

P63
E3 E4

S2

E1

HI4

P14 P24 P34 P44
A14   A24

P64

S3

HI5

P15 P25 P35 P45 P55
A15   A25

P65

AO

E2

▽ L2,3

20 | 20 | 40 | 40 | 40 | 20 | 20

200

Flexible Pipes
for Collecting
Drained Water

Z ⊕ ↑ ↓ ⊖ ①

Direction of Vibration

⊖X ← → ⊕X
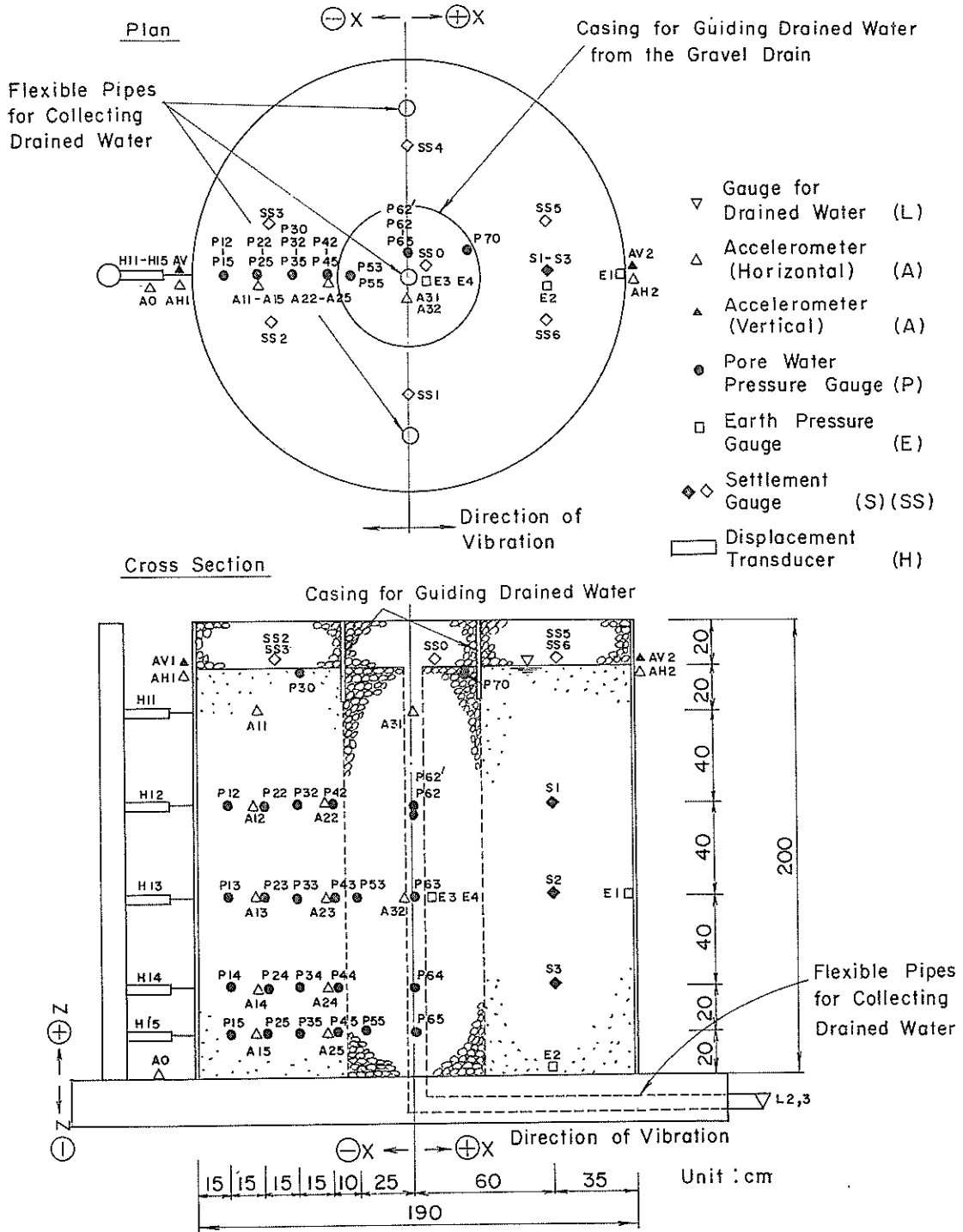
|15|15|15|15|10| 25 | 60 | 35 |

190

Unit : cm

Fig. 3 Typical locations of the instruments

up the container with water. The measurements were conducted two times. The results gave the value of 189.6 cm as the exact inside diameter.

2.4 Instrumentation

(1) Measured quantities

As mentioned earlier, the performance of the gravel drains is characterized by excess pore water pressures and settlements. Threfore, these quantities were measured with the greatest care. The amount of the drained water from the gravel drain or from the sand deposit has a close relation with the settlement. Therefore, the amount of the drained water was also measured. The amount of the excess pore water pressures and the settlements are affected by the dynamic response of the model ground. Therefore, accelerations and displacements of the ground were also measured.

(a) Details   (b) Overall view
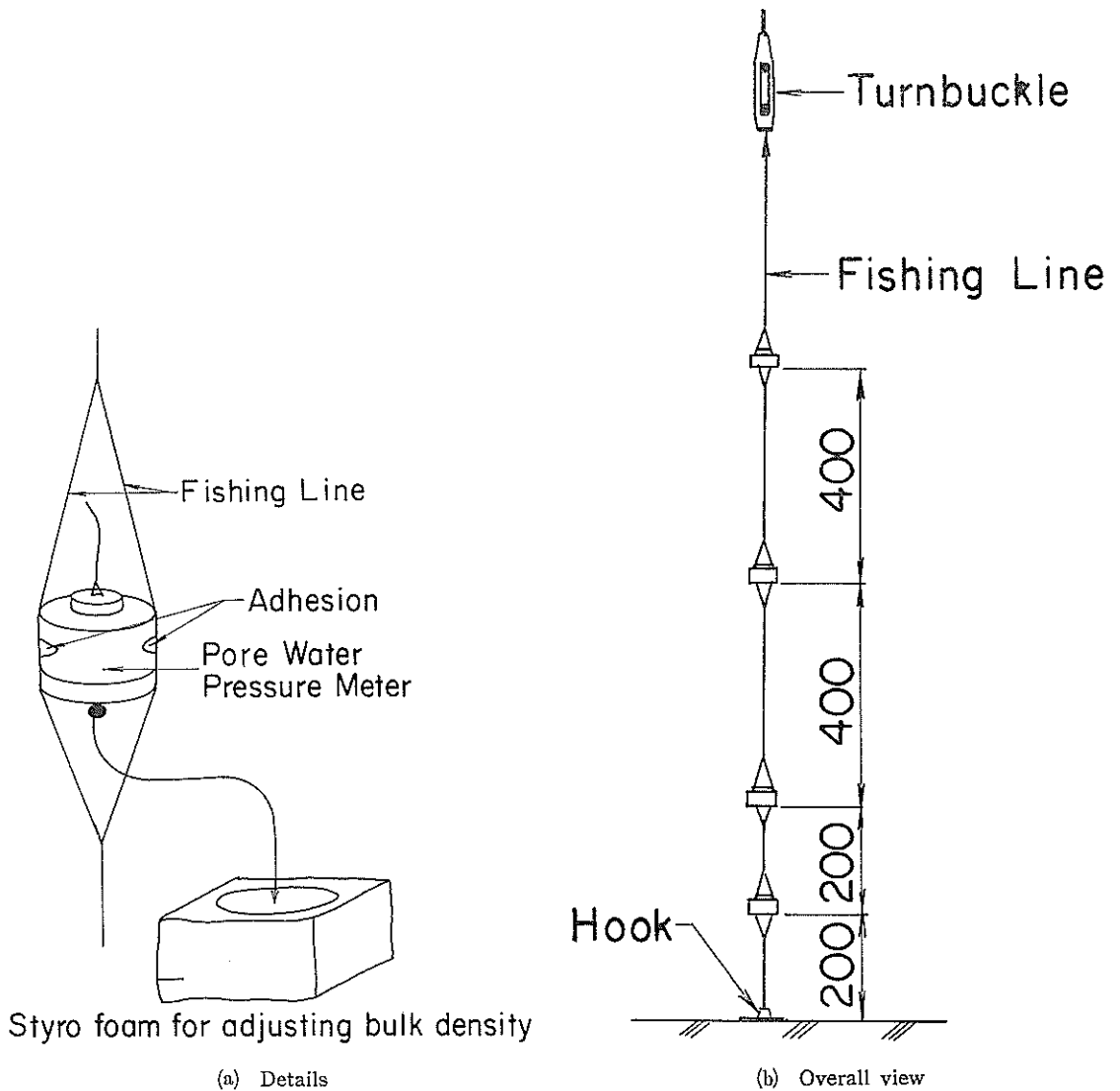
Fig. 4 Attachment for the pore water pressure meter

The performance of the gravel drain is also affected by densities of the sand deposit and the gravel drain. Therefore, weight and volume of the sand and the gravel were also measured. Cone penetration resistance was also measured for confirming the uniformity of the density of the sand deposit.

(2) Arrangement of the instruments

As mentioned earlier, when the composite ground, made of the sand deposit and the gravel drain, is horizontally shaken, excess pore water pressures are generated in the sand deposit and initiate the flow of pore water towards the gravel drain. Length of the path of the flow towards the gravel drain varies with the position from which each flow initiates. As a result, excess pore water pressures which will be measured in the composite ground may vary with the distance measured from the center of the gravel drain. Apart from the distribution of the excess pore water pressures in the horizontal direction, excess pore water pressures will vary with depth. With these phenomena in mind, the instruments were deployed in an array configuration as shown in **Fig. 3**.

Because the instruments were deployed in the array configuration, it will be useful to define the levels and the lines, which correspond to the rows and the columns of the array in the cross section. The levels are numbered downward; level 1 denotes the horizontal cross section at the height of 160 cm measured from the bottom of the container, level 2 at 120 cm, the level 3 at 80 cm, level 4 at 40 cm, and level 5 at 20 cm. The lines are numbered inward; line 1 denotes the position at 15 cm from the outer edge, line 2 at 30 cm, line 3 at 45 cm, line 4 at 60 cm, line 5 at 70 cm, and line 6 at 95 cm which coincides with the center of the model ground. The numbers given to the instruments are the combinations of the numbers of the lines and the levels.

For the tests without gravel drain, the same deployment was adopted. However, for R-700 series, at which the gravel drain of a larger diameter was used, the locations of the lines were slightly changed. The exact locations will be given later when they become necessary.

(3) Instruments

Accuracy in the results of the model tests generally depend on the accuracy of the instruments used for the model tests. The reliability of the instruments can generally be judged with the detail information on the instruments. The detail information is given here on the instruments used for the present study.

a) Pore water pressure meters

Specific weight of the pore water pressure meters was adjusted to be same as that of the saturated sands by using attachments made of styrofoam as shown in **Fig. 4 (a)**. Locations of the pore water pressure meters were fixed by using fishing lines. As shown in **Fig. 4 (b)**, the fishing lines were suspended from the cross beams at the top of the container. The other ends of the fishing lines were fixed at the bottom of the container. The tensions given to the fishing lines were adjusted with the turnbuckles in order to mitigate the undesirable effects on the dynamic response of the model ground.

After setting the pore water pressure meters by the fishing lines, the model ground was made by pouring the sand into the water; the details of the pouring will be decribed in the later section. The water was gradually leveled up. When the level of the water became high enough, small air bubbles were removed within the water from the pore water pressure meters in order to assure the accurate measurements of the pore water pressures.

b) Settlement gauges

Two types of settlement gauges were used for the present study. One type of settlement gauges measures the residual values of the settlements after the shaking. The other measures the settlements which are varying with time as the drainage takes place. The former type of settlement gauge was made of acrylic plates and strings. The plates were placed at the surface of the sand deposit above which lays a gravel layer of 20 cm thickness as shown in **Fig. 5**. Relative levels of the weights at the end of the strings were read off as the residual values of the settlements at the surface of the sand deposit.
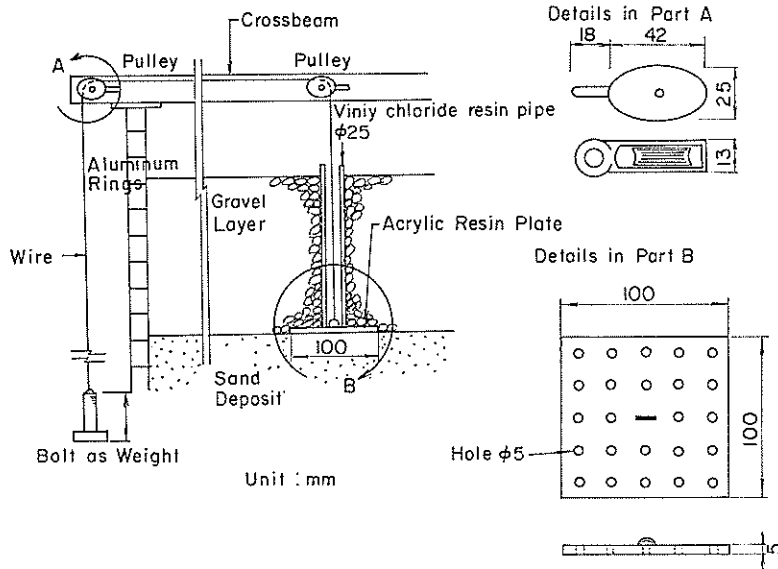
Fig. 5 Residual settlement gauge (denoted by SS in Fig. 3)
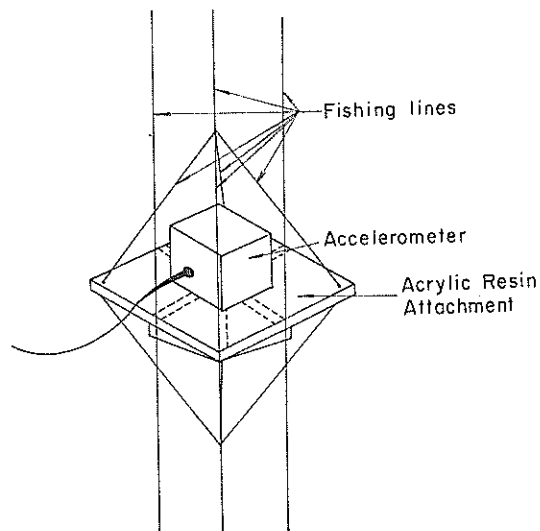
Fig. 6 Attachment for the accelerometer

The latter type of the settlement gauge was made of two parts; one was a pressure meter put in a cell which is filled with water, the other a container filled with water. These parts were connected with flexible vinyl pipes. In order to measure the settlements with this type of gauge, level of the container was fixed throughout the shaking tests while the cell was placed in the sand deposit. If the level of the cell changes, water pressure in the cell changes. Thus the settlements were measured. Undesirable dynamic components of the pressure were removed by appropriate high-cut filters.

c) Measuring the amount of drained water

The amount of drained water from the gravel drain was measured by guiding the drained water into a flexible pipe, which went through the base of the container and out into a tank. A casing was placed as shown in **Fig. 3** at the top of the gravel drain and used as a guide for collecting the drained water from the gravel drain. The drained water thus flowed through the flexible pipe and flowed into the tank. The pipe was 5 cm in diameter and was flexible even in the longitudinal direction so as to smoothly follow the settlement in the model ground.

Two more flexible pipes were used for measuring the amount of the water drained from the sand deposit. Weights of the water collected from the gravel drain and from the sand deposit were separately measured with the load cells.

d) Accelerometers

Two types of accelerometers were used for the present study. One had the bulk density being approximately the same as that of the saturated sand. The other had larger bulk density but had attachments such as shown in **Fig. 6** for securing better fit with the sand deposit. The fishing lines were used for fixing the positions of the accelerometers as in the same manner as for the pore water pressure meters. At the final stage in placing the accelerometers in the sand deposit, fine adjustments were made for levelling the accelerometers by monitoring the output of each instrument. The fishing lines suspended from the crossbeams were cut, when the model ground was completely made, in order to minimize the undesirable effect of the fishing lines on the accelerometers.

e) Displacement tranceducers

Displacement tranceducers were attached to a rigid steel pole which was fixed to the shaking table as shown in **Fig. 3**. Relative displacement between the container and the fixed pole was measured. Inductance type was used as the displacement tranceducer in order to minimize the undesirable reaction force applied by the tranceducers to the model ground.

f) Other instruments

Loadcells were used for measuring the weights of the sand and the gravel. The measured weights were used for calculating the density of the sand deposit and the gravel drain. A cone penetrometer was also used for confirming the uniformity of the density of the sand deposit.

Earth pressures were measured at the locations indicated in **Fig. 3**. However, the measured values were later determined unreliable and abandoned.

g) Specification for the instruments

Specifications for the above-mentioned instruments are summarized in **Table 2**.

(4) Calibration of instruments

All the instruments were calibrated carefully for the present study. Pore water pressure meters were calibrated by changing the level of the pore water pressure meters within the water, which was filled in a water pool of about 1.2 m in depth. The outputs of the pore water pressure meters were examined for the linearity and

Table 2 Specifications of instruments

Kind of Instrument	Mechanism of Sensor	Capacity	Dimensions (mm)	Weight (gf)	Frequency range of uniform sensitivity (Hz)	Locations of the instruments in Fig. 3
Pore water pressure meter	Strain gauge type	0.5kgf/cm²	$\phi 40$, t$=30$	170	0~3000	P12-15, P22-25, P30, P32-35, P42-45, P53, P62-65, P62', P63', P70
Pressure meter for settlement gauge	Semiconductor type	0.2kgf/cm²	$\phi 10$, t$=2.5$	1	0~2000	S1-3
Loadcell	Strain gauge type	1000kgf	$\phi 68$, t$=143$	2700	—	L1 for measuring the weights of sands and gravels
		200kgf	$\phi 68$, t$=111$	2300	—	L2, L3 for measuring the weights of drained water
Accelerometer	Strain gauge type	±2 G	56×61×27	200	0~90	A0, A11-15
		±2 G	30×27×22	60	0~56	AV1-2, AH0-2, A22-25, A31-32
Displacement transducer	Inductance type	±200mm	830×75×70	2600	—	H11
		±50mm	330×65×60	900	—	H12-13
		±10mm	330×65×60	900	—	H14-15
Cone penetrometer	Portable single tube type, Capacity: 100 kgf					

Cone: angle$=30°$; projected area$=3.23$ cm²; reversally tapered

the hysteresis. The results confirmed that noises and errors contained in the outputs were less than 1% in the pressure ranges to be used for the present study. The stability of these instruments was confirmed.

The settlement gauges used for measuring the continuous value were calibrated by changing the level of the gauges. The results indicated that undesirable drift was contained in the measured value at the rate of about 1 mm/min. The drift was usually a monotonously increasing or decreasing function of time. Loadcells were calibrated six times during the present study by using iron weights. The result of the calibration revealed 0.8% fluctuation in the calibrated values. This fluctuation amounts to 3.5% errors in estimating the relative densities of the sand deposit in the present study.

2.5 Sand and gravel
(1) Sand

The sand used for the present study was taken at Gaikou district of Akita Port in Japan. The location for sampling the sand is shown by x-mark in **Fig. 7**. The area around this location was reclaimed with sand which was dredged from the nearby sea bottom. The area liquefied during the 1983 Nihonkai-Chubu Earthquake of Magnitude 7.7.[1]

The sand taken from the Akita Port had fines content (i.e., percentage of soil particles finer than 0.074 mm by weight) of less than 5%. Therefore, influence of the fines on the liquefaction strength of the sand was considered negligibly small. However, the fines were completely washed out for the present study. The reason for this is, as given below, related to the uniformity in permeability of the model of sand deposit.

As mentioned earlier, the sand was poured into the water to form the model sand deposit. When the sand, without washing out the fines, was poured into the water at one of preliminary experiments, the fines tended to separate from the coarser particles and to form a thin layer spread out in a horizontal plane. Because of the thin layer of the fines, apparent permeability of the sand deposit in the
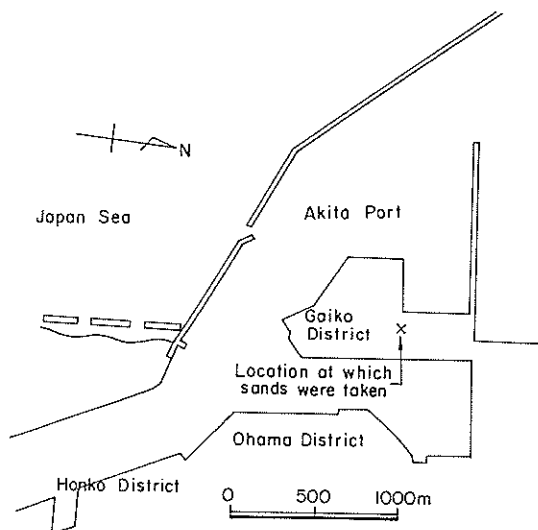
Fig. 7 Plan of Akita port and location at which sands were taken for the present study

vertical direction decreased into less than about one tenth of the original permeability of the sand. On the contrary, when the fines were washed out beforehand, permeability of the sand deposit in the vertical direction was always the same as the original permeability of the sand. Because it was desirable to use model sand deposits with the same permeability through out the series of the tests, the fines were completely washed out for the present study.

The grain size accumulation curves are shown in **Fig.** 8 for the sand thus prepared for the present study. Physical properties and permeability of the sand are shown in **Table 3** and **Fig.** 9. The maximum and the minimum density of the sand, shown in **Table 3**, were obtained by adopting the testing method shown by
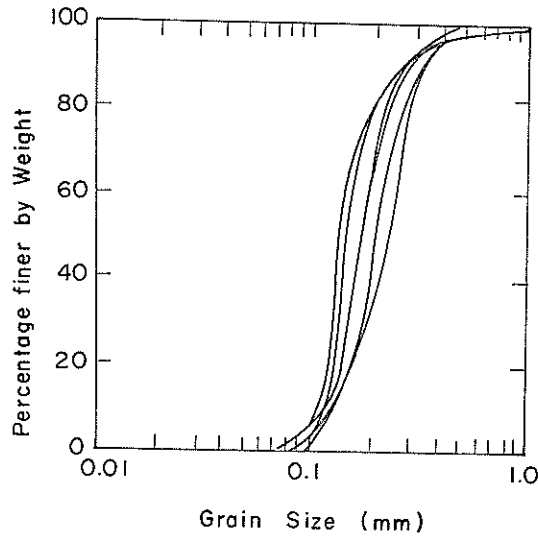
Fig. 8 Grain size accumulation curves of the sands used for the present study

$$k_{15} = 0.0125 \frac{e^3}{1+e}$$

k_{15}=Coefficient of Permeability at 15°C

e : Void Ratio

$e^3/(1+e)$
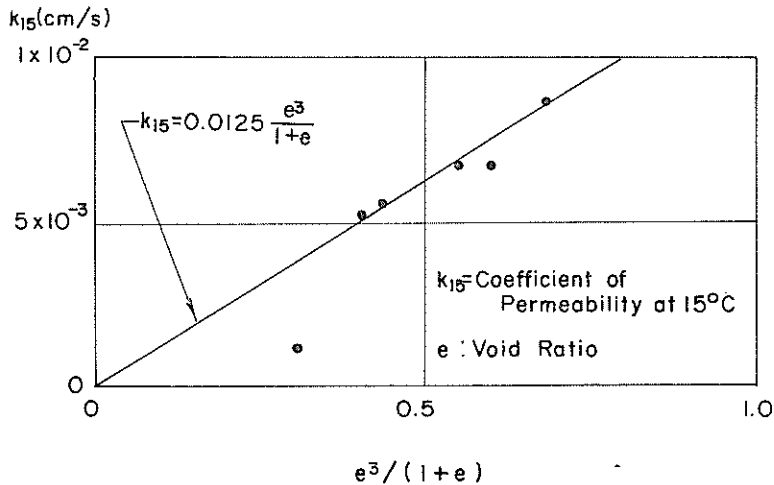
Fig. 9 Coefficient of permeability of the sands used for the present study

Table 3 Test results of the physical properties of the sands used for the present study

Date of Test	Oct. 18, 1984	Nov. 13, 1984	Nov. 13, 1984	Nov. 15, 1984	Nov. 15, 1984	Jan. 9, 1985	Jan. 29, 1985	Average	Standard Deviation
Specific Gravity G_s	2.665	2.662	2.667	2.672	2.676	2.662	2.663	2.667	0.005
Grading ⎰Gravel	0.4	0.4	0.4	0.3	0.4	0.1	0.3	0.33	0.10
Sand	99.3	99.2	99.1	98.7	99.0	99.2	99.3	99.1	0.2
⎱Silt	0.3	0.4	0.5	1.0	0.6	0.7	0.4	0.56	0.2
D_{60} (mm)	0.14	0.18	0.23	0.18	0.21	0.15	0.18	0.181	0.03
D_{10} (mm)	0.11	0.12	0.14	0.12	0.14	0.12	0.13	0.126	0.01
Cofficient of Uniformity U_c	1.3	1.5	1.6	1.5	1.5	1.3	1.4	1.44	0.10
e_{max}	1.346	1.355	1.349	1.342	1.361	1.375	1.341	1.353	0.011
e_{min}	0.879	0.866	0.856	0.849	0.870	0.886	0.851	0.865	0.013
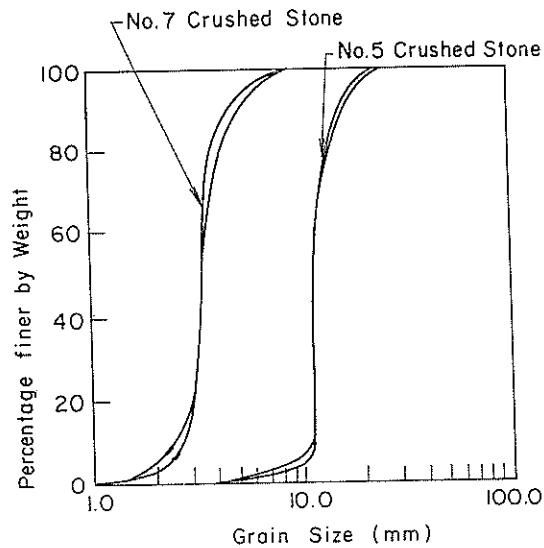
Fig. 10 Gaain size accumulation curves of the crushed stones used for the present study

Table 4 Test results of the physical properties of the crushed stones used for the present study

Kind of Stone	No. 5 Crushed Stone			No. 7 Crushed Stone		
Date of Test	Oct. 19, 1984	Jan. 10, 1985	Jan. 29, 1985	Dec. 5, 1984	Jan. 10, 1985	Jan. 29, 1985
Specific gravity ⎰under saturated surface-dry	2.711	2.700	2.702	2.634	2.656	2.643
under oven-dry	2.657	2.655	2.608	2.589	2.608	2.597
⎱Apparent	2.810	2.780	2.782	2.712	2.739	2.721
Amount of water Absorption	2.1	1.7	1.7	1.8	1.9	1.8

Japanese Society of Soil Mechanics and Foundation Engineering[15].
(2)   Gravel
   Two kinds of crushed stones were used as materials of the gravel drain; i.e., one was taken from Iiyama of Atsugi City in Kanagawa Prefecture in Japan, the other from Aso-Gun in Tochigi Prefecture in Japan. The former will be denoted as "No. 5 crushed stones", the latter as "No. 7 crushed stones" hereafter. The crushed stones were washed before they were used for the tests. The grain size accumulation curves are shown in **Fig. 10**. Physical properties are shown in **Table 4**.
   Except for R-100 series, only No. 7 crushed stones were used as the material of the gravel drain. No. 5 crushed stones were mainly used as the gravel layer of 20 cm thickness above the sand deposit or above the composite ground made of the sand deposit and the gravel drain. As will be mentioned later, R-100 series turned
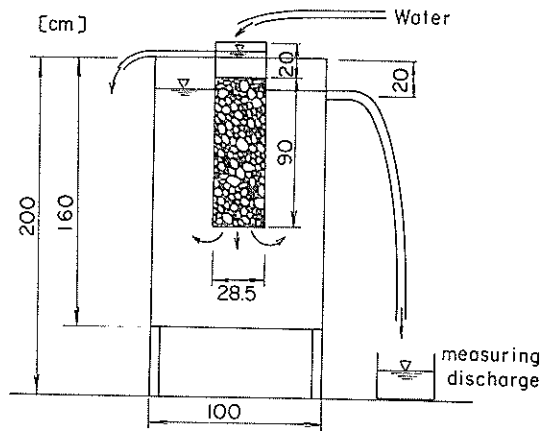
Fig. 11   Apparatus for measuring the coefficient of permeability
of No. 7 crushed stone used for the present study
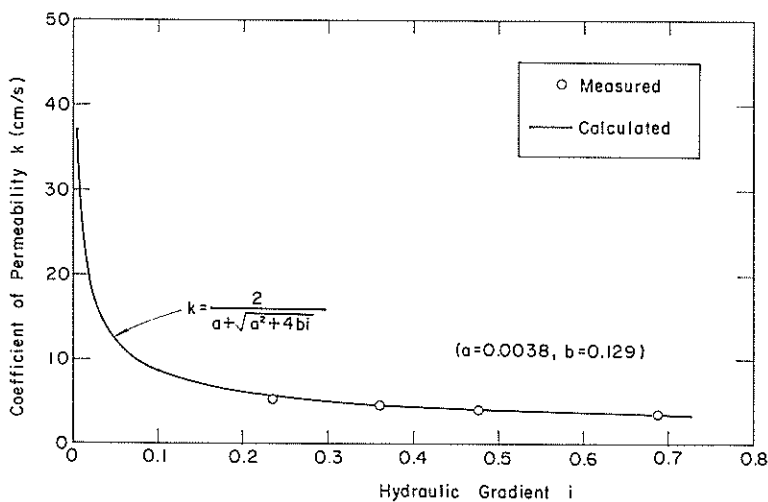
Fig. 12   Coefficient of permeability of No. 7 crushed stone used for the
present study

out to be a failure as a test of the gravel drain because the gravel drain made of No. 5 crushed stones had completely clogged with the sand even before the model was shaken. Therefore, only about No. 7 crushed stones will be explained hereafter.

The permeability of the material used for the gravel drain is one of the important factors which govern the performance of the gravel drain. For measuring the permeability, several considerations should be given to the particular nature of the flow through the gravel drain. First of all, rate of the flow through the gravel drain will be so high during the shaking that the flow will no longer remain a laminar flow but will be a turnbulent flow. As a result, the apparent permeability of the material used for the gravel drain will vary with the hydraulic gradient. Secondly, the grain size of the material used for the grave drain is far more greater than that of the sand. Therefore, the apparatus generally used for measuring the permeability of sands is too small for accurately measuring the permeability of the material used for the gravel drain. Consequently, a large apparatus shown in **Fig. 11** was used for measuring the permeability of No. 7 crushed stones. The permeability was measured at several hydraulic gradients. The results are shown in **Fig. 12**. The equation shown in the same figure is derived by assuming that the hydraulic gradient is the quadratic function of rate of flow. The constants given for the equation were obtained by the least square method.

2.6 Model preparation

The model of the composite ground, which was made of the sand deposit and the gravel drain, was prepared, as shown in **Fig. 13**, by the following procedure.

(1) Pouring water

First of all, the instruments were arranged with fishing strings and others. Secondly, temporary scaffolds were suspended from the crossbeams. The scaffolds supported the engineers for preparing the model ground so that the model ground would not be disturbed during the model preparation, except at finely adjusting the accelerometers. After thus preparing the instruments and the scaffolds, water was poured into the container up to the level of 30 cm. As mentioned earlier, small air
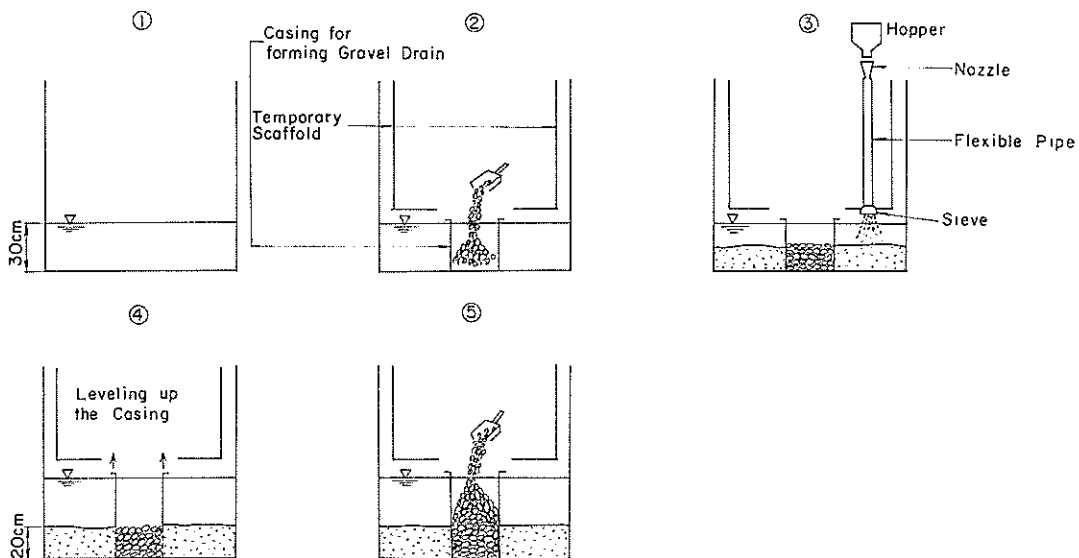
Fig. 13 Procedure for model preparation

bubbles were removed from the front surface of the pore water pressure meters when the level of water became higher enough.

(2) Pouring crushed stones

Crushed stones were poured into the water for forming the gravel drain. Before poured into the water, the crushed stones had been dried and the weight had been measured with a loadcell. Then, the engineer on the temporary scaffold carefully poured the crushed stones with a scoop into the temporary casing as shown in **Photo 2**. The deposit of the crushed stones was leveled up to about 20 cm.

(3) Pouring sands

Sands were poured into the water for forming the model ground surrounding the gravel drain. Before poured into the water, the sands had been dried and stored in a hopper of which capacity is 0.5 m³. The weight was measured with a loadcell. Then, the engineer on the temporary scaffold carefully poured the sands into the water with a hose attached to the hopper. At the other end of the hose, a screen of 5 mm mesh was attached to the nozzle for reducing the speed of the pouring sands. The level of the screen was kept at the level of about 20 cm higher than the water level. While the sands were poured into the water, the level of the sand deposit was monitored by the other engineer for keeping the level of the sand deposit at least 5 cm below the water level. The sand deposit was leveled up to about 20 cm. Then, the casing for forming the gravel drain was carefully leveled up to about 20 cm. The temporary scaffold was also leveled up.

(4) Forming upper gravel layer

After the above-mentioned process of pouring water, crushed stones, and sands was repeated nine times, the surface of the sand deposit was carefully leveled at the height of 180 cm. The exact level of the model ground was measured at the grid points shown in **Fig. 14** (a) for determining the density of the model ground. The cone penetration tests were also conducted for confirming the uniformity of the density.

The upper gravel layer was formed to the thickness of 20 cm by carefully placing the crushed stones on the top of the composite ground. On the surface of the upper
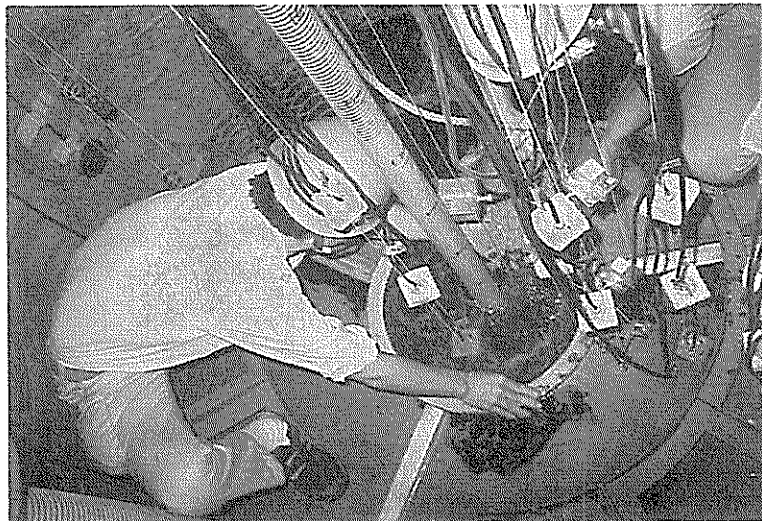
Photo 2 Carefully poring the crushed stones into the casing for forming the gravel drain

Direction of Vibration
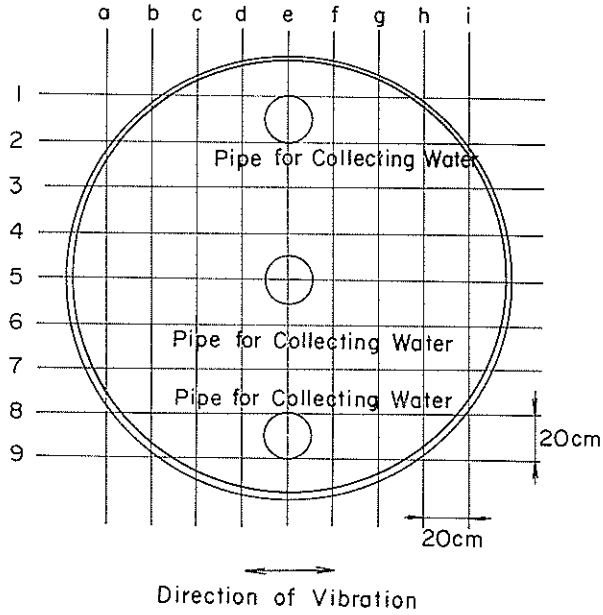
(a)　At the surface of the sand deposit

Direction of Vibrition
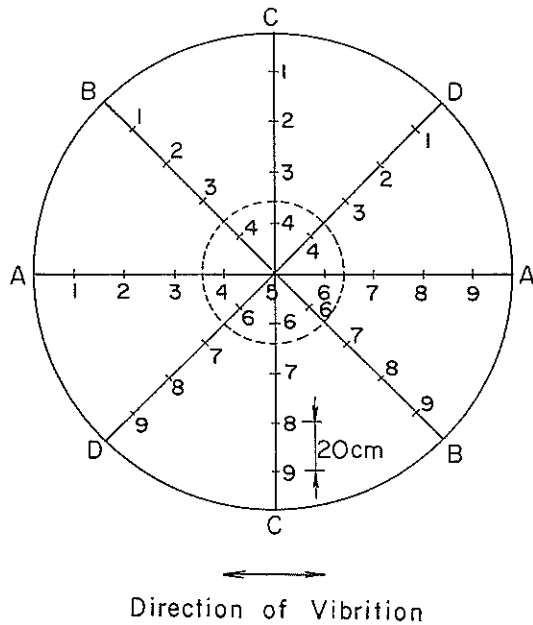
(b)　At the surface of the upper gravel layer

Fig. 14　Locations for measuring the level of the model

Table 5 Initial properties of the model

Series No.	a/b	$H1$ (cm)	$H2$ (cm)	γ_{sat} (gf/cm³)	γ_d (gf/cm³)	e	Dr (%)	k_{15} (cm/sec)	T (°C)	k_T (cm/sec)	$\gamma_{sat\,d}$ (gf/cm³)	γ_{dd} (gf/cm³)	e_d	γ_{do} (gf/cm³)	G_0 (kgf/cm²)
R-100	0.3	200.4	179.5	1.782*	1.252*	1.129*	47*	8.5×10^{-3}	19.5	9.5×10^{-3}	1.922	1.463	0.848	1.416	115/79
R-200	—	201.0	182.4	1.754	1.206	1.210	29	10.0×10^{-3}	18	10.8×10^{-3}				1.476	122/72
R-300	—	201.2	181.0	1.757	1.211	1.201	31	9.8×10^{-3}	14	9.6×10^{-3}				1.501	126/84
R-400	0.3	199.9	182.5	1.760	1.217	1.190	33	9.6×10^{-3}	12	8.9×10^{-3}	1.881	1.417	0.866	1.403	140/89
R-500	0.3	200.1	181.5	1.760	1.217	1.190	33	9.6×10^{-3}	9	8.1×10^{-3}	1.894	1.437	0.840	1.401	136/76
R-600	—	200.6	184.1	1.753	1.205	1.212	29	10.1×10^{-3}	13	9.5×10^{-3}				1.425	108/93
R-700	0.45	200.2	183.0	1.760	1.216	1.192	33	9.7×10^{-3}	14	9.4×10^{-3}	1.892	1.435	0.843	1.398	139/87
R-800	—	203.2	182.9	1.747	1.196	1.228	25	10.4×10^{-3}	9	8.8×10^{-3}				1.377	116/91
R-900	0.3	200.3	181.8	1.759	1.215	1.193	33	9.7×10^{-3}	11	8.6×10^{-3}	1.880	1.415	0.869	1.380	130/89

a, b : radii of gravel drain and composite ground

$H1, H2$: heights of top of the gravel layer and surface of the sand deposit

γ_{sat}, γ_d : saturated and dry unit weights of sand deposit

e : void ratio of sand deposit

Dr : relative density of sand deposit

k_{15}, k_T : coefficients of permeability of sand deposit at 15°C and at T°C

T : temperature of water in centigrade

$\gamma_{sat\,d}, \gamma_{dd}$: saturated and dry unit weights of gravel drain

e_d : void ratio of gravel drain

γ_{do} : dry unit weight of gravel layer

G_0 : shear modulus at small strain level
(value obtained by impulse test/value obtained by resonant test)

$$Dr = \frac{e_{max} - e}{e_{max} - e_{min}} = \frac{1.346 + e}{1.346 - 0.879}$$

Sand $G_s = 2.665$, No. 5 Crushed Stone $G_s = 2.704$
No. 7 Crushed Stone $G_s = 2.644$

$k_{15} = 0.0125 \dfrac{e^3}{1+e}$ (after Fig. 9)

* : influenced by sand migration into gravel drain
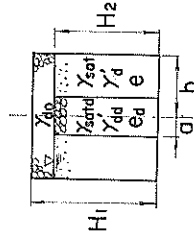
gravel layer, level markers were placed at the points shown in **Fig. 14** (b). The initial levels of the surface of the upper gravel layer were measured at these points. The measured levels were used later for determining the settlement of the model ground. Finally, as mentioned earlier, a weight was placed at the top of the container for preventing the rocking motion of the model ground. This vertical load was applied only to the container.

2.7 Initial densities and other properties of models

Completed model grounds for the present study had initial properties summarized in **Table 5**. In addition to these properties, shear moduli at small strain level were obtained before and after the shaking test by two methods; one used shear wave velocity measured by impulse response of the model, the other used resonant frequency of the model. A typical record of the impulse test and a typical result of the resonant test are shown in **Appendix A**. The shear moduli before and after the test are summarized in **Tables 5** and **6**. The results of the cone penetratin tests are also shown in **Fig. 15**. The results in this figure indicate that initial densities of the sand deposit are uniform along the depth. However, the densities after the shaking tests seem irregular along the depth.

2.8 Input motions

Input motions used for the present study were of sinusoidal and earthquake wave forms. The sinusoidal input motion was of 2 Hz and of 20 cycles. The earthquake motion was of the recorded acceleration at Akita Port during 1983 Nihonkai-Chubu Earthquake of Magnitude 7.7 recorded at about 100 km off from the epicenter. The wave form is shown in **Fig. 16**.

As mentioned earlier, each series of the tests consisted of several shaking tests at several amplitudes of the input motions. Case numbers of these tests and the maximum accelerations of the input motions are summarized in **Table 7**. As shown in this table, many shaking tests have been conducted. However, most of the tests were conducted after undergoing some degree of stress history in cyclic shear. Obviously, the influence of the stress history in cyclic shear on the gravel drains

Table 6 Properties of the model after the shaking test

Series No.	Dr (%)	γ_{sat} (gf/cm³)	e	G_0 (kgf/cm²)
R–100	53*	1.794*	1.907*	160/85
R–200	58	1.801	1.077	139/71
R–300	48	1.779	1.124	110/69
R–400	51	1.789	1.109	160/86
R–500	60	1.805	1.068	156
R–600	41	1.772	1.155	121/73
R–700	45	1.780	1.134	140
R–800	50	1.789	1.112	151/90
R–900	52	1.791	1.105	156

Dr : relative density
γ_{sat} : saturated unit weight of sand deposit
e : void ratio of sand deposit
G_0 : shear modulus at small strain level
        (value obtained by impulse test/value obtained by resonant
        test)
* : influenced by sand migration into gravel drain
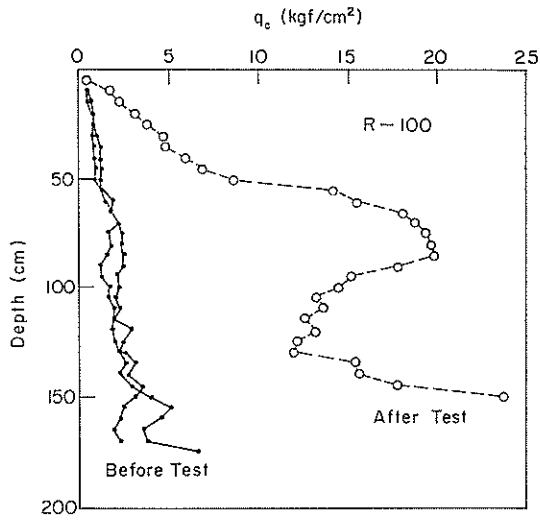
(a) R-100 series
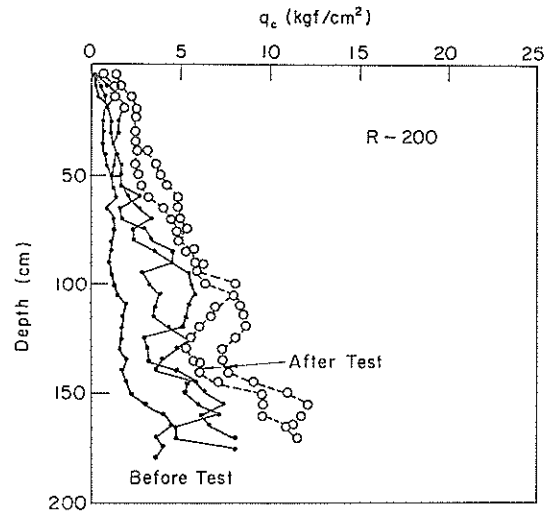
(b) R-200 series
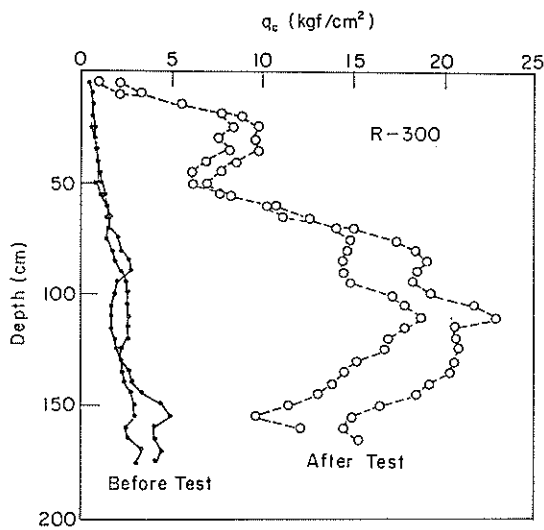
(c) R-300 series
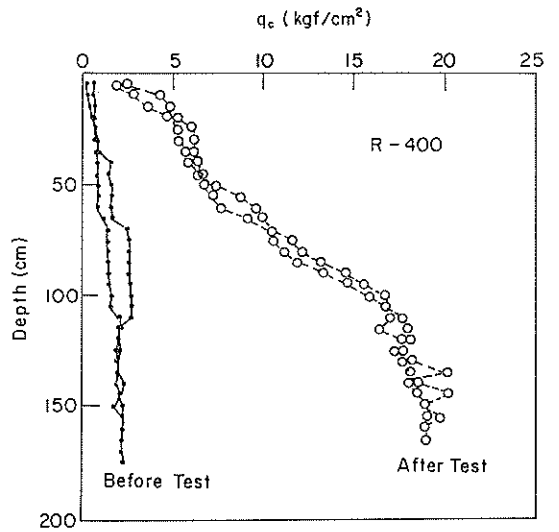
(d) R-400 series

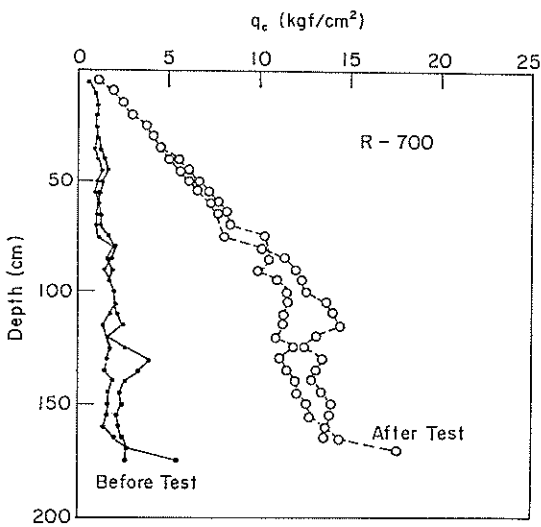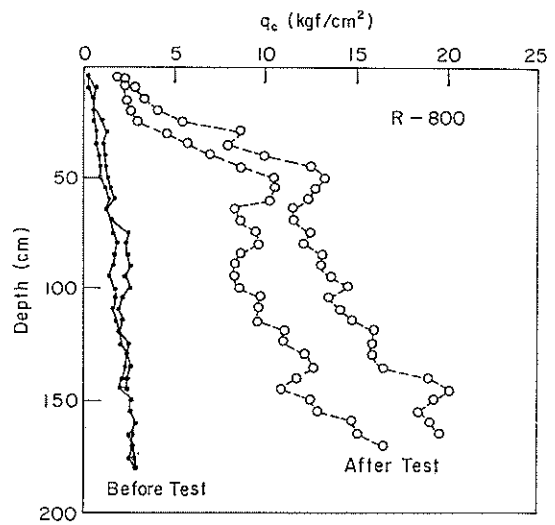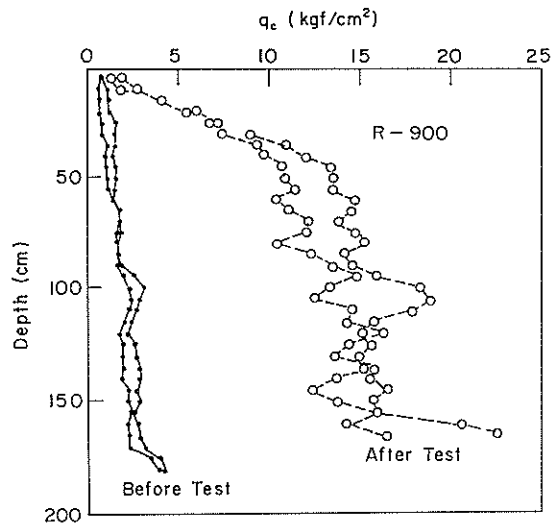**Fig. 15** Results of cone peneration tests before and after the tests (to be continued)
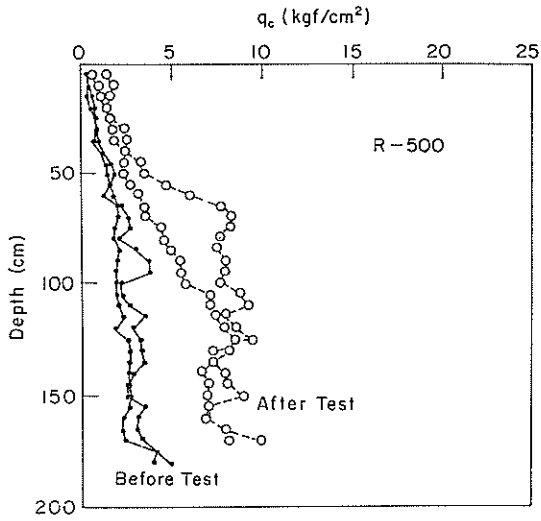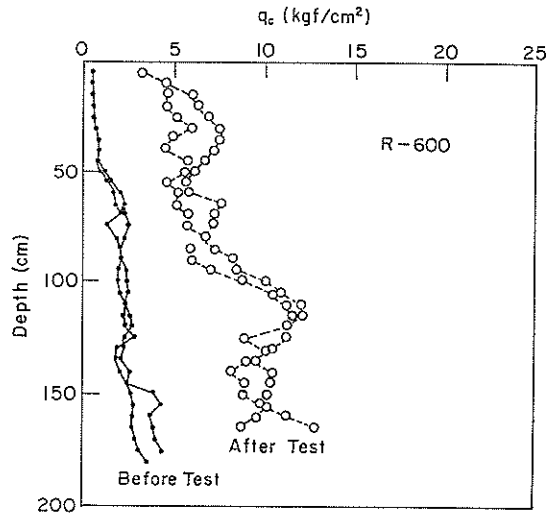
(e) R-500 series

(f) R-600 series

(g) R-700 series

(h) R-800 series

Fig. 15 Results of cone penetration tests before and after the tests (to be continued)

q_c (kgf/cm^2)

R – 900

After Test

Before Test

(i) R-900 series

Fig. 15 Results of cone penetration tests before and after the tests

CAS-R802

PIC-AD

PIC-AD

PIC-AD

ACCELERATION (GAL)

TIME (SECONDS)
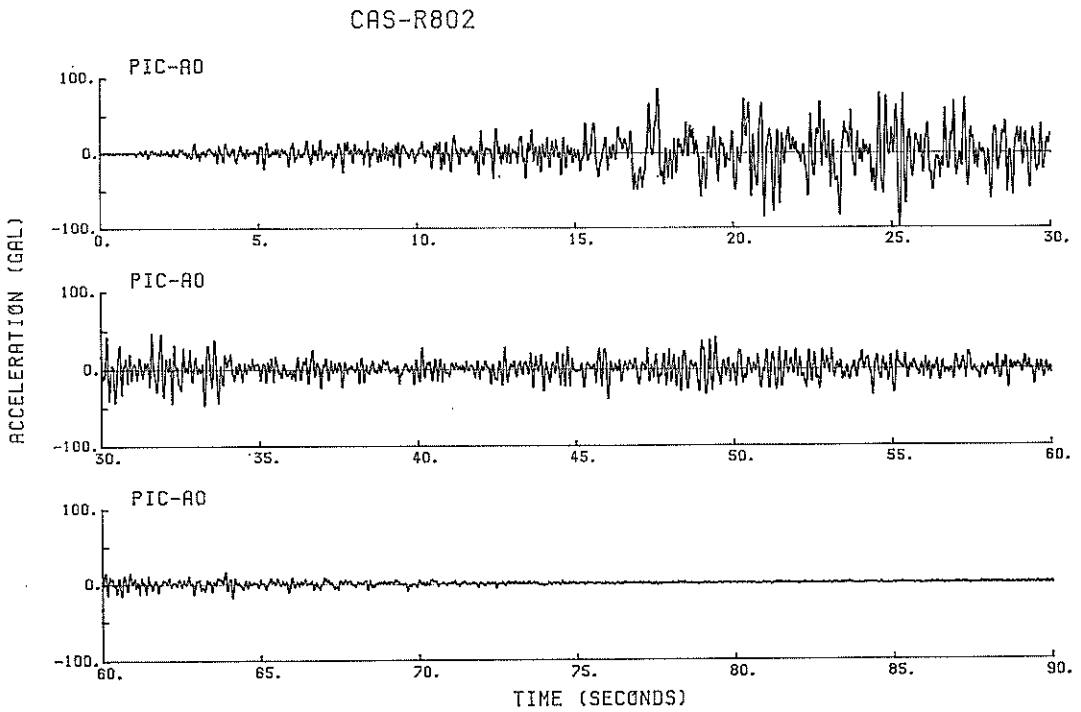
Fig. 16 Input earthquake motion used for R-800 and R-900 series

Table 7 Levels of the input acceleration and result of maximum
excess pore water pressure ratios

Table 7(a) R-100 series

Date: Oct. 29, 1984.
Temperature: 19.5°C in water

Case No.	α_{max} (Gal)	u_{max}/σ_{v0}'	Dr (%)
R-101	18**	0.08	46.5
102	18**	0.06	
103	11**	0.09	
104	29	0.04	
105	32	0.07	
106	32.5	0.13	
107	32	0.26	
108	36.5	0.30	
109	47	0.05	
110	48	0.06	
111	51	0.05	
112	56	0.11	
113	61	0.08	
114	65	0.15	
115	68	0.22	
116	70.5	0.19	
117	75	0.19	
118	80	0.23	
119	84	0.28	
120	86	0.44	
121*	88	0.83	
122	96	0.88	
123	100	0.79	
124	105	0.69	
125	108	0.55	
126	113	0.39	80.5

α_{max}: Max. Acceleration of Input Motion
u_{max}/σ_{v0}': Max. Excess Pore Water
      Pressure Ratio at P 15 in Fig. 3
Dr : Relative Density
  * : To be presented in detail in this report
 ** : Resonant Test

Table 7(b) R-200 series

Date: Nov. 8, 1984
Temperature: 18°C in air

Case No.	α_{max} (Gal)	u_{max}/σ_{v0}'	Dr (%)
R-201	11**	—	29.1
202	19**	—	
203	14**	—	
204*	42.9	0.92	
205	30.9	0.18	
206	34.3	0.10	
207	51.5	0.33	
208	63.5	0.26	
209	72.0	0.33	
210	77.2	0.78	
211	86.9	1.01	46.9

α_{max}: Max. Acceleration of Input Motion
u_{max}/σ_{v0}': Max. Excess Pore Water
      Pressure Ratio at P 15 in Fig. 3
Dr : Relative Density
  * : To be presented in detail in this report
 ** : Resonant Test

Table 7(c) R-300 series

Date: Nov. 19, 1984
Temperature: 14°C in air

Case No.	α_{max} (Gal)	u_{max}/σ_{v0}'	Dr (%)
R-301	5.5**	0.01	31.0
302*	50	0.63	
303	81	1.01	
304	48	0.98	
(305)	—	—	
306	6.2**	0.15	
307	34	0.14	
308	49	0.15	
309	74	0.96	
310	68.5	0.92	
311	6.7**	0.02	
312	33.5	00.8	
313	47	0.14	
314	76	0.89	
315	107	0.81	
316	5.4**	—	65.7

α_{max}: Max. Acceleration of Input Motion
u_{max}/σ_{v0}': Max. Excess Pore Water
      Pressure Ratio at P 23 in Fig. 3
Dr : Relative Density
  * : To be presented in detail in this report
 ** : Resonant Test

Table 7(e) R-500 series

Date: Dec. 7, 1987
Temperature: 9℃ in water
            12.5℃ in air

Case No.	α_{max} (Gal)	u_{max}/σ_{v0}'	Dr (%)
R-500	6.9**	—	33.4
502*	49.7	0.39	(34.7)
503	63.5	0.92	(40.1)
504	51.4	0.34	(41.3)
505	7.6**	—	57.5

α_{max}: Max. Acceleration of Input Motion
u_{max}/σ_{v0}': Max. Excess Pore Water
          Pressure Ratio at P 13 in Fig. 3
Dr : Retlaive Density, ( ) is obtained by
      Settlement gauges (SS in Fig. 3)
 * To be presented in detail in this report
** Resonant Test

Table 7(d) R-400 series

Date: Nov. 28, 1984
Temperature: 12℃ in water
            14℃ in air

Case No.	α_{max} (Gal)	u_{max}/σ_{v0}'	Dr (%)
R-401	5.1**	—	33.4
402*	50	0.18	(33.8)
403	55	0.23	(34.4)
404	58	0.31	(35.3)
405	67	0.30	(36.0)
406	70.2	0.17	(36.9)
407	71.9	0.30	(37.6)
408	77.1	0.34	(38.5)
409	83.0	0.15	(39.1)
410	90.9	0.12	(39.4)
411	94.8	0.20	(40.0)
412	102.8	0.23	(40.5)
413	106.7	0.26	(41.3)
414	110.7	0.30	(42.1)
415	114.6	0.40	(43.0)
416	118.6	0.54	(44.4)
417	122.5	0.91	(47.7)
418	126.5	1.03	(53.4)
419	4.6**	0.02	
420	49.7	0.16	(53.8)
421	80	0.35	(54.8)
422	120	0.88	60.6 (57.9)

α_{max}: Max. Acceleration of Input Motion
u_{max}/σ_{v0}': Max. Excess Pore Water
          Pressure Ratio at P 13 in Fig. 3
Dr : Relative Density, ( ) is obtained by
      settlement gauges (SS in Fig. 3)
 * : To be presented in detail in this report
** : Resonant Test

Table 7(f) R-600 series

Date: Dec. 17, 1984
Temperature: 13℃ in water
            13.5℃ in air

Case No.	α_{max} (Gal)	u_{max}/σ_{v0}'	Dr (%)
R-601	3.4**	0.01	28.7
602*	30.0	0.16	(29.0)
603*	84.0	1.01	(39.6)
604	61.0	1.03	(47.6)
605	9.1**	0.03	—
606	59.5	0.99	(52.8)
607	59.5	0.97	(56.7)
608	13.1**	0.02	58.2

α_{max}: Max. Acceleration of Input Motion
u_{max}/σ_{v0}': Max. Excess Pore Water
          Pressure Ratio at P 13 in Fig. 3
Dr : Relative Density, ( ) is obtained by
      settlement gauges (SS in Fig. 3)
 * : To be presented in detail in this report
** : Resonant Test

Table 7(g) R-700 series
Date: Dec. 25, 1984
Temperature: 14°C in water
10°C in air

Case No.	α_{max} (Gal)	u_{max}/σ_{v0}'	Dr (%)
R-701	5.2**	0.01	33.0
702*	51.0	1.14	(33.5)
703*	81.6	0.96	(41.5)
704	78.2	0.89	(47.1)
705	100.3	0.89	(50.7)
706	4.0**	0.02	—
707	50.6	0.13	—
708	84.3	0.23	(51.1)
709	121.3	0.37	(51.9)
710	157.2	0.89	(53.3)
711	5.7**	0.01	(59.5) 69.4

α_{max}: Max. Acceleration of Input Motion
u_{max}/σ_{v0}': Max. Excess Pore Water Pressure Ratio at P13 in Fig. 3
Dr: Relative Density, ( ) is obtained by settlement gauges (SS in Fig. 3)
*: To be presented in detail in this report
**: Resonant Test

Table 7(h) R-800 series
Date: Jan. 12, 1985
Temperature: 9°C in water
10°C in air

Case No.	α_{max} (Gal)	u_{max}/σ_{v0}'	Dr (%)
R-801	7.0**	0.01	25.3
802*	104.5	0.90	(29.1)
803	157.6	0.98	(34.6)
804	226.4	1.02	(40.8)
805	8.5**	0.02	—
806	95.9	0.55	(42.0)
807	150.7	0.55	(43.6)
808	192.5	0.57	(45.3)
809	13.4**	0	46.3

α_{max}: Max. Acceleration of Input Motion
u_{max}/σ_{v0}': Max. Excess Pore Water Pressure Ratio at P13 in Fig. 3
Dr: Relative Density, ( ) is obtained by settlement gauges (SS in Fig. 3)
*: To be presented in detail in this report
** Resonant Test

Table 7(i) R-900 series
Date: Jan. 23, 1985
Temperature: 11°C in water
12°C in air

Case No.	α_{max} (Gal)	u_{max}/σ_{v0}'	Dr (%)
R-901	5.1**	—	32.8
902*	99.3	0.71	(36.6)
903	150.7	0.80	(41.3)
904	202.1	0.87	(46.8)
905	213.4	0.71	(50.2)
906	5.2**	—	—
907	91.7	0.05	(50.3)
908	132.5	0.12	(50.6)
909	216.9	0.31	(51.6)
910	5.2**	—	52.0

α_{max}: Max. Acceleration of Input Motion
u_{max}/σ_{v0}': Max. Excess Pore Water Pressure Ratio at P13 in Fig. 3
Dr: Relative Density, ( ) is obtained by settlement gauges (SS in Fig. 3)
*: To be presented in detail in this report
**: Resonart Test

are one of the interesting research subjects because there is a good chance that the gravel drains will experience several earthquakes. However, it is later found too difficult to get a simple conclusion on this subject from the present test results. Therefore, results of the model tests considered to be at the virgin (i.e. without any stress history in cyclic shear) conditions will mainly be presented in the following chapters.

3. Results of large scale model tests

3.1 Outline of test results

R-100 series was conducted as preliminary tests. Strictly speaking this series of tests could not be regarded as successful one because the gravel drain had been clogged with sands even before the shaking. However, the results indicate importance of appropriate selection of materials to be used for the gravel drain. The results also indicate the interesting performance of the gravel drain if the gravel drain happens to be clogged with sands.

R-200, R-300, and R-600 series were conducted as index tests for the performance of the sand deposits without gravel drain. When the model was shaken with a sinusoidal input motions of 2 Hz for a duration of 10 seconds, excess pore water pressures gradually increased. After the shaking stopped, the excess pore water

pressures gradually decreased. Throughout these processes, the sand deposit gradually settled. As results of these tests, definitive data were obtained on the liquefaction properties of the sand deposit.

R-400 and R-500 series were conducted with the gravel drain with the spacing ratio of $a/b=0.3$, in which a and b denote radii of a gravel drain and the equivalent circle as indicated in **Figs. 1** and **2**. R-700 series were conducted with the gravel drain with the spacing ratio of $a/b=0.45$. When the model was shaken with sinusoidal input motions of 2 Hz for a duration of 10 seconds as in the same manner as for the sand deposit without gravel drains, excess pore water pressures gradually increased and, at the same time, pore water began to flow from the gravel drain. Hydraulic gradient towards the gravel drain was also observed. The rate of the increase in excess pore water pressures was lower than that in the case without the gravel drain. When the increasing rate in excess pore water pressure was low enough, the maximum value of the excess pore water pressure did not reach the value of the initial vertical effective stress. In this case, the gravel drain was successful in reducing the maximum value of the excess pore water pressure and thus preventing the liquefaction. However, when the intensity of the shaking was stepped up to a higher level, the increasing rate in excess pore water pressure became high and the maximum value of the excess pore water pressure reached the value of the initial vertical effective stress. At this instance, the sand deposit liquefied even though the gravel drain was installed. This result indicates that a very careful design is necessary for installing the gravel drains if one intends to reduce the maximum value of the excess pore water pressure to a low enough value in which no liquefaction occurs.

After the shaking stopped, the excess pore water pressure gradually decreased. The rate of the decrease in excess pore water pressure was remarkably higher than that in the case without the gravel drain. In contrast to the delicate performance on reducing the maximum value of the excess pore water pressures, the gravel drain was almost always effective for faster dissipation of the excess pore water pressure after the shaking. Throughout these processes, including the process of increasing in excess pore water pressures, the sand deposit gradually settled. This result indicates that, even if the gravel drains are installed, some amounts of settlements are inevitable in the sand deposit.

R-800 and R-900 were conducted under the earthquake motions; R-800 being without the gravel drain, R-900 with the gravel drain at the spacing ratio of $a/b=0.3$. Results of these tests confirm that the effects of the gravel drain mentioned earlier are valid under the earthquake motions as well as under the sinusoidal input motions.

3.2 Test results under sinusoidal input motions

(1) Model tests without a gravel drain (R-200, R-300, and R-600 series)

a) Excess pore water pressures

When the model ground without a gravel drain was shaken, time histories of excess pore water pressures were measured as shown in **Figs. 17** through **20**. The alphabets and numbers shown at the vertical axes on these figures such as "PIC-P12" correspond to the alphabets and numbers given to the instruments shown in **Fig. 3**. In **Figs. 17** through **20**, measured excess pore water pressures are normalised by the initial vertical effective stresses. The layout of the time histories in those figures approximately corresponds to the layout of the instruments in the cross section of the model ground if the lower half of the figures could be rearranged to the right of the upper half of the figures. The duration of the shaking was, as mentioned earlier, 10 seconds. In these figures, the excess pore water pressures during dis-

sipation are more clearly shown in (b), in which the excess pore water pressures are plotted for the duration of 120 seconds.

The maximum pore water pressure ratios attained in these tests are about 0.2 (in case R-602), 0.6 (in case R-02), 0.9 (in case R-204), and 1.0 (in case R-603). Relative densities of the model sand deposits before the shaking are about 29% for all of these tests as shown in **Table 5**. These four test results are considered as representative cases in various degree of liquefaction at the sand deposit without gravel drains. As shown in these figures, the same amount of pore water pressures is generated at the same level but the pore water pressure ratios slightly vary with the depth.

The excess pore water pressures at the sand deposit, as shown in **Figs. 17** (b) and 18 (b), dissipate logarithmically when the maximum excess pore water pressures attained during the shaking are less than about half of the initial vertical effective stress. Once the maximum excess pore water pressures reach the initial vertical effective stress, the rate of dissipation, as shown in **Figs. 19** (b) and 20 (b), becomes drastically low and becomes dependent on the stress or strain histories applied to the sand deposit.

Presented above are the results of the tests for the excess pore water pressures. It is now necessary to know how these excess pore water pressures are generatd by the shaking. Obviously the acceleration and the displacement of the model sand deposits are two of the most relevant quantities. These quantities will be presented in the next subsection.

b) Accelerations and displacements

Accelerometers and displacement transducers were, as mentioned earlier, deployed at the locations shown in **Fig. 3**. Time histories of the accelerations and the displacements measured at these locations are shown in **Figs. 21** through 24. Distributions of the maximum accelerations are shown in **Fig. 25**. It is easy to recognize in these figures that, although the input motions are of the same sinusoidal wave, dynamic responses of the model grounds depend on the degree of liquefaction.

In **Figs. 21** through 24, AH0, shown in the third rows from the left lower corner, is the acceleration of the weight put on the container for suppressing the rocking motion of the model. AV1 and AV2, shown above the time histories of AH0, are measured in order to confirm the effect of the weight for suppressing the rocking motion.

In addition to the displacements shown in these figures, the shear strain is one of the important quantities which govern the performance of the sand deposit. The shear strains computed from the measured displacements are presented in **Appendix C**.

c) Drained water and settlements

As a result of the excess pore water pressure generation due to the shaking, pore water was drained from the surface of the sand deposit and the sand deposit settles. The amount of drained water and the settlements after the shaking are shown in **Table 8**. Relative densities after the shaking are shown in the **Table 7**. Some of the time histories of the settlements are shown in **Fig. 26**. As mentioned earlier, drift like errors contained in the measurement of the settlements are about 1 mm/min. Figure 26 shows that the settlements do occur not only after the shaking when only the dissipation takes place but also during the shaking when the dissipation as well as generation of excess pore water pressures takes place.

The settlements, which were measured after the series of the shaking tests at the surface of the sand deposit, are shown in **Fig. 27**. In this figure, A-A, B-B,

R602

Fig. 17 Time histories of measured excess pore water pressures at Case R-602 (without a gravel drain; under sinusoidal input motion; maximum input acceleration 30 Gals) (to be continued)
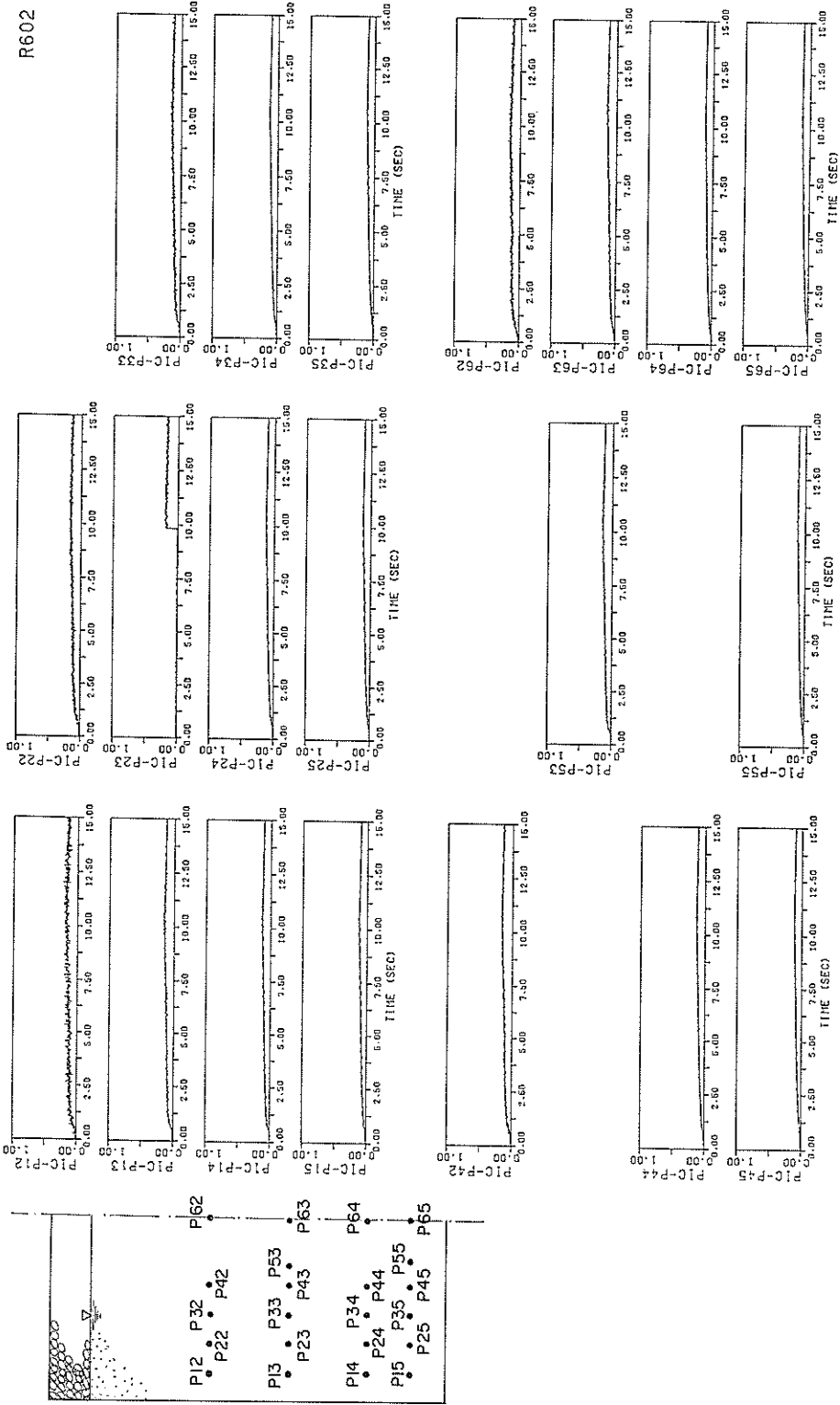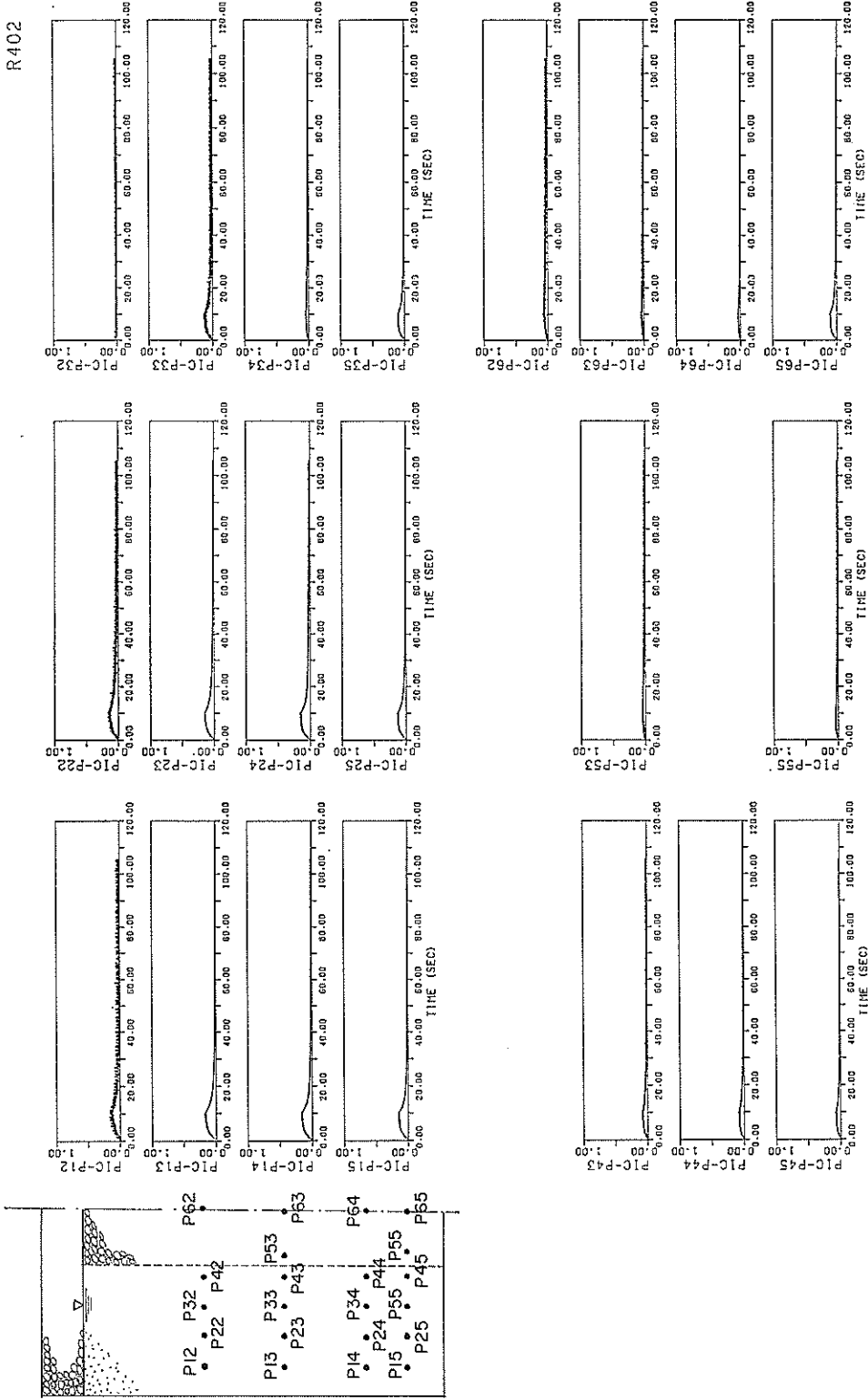
(a) short term

Fig. 17 Time histories of measured excess pore water pressures at Case R-502 (without a gravel drain ; under sinusoidal input motion ; maximum input acceleration 30 Gals)

(b) long term

R302

Fig. 18 Time histories of measured excess pore water pressures at Case R-302 (without a gravel drain; under sinusoidal input motion; maximum input acceleration 50 Gals) (to be continued)
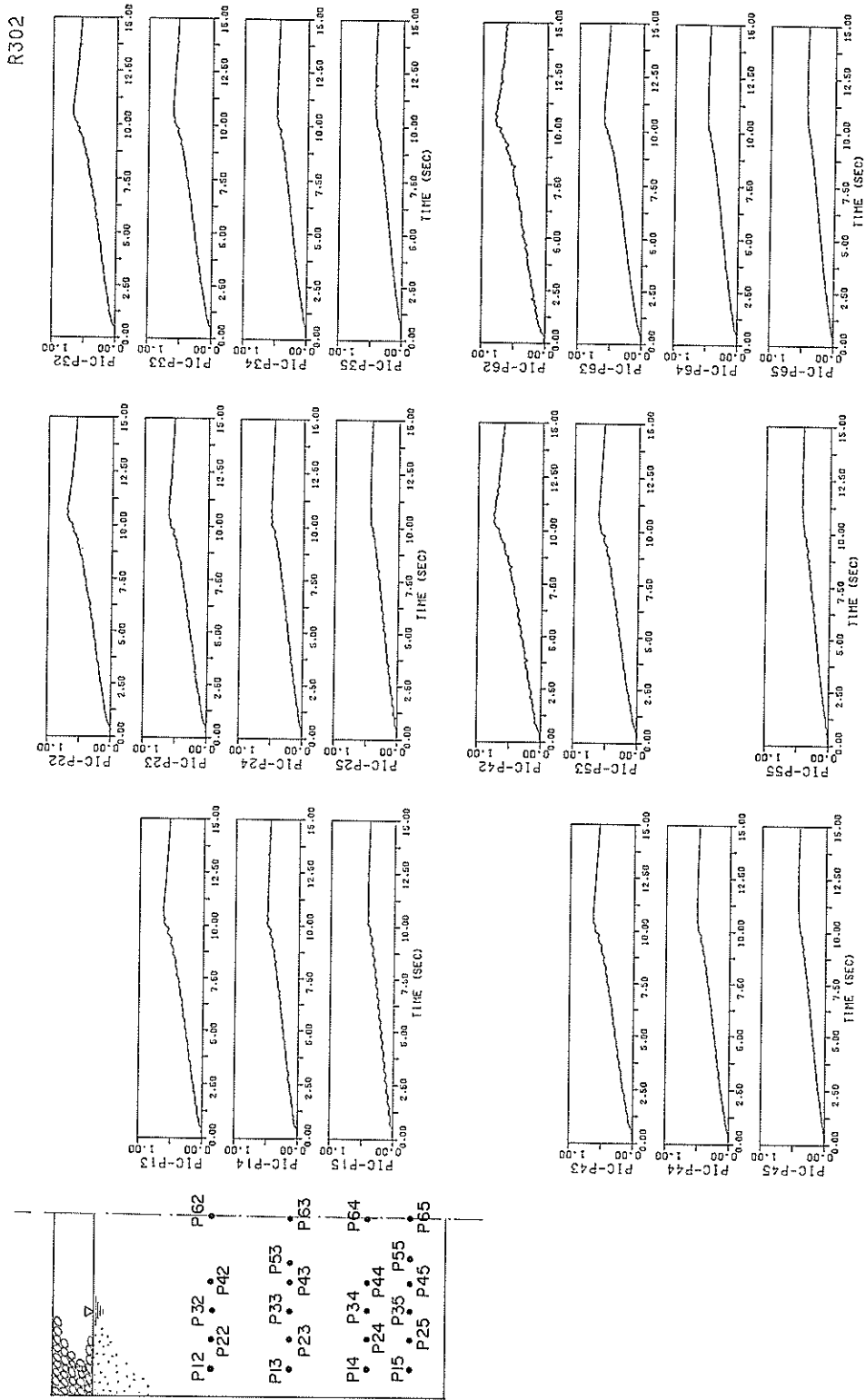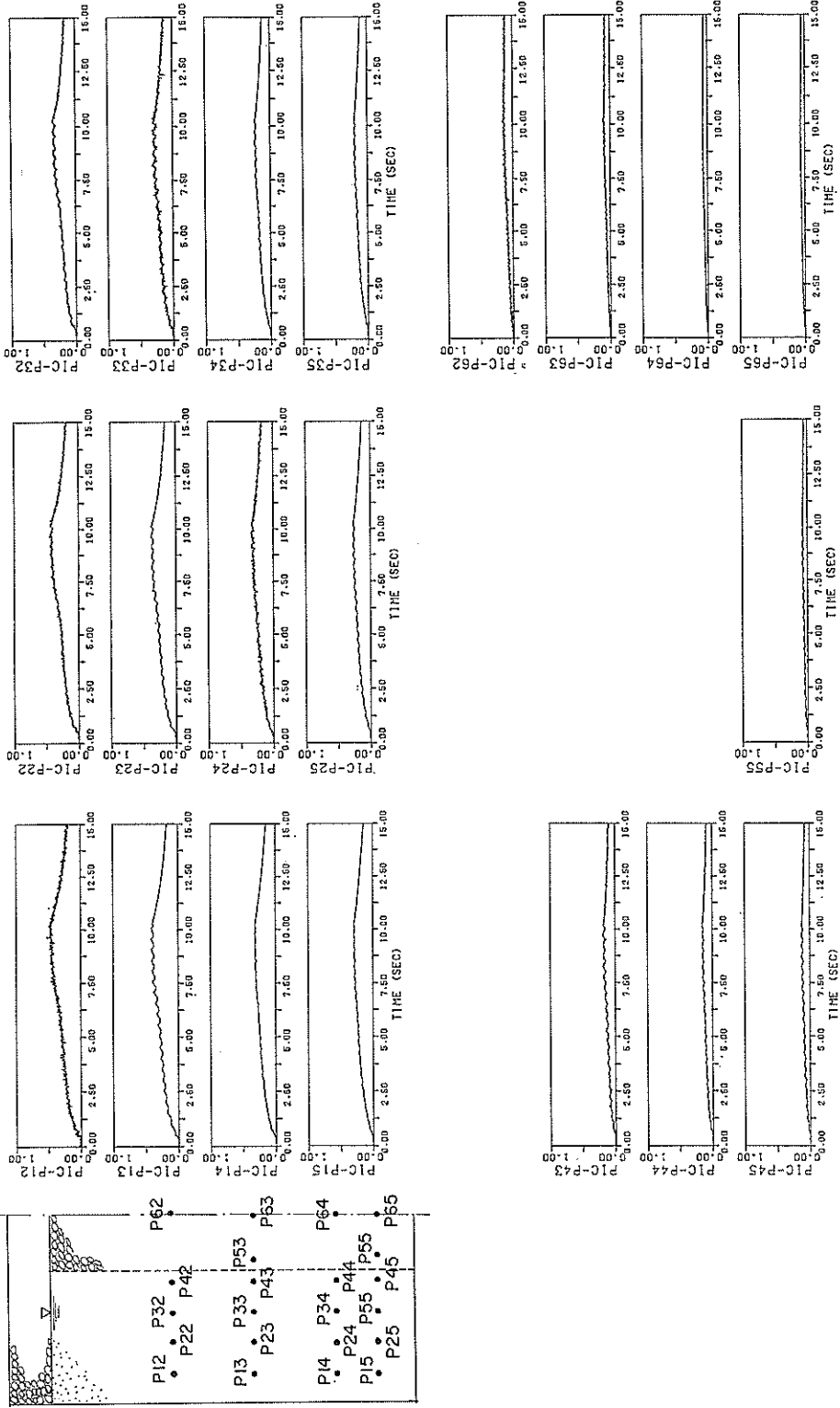
(a) short term

Fig. 18 Time histories of measured excess pore water pressures at Case R-302 (without a gravel drain; under sinusoidal input motion; maximum input acceleration 50 Gals)

(b) long term

R204
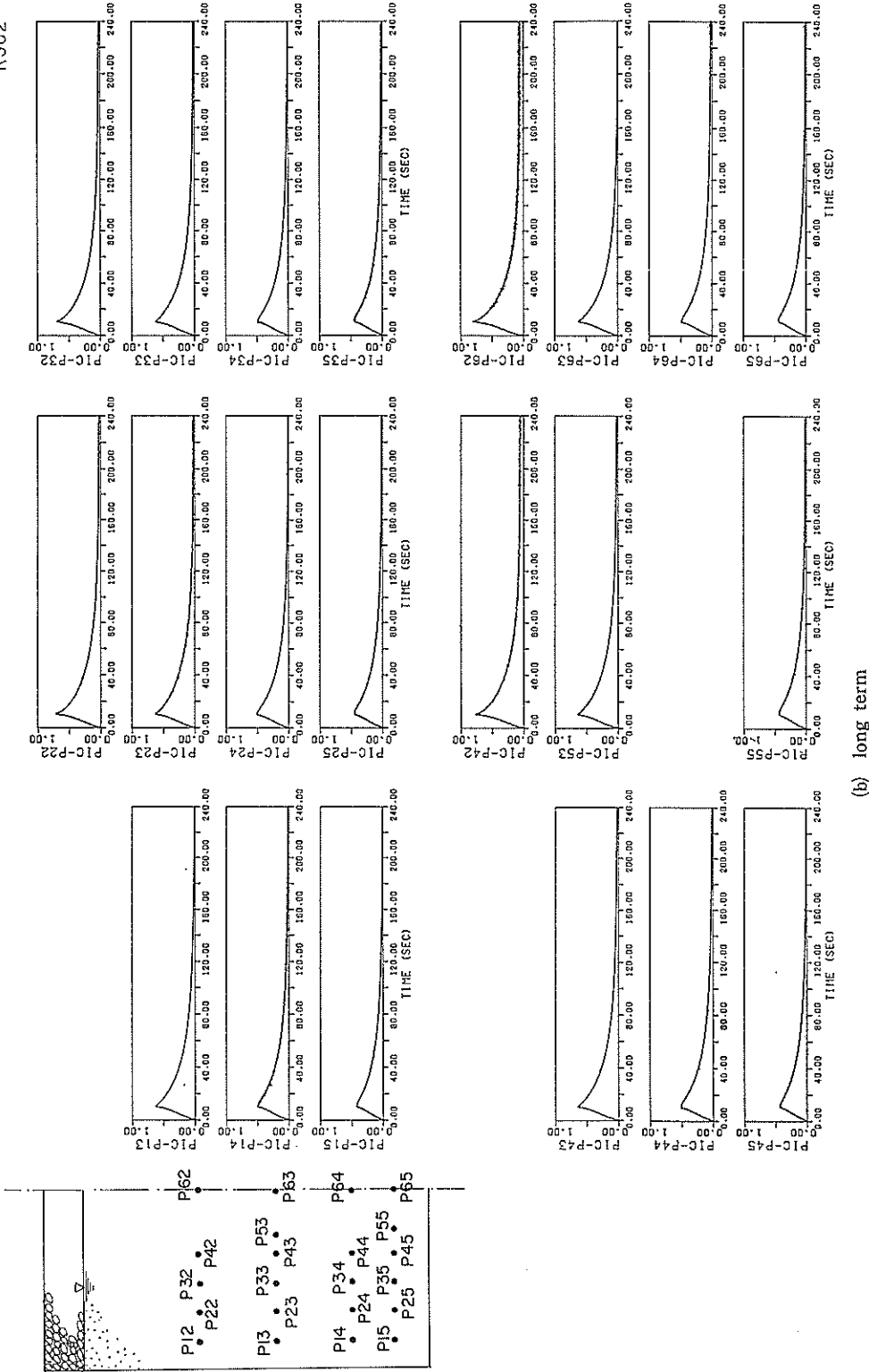
(a) short term

Fig. 19 Time histories of measured excess pore water pressures at Case R-204 (without a gravel drain ; under sinusoidal input motion ; maximum input acceleration 43 Gals) (to be continued)
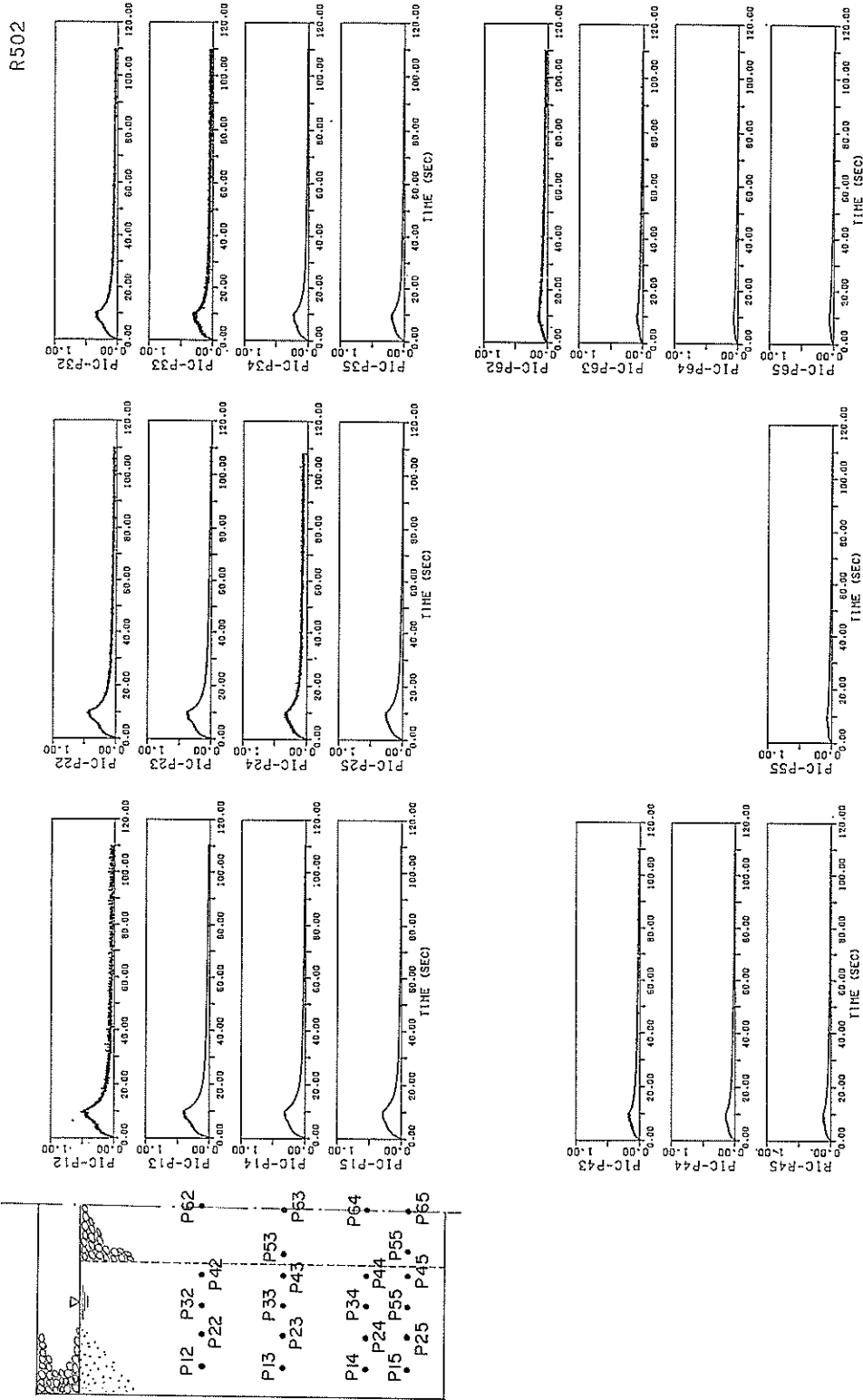
Fig. 19 Time histories of measured excess pore water pressures at Case R–204 (without a gravel drain; under sinusoidal input motion; maximum input acceleration 43 Gals)

(b) long term

Fig. 20 Time histories of measured excess pore water pressures at Case R-603 (without a gravel drain; under sinusoidal input motion; maximum input acceleration 84 Gals) (to be continued)
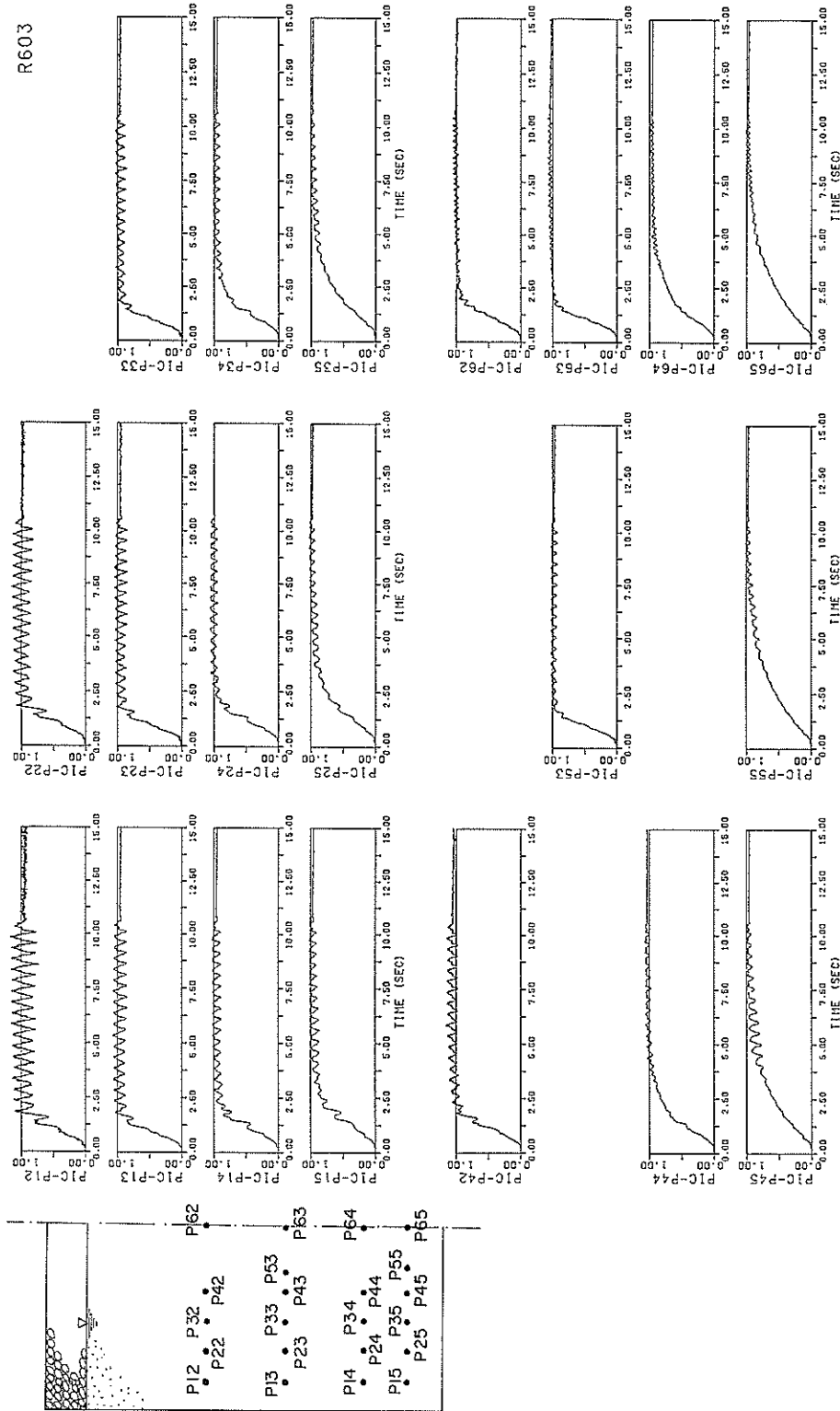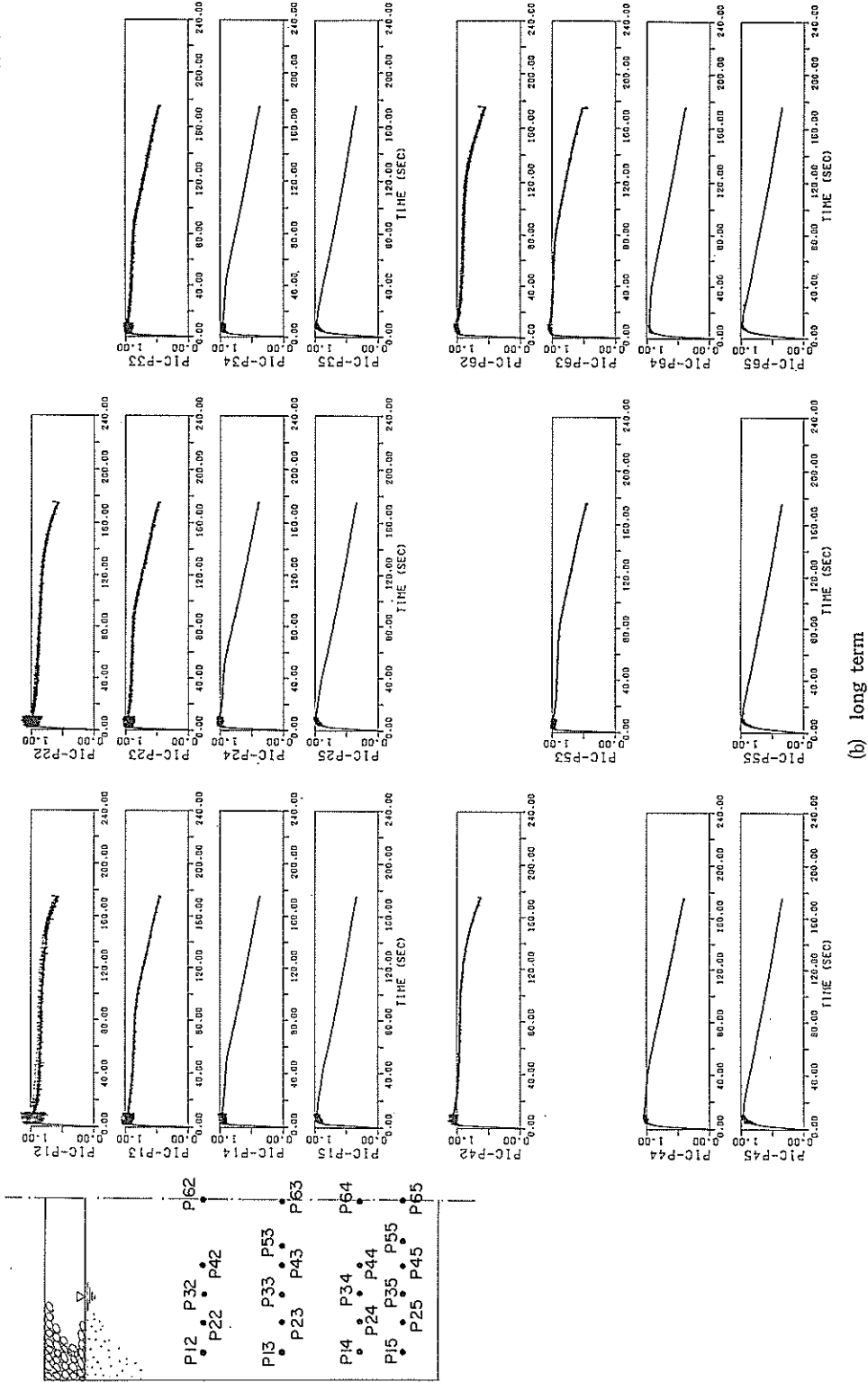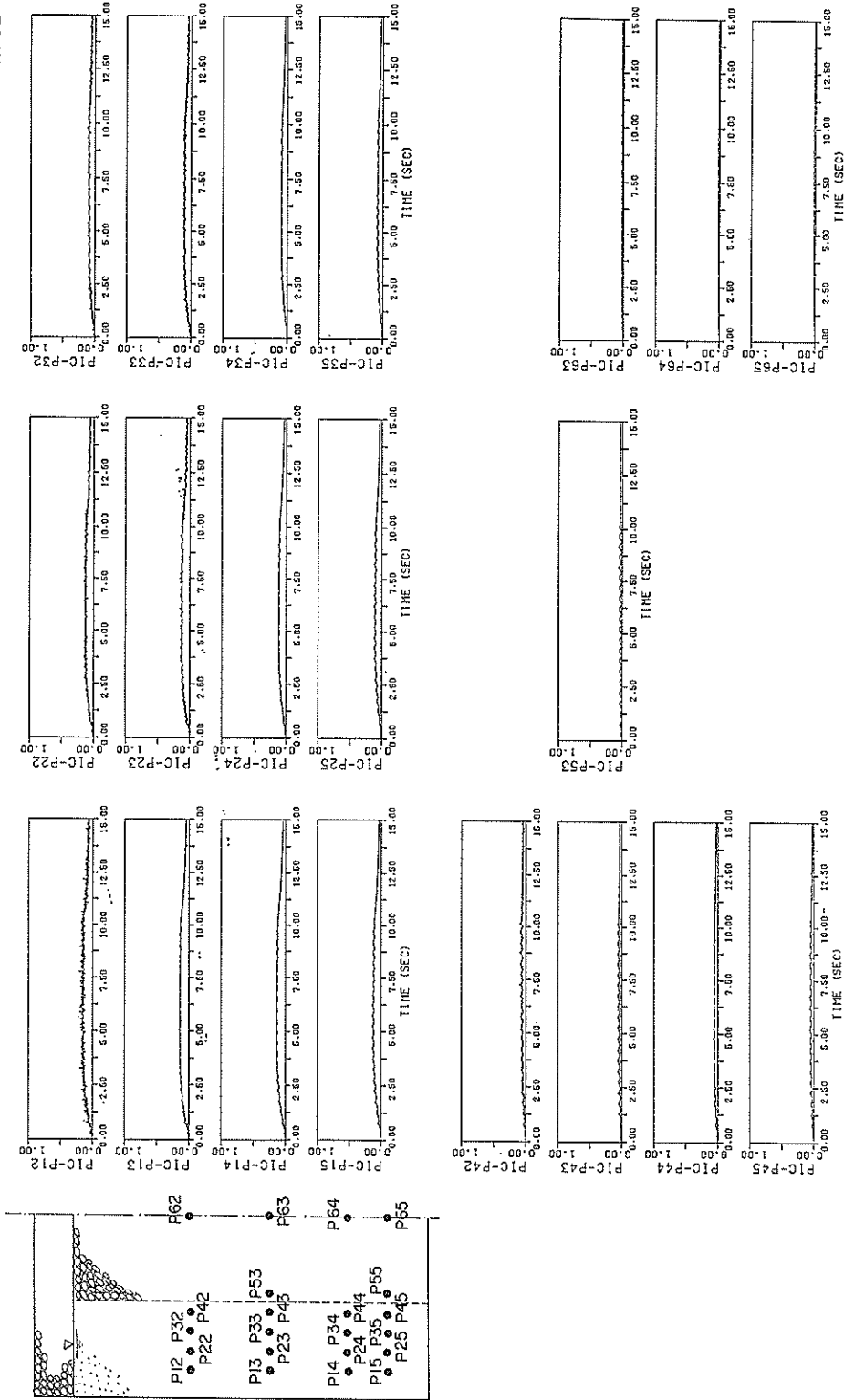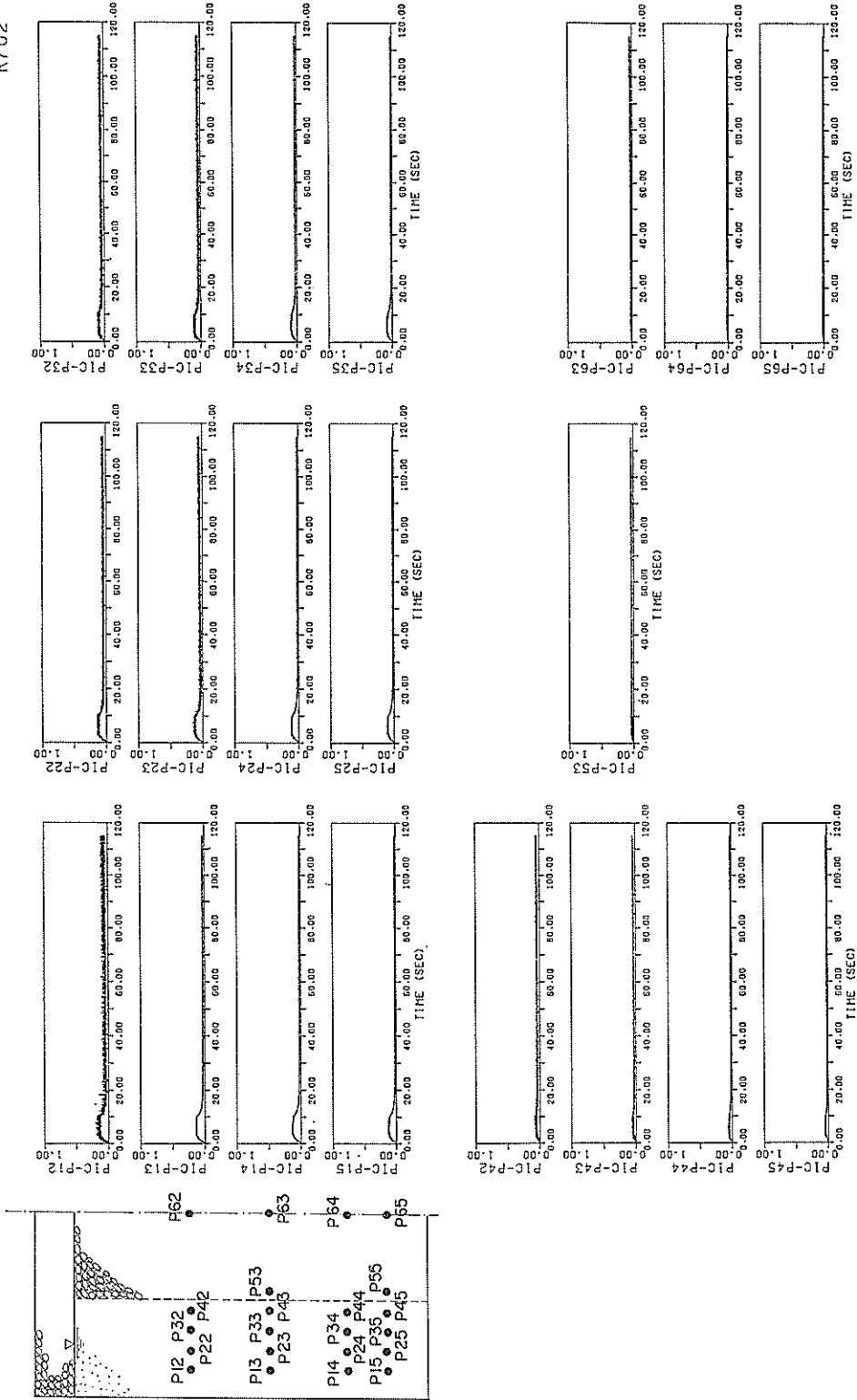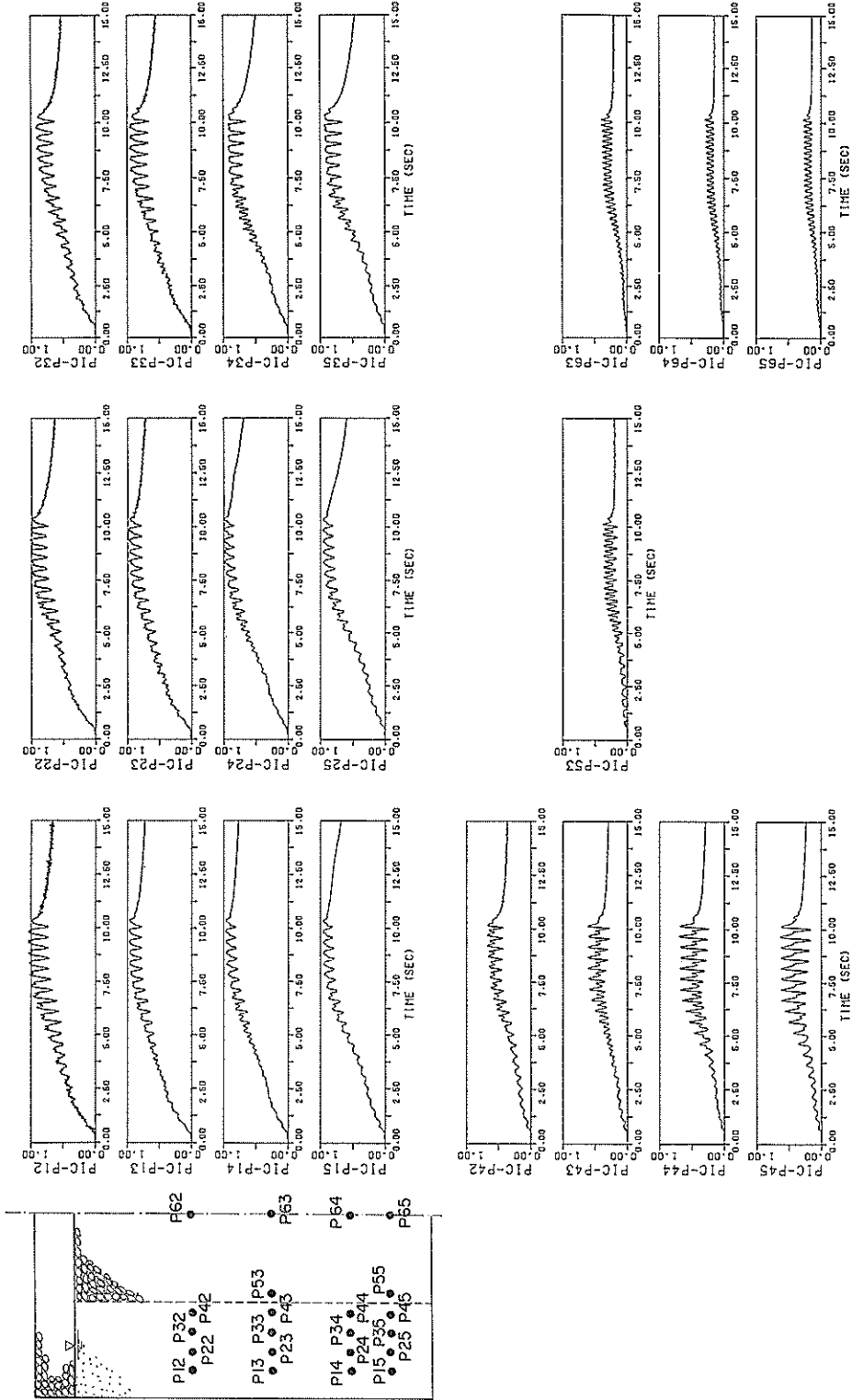
(a) short term

Fig. 20 Time histories of measured excess pore water pressures at Case R-603 (without a gravel drain; under sinusoidal input motion; maximum input acceleration 84 Gals)

(b) long term
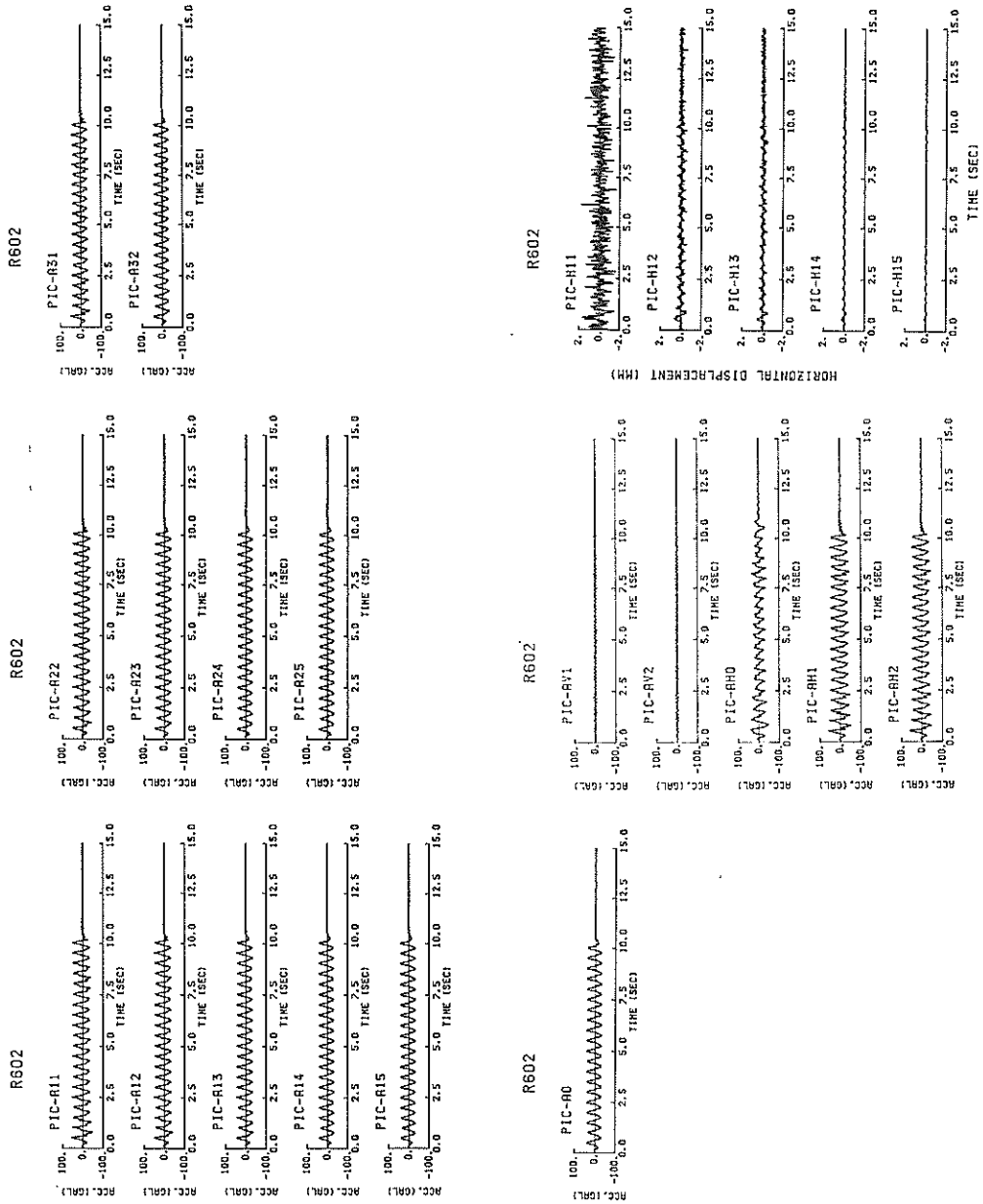
Fig. 21 Time histories of measured acceleration and displacement at Case R-602 (without a gravel drain; maximum input acceleration 30 Gals)
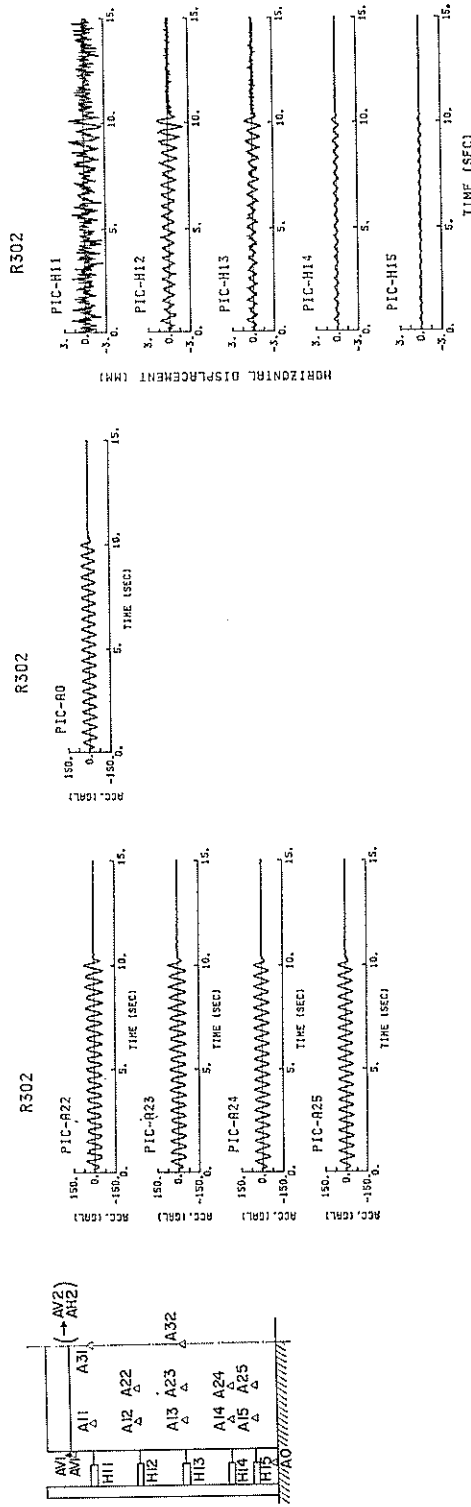
Fig. 22 Time histories of measured acceleration and displacement at Case R-302 (without a gravel drain ; maximum input acceleration 50 Gals)
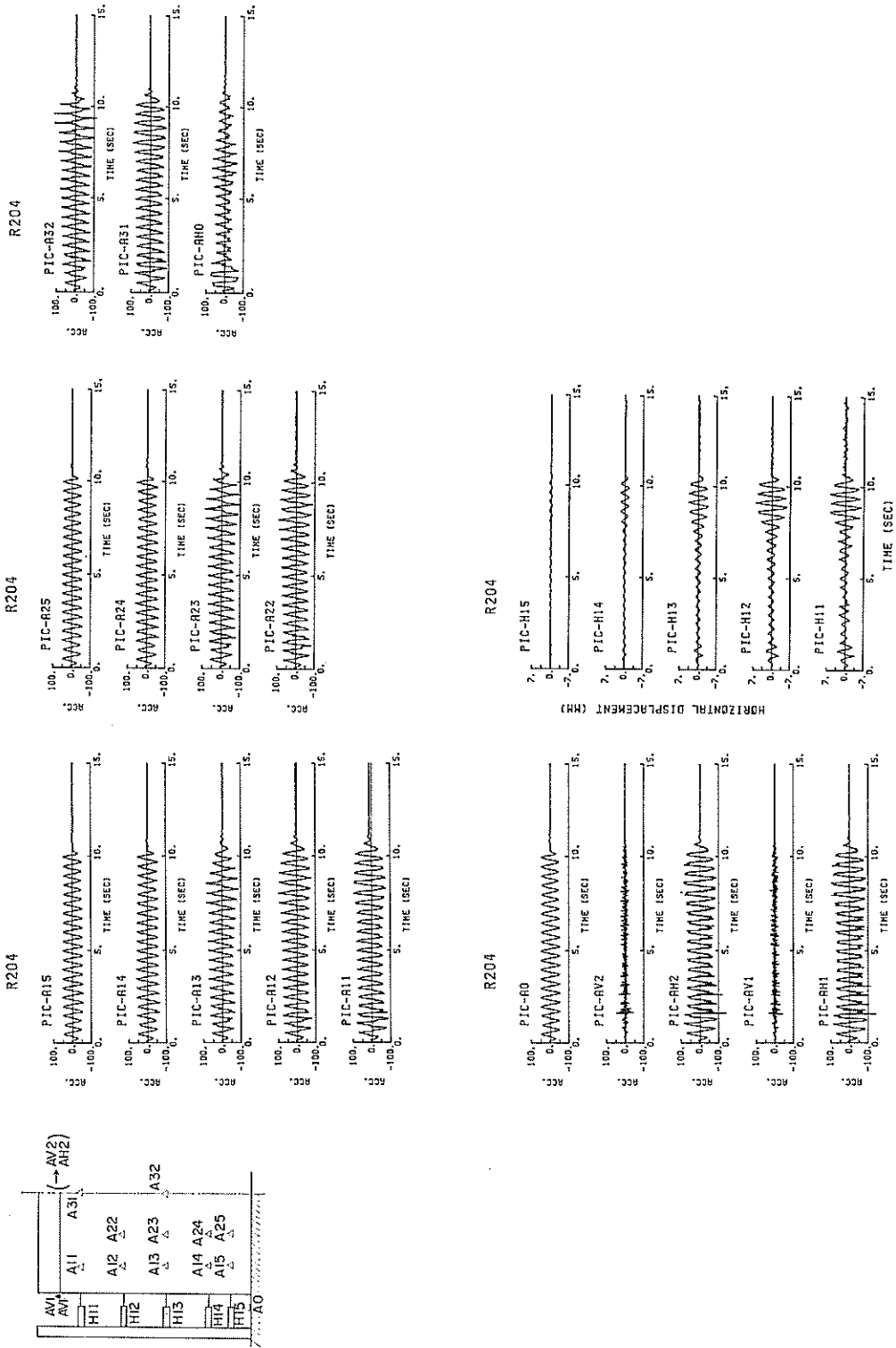
Fig. 23 Time histories of measured acceleration and displacement at Case R-204 (without a gravel drain; maximum input acceleration 43 Gals)
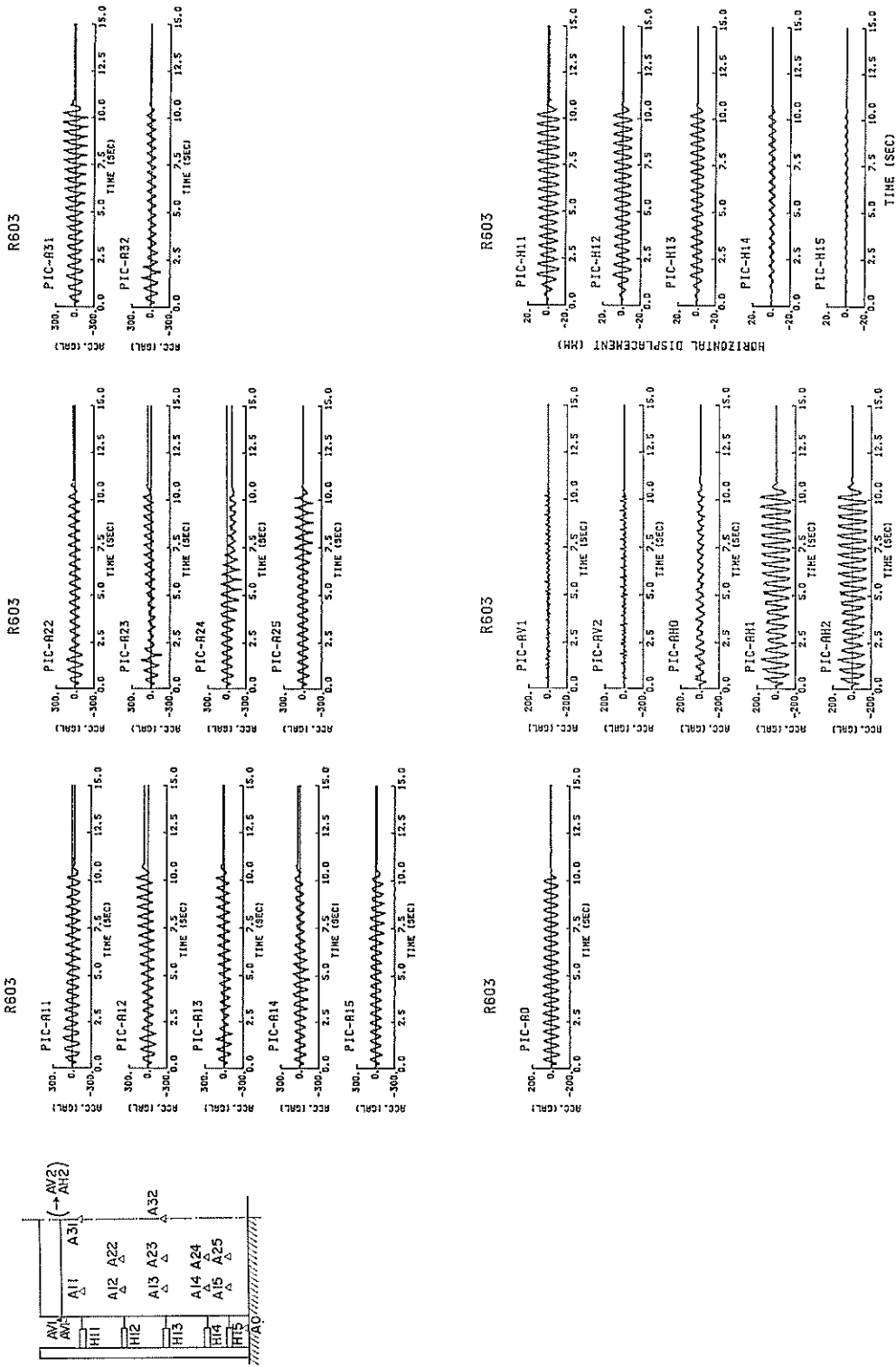
Fig. 24 Time histories of measured acceleration and displacement at Case R–603 (without a gravel drain ; maximum input acceleration 84 Gals)
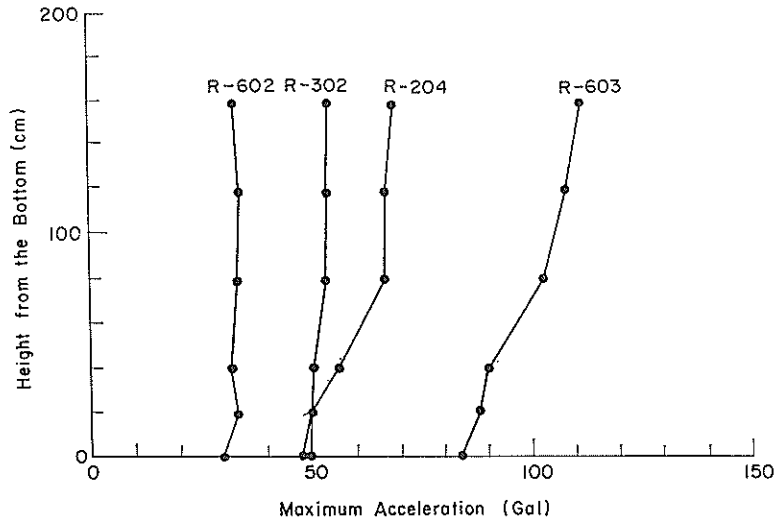
Fig. 25 Distribution of maximum accelerations at Cases R–602, R–302, R–204, R–603 (without a gravel drain; under sinusoidal input motion)

(a) R–302

(b) R–602

(c) R–603
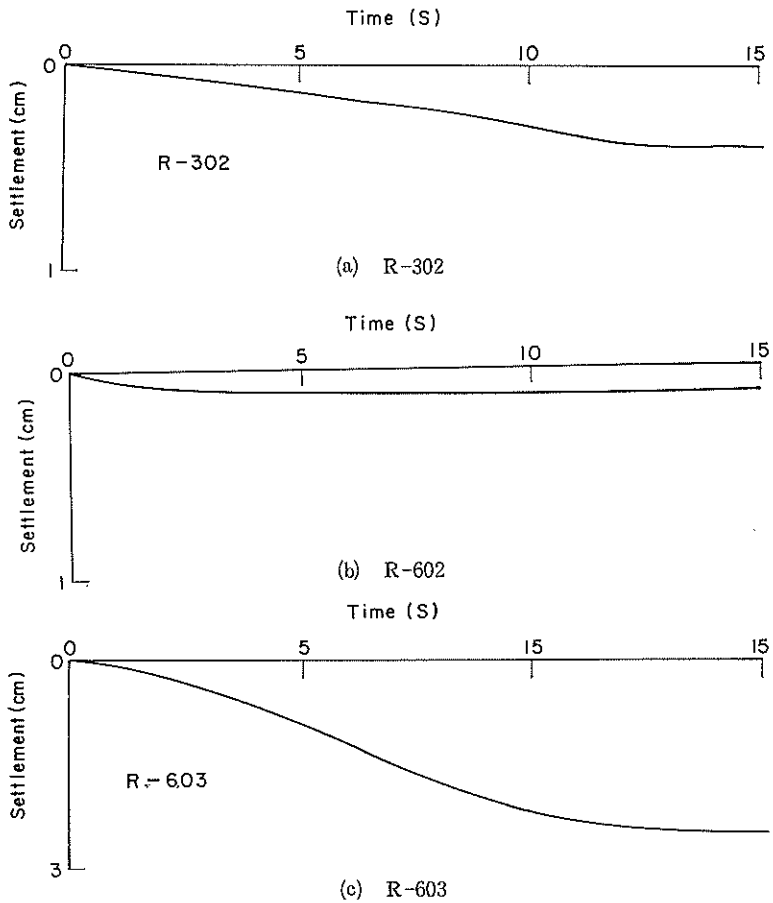
Fig. 26 Time histories of settlements at Cases R–302, R–602 and R–603 (without a gravel drain; under sinusoidal input motion)

Table 8 Settlements and drained water at the tests without a
gravel drain under sinusoidal input motion

Case	Settlement (cm)			Drained Water (kgf)
No.	S S*	S 1	S 2	L 2 + L 3
R-602	0.1	0.4	−0.2	2.4
R-302	—	0.4	0.2	11.1
R-204	—	1.3	1.3	43.5
R-603	4.1	4.8	4.7	106.0

* Average from SS 1~SS 6
Locations of the instruments are as shown in Fig. 3 ;
    S S (at 180cm level)
    S 1 (at 120cm level)
    S 2 (at 80cm level)

(a) After R-200 series   (b) After R-300 series
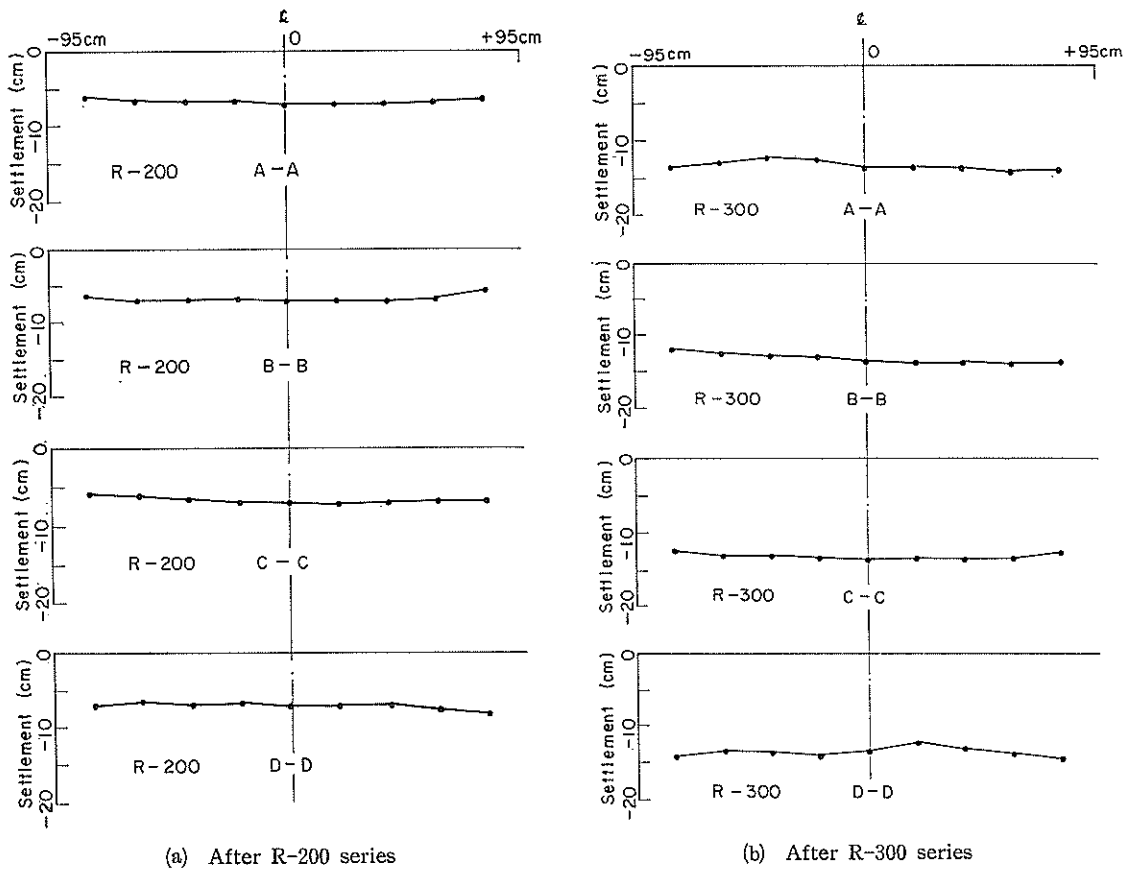
Fig. 27 Settlements at the end of the series R-200, R
-300 and R-600 (without a gravel drain ; under
sinusoidal input motions) (to be continued)

etc. denote the sections along the lines shown in **Fig. 14** (b). The settlements show no sign of arching effect due to the friction along the rubber membrane inside the container.

Presented above are the results of the tests for the model ground without gravel drain when shaken by the sinusoidal input motions. Now that the performance of the sand deposit without gravel drain is known, the tests results with the gravel drains are ready to be presented.

(2)   Model tests with a gravel drain (R-400, R-500, and R-700 series)
a)   Excess pore water pressures

When the model grounds with the gravel drain were shaken, the excess pore water pressures were measured as shown in **Figs. 28** through **31**. The relative densities of the sand deposit surrounding the gravel drain were about 33%. The locations of the instruments were basically the same as those shown in **Fig. 3** except for R-700 series. In R-700 series, radius of the gravel drain was 1.5 times as large as that in R-400 and R-500 series. Therefore, the locations of the instruments were slightly varied for R-700 series; if we denote P12-P15 as Line 1, P22-P25 as line 2, etc. as defined earlier, the intervals between these lines are 10 cm, the distance between the line 1 and the outer edge of the container 15 cm.

(c)   After R-600 series

Fig. 27   Settlements at the end of the series R-200, R-300 and R-600 (without a gravel drain ; under sinusoidal input motions)

Fig. 28 Time histories of measured excess pore water pressures at Case R-402 (with a gravel drain $a/b=0.3$; under sinusoidal input motion; maximum input acceleration 50 Gals) (to be continued)

(a) short term

Fig. 28 Time histories of measured excess pore water pressures at Case R–402 (with a gravel drain $a/b=0.3$; under sinusoidal input motion; maximum input acceleration 50 Gals)

(b) long term

R502

Fig. 29 Time histories of measured excess pore water pessures at Case R-502 (with a gravel drain $a/b=0.3$; under sinusiodal input motion; maximum input acceleration 50 Gals) (to be continued)

(a) short term

R502

(b) long term

Fig. 29 Time histories of measured excess pore water pessures at Case R-502 (with a gravel drain $a/b = 0.3$; under sinusoidal input motion; maxmium input acceleration 50 Gals)

(a) short term

Fig. 30 Time histories of measured excess pore water pressures at Case R-702 (with a gravel drain $a/b=0.45$; under sinusoidal input motion; maximum input acceleration 51 Gals) (to be continued)

R702

(b) long term

Fig. 30 Time histories of measured excess pore water pressures at Case R-702 (with a gravel drain $a/b=0.45$; under sinusoidal input motion; maximum input acceleration 51 Gals)

Fig. 31 Time histories of measured excess pore water pressures at Case R-703 (with a gravel drain $a/b=0.45$; under sinusoidal input motion; maximum input acceleration 82 Gals) (to be continued)

(a) short term
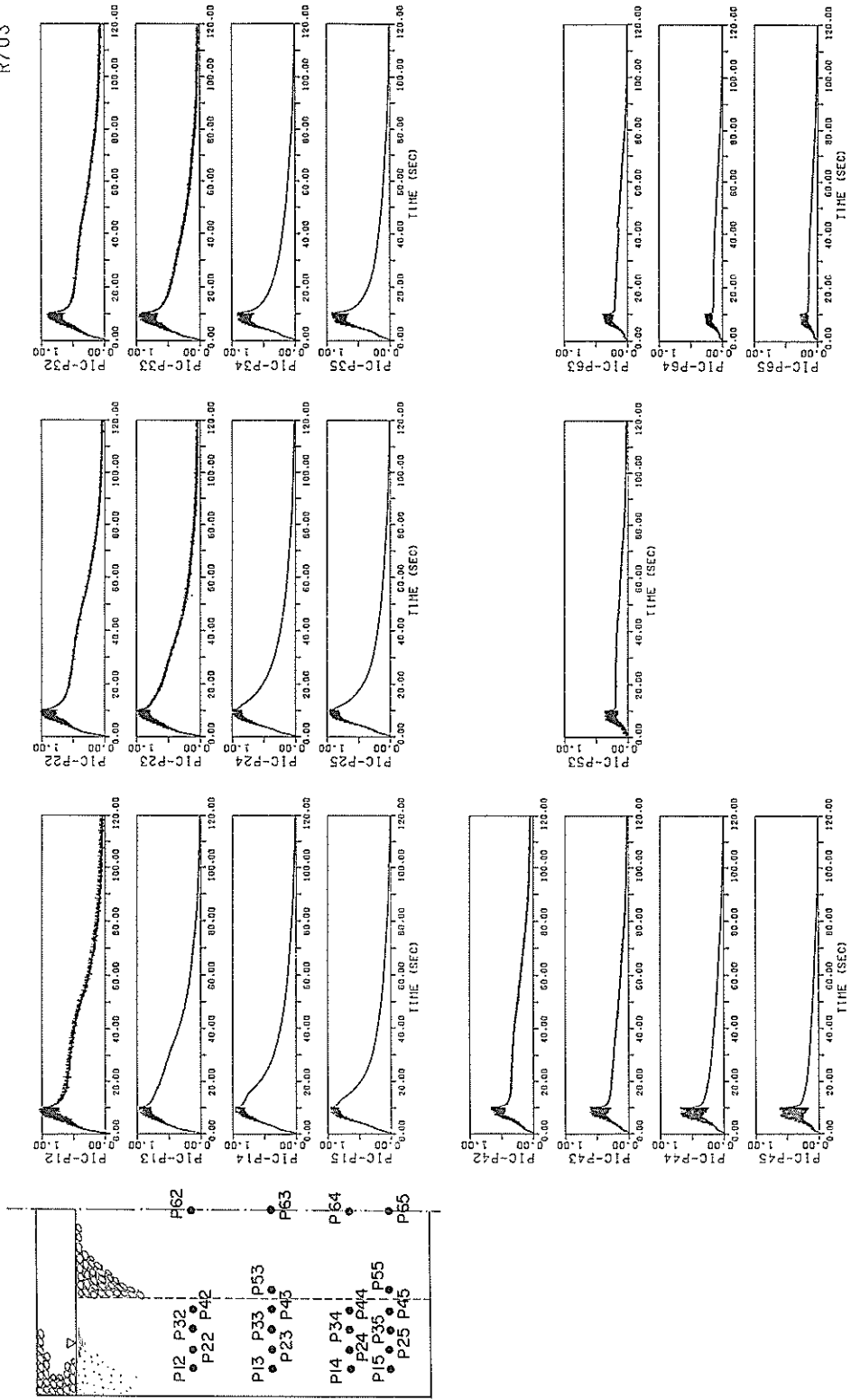
(b) long term

Fig. 31 Time histories of measured excess pore water pressures at Case R-703 (with a gravel drain $a/b=0.45$; under sinusoidal input motion; maximum input acceleration 82 Gals)
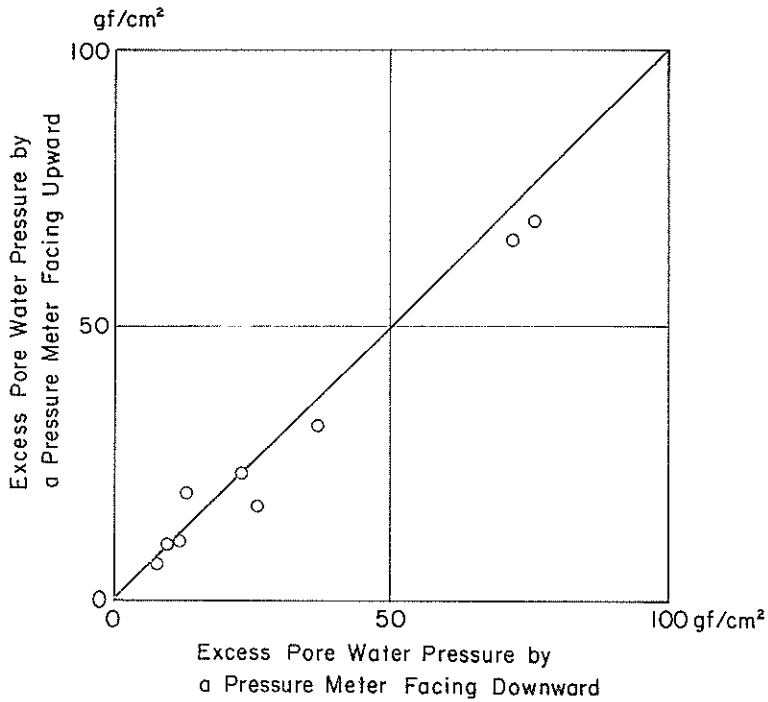
Fig. 32 Comparison of the excess pore water pressures in the gravel drain
measured by pressure meters facing downward and upward

At the R-400 series, pore water pressure meters including the ones located within the gravel drain such as P62, P63, etc. faced downward. It was later considered that the direction of the pore water pressure meters might have affected the measured values within the gravel drain because the rate of flow within the gravel drain was considered high. Therefore, pairs of the pore water pressure meters, one facing downward and the other facing upward, were put at the same location to measure the influence of the direction of the pore water pressure meters for R-500 series. P62 and P62', P63 and P63' in **Fig. 3** are the pairs of the instruments used for this purpose. The result indicates, as shown in **Fig. 32**, the influence of the rate of the flow through the gravel drain is negligibly small.

Distributions of the excess pore water pressures are shown in **Fig. 33**. Hydraulic gradient towards the gravel drains are clearly recognized in this figure.

Comparison between the tests with and without the gravel drain will be given later.

b) Accelerations and displacements

Accelerations and displacements for the tests with the gravel drain are shown in **Figs. 34** through **37**. Distributions of the maximum values are shown in **Fig. 38**.

c) Drained waters and settlements

When the composite ground, made of sand deposit and the gravel drain, is shaken, pore water is drained from the gravel drain. Some of the pore water is drained directly from the surface of the sand deposit. Both of the drained waters were, as mentioned earlier, collected by using the casing in the gravel layer at the top of the composite ground. The collected waters were guided out through the
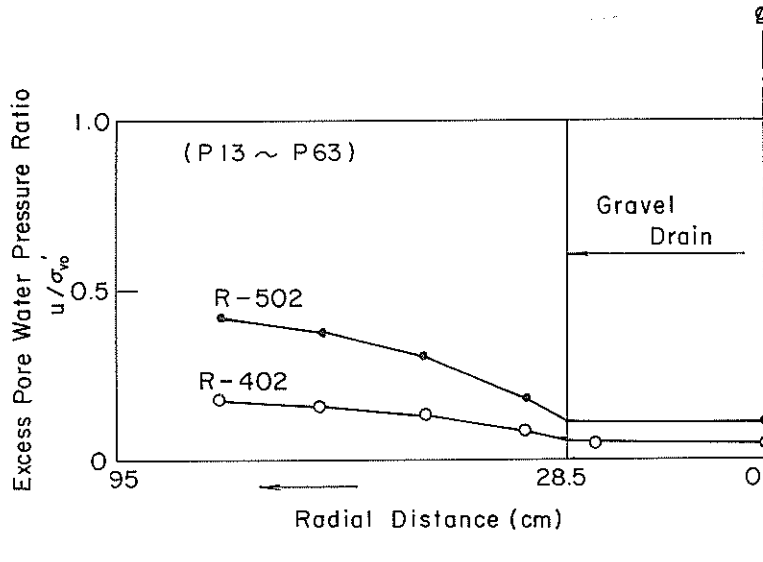
(a) Case R–402 and R–502 (with a gravel drain $a/b=0.3$)
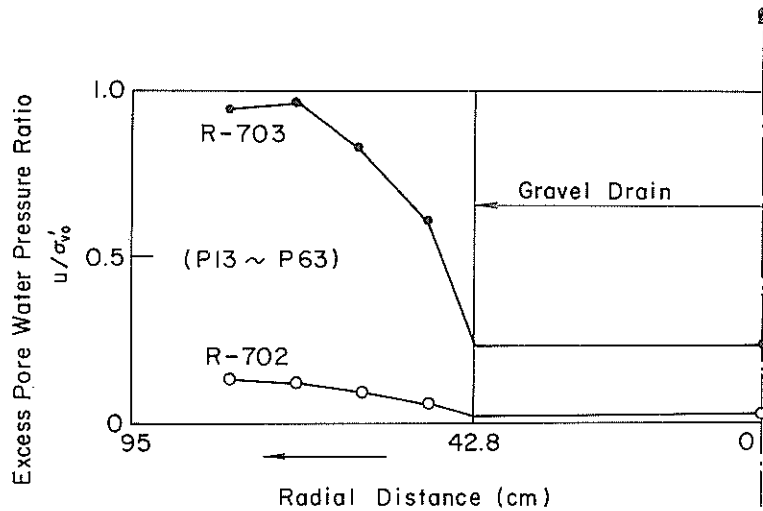
(b) Case R–702 and R–703 (with a gravel drain $a/b=0.45$)

Fig. 33 Distribution of maximum excess pore water pressure ratio

flexible pipes for measuring the amount of drained waters. The drained waters and settlements after the shaking resulted in as shown in **Table 9**. The pattern of the settlements measured at the surface of the composite ground after the series of the tests are shown in **Fig. 39**. Implications from these results will be given below.

(3)   Implications of the test results under sinusoidal excitations

The results of the tests under sinusoidal excitations have been presented so far as they are. The quantities of the aquired data might be too large to get a fast grasp of the results of the tests. In the later chapter, all of these data will be used
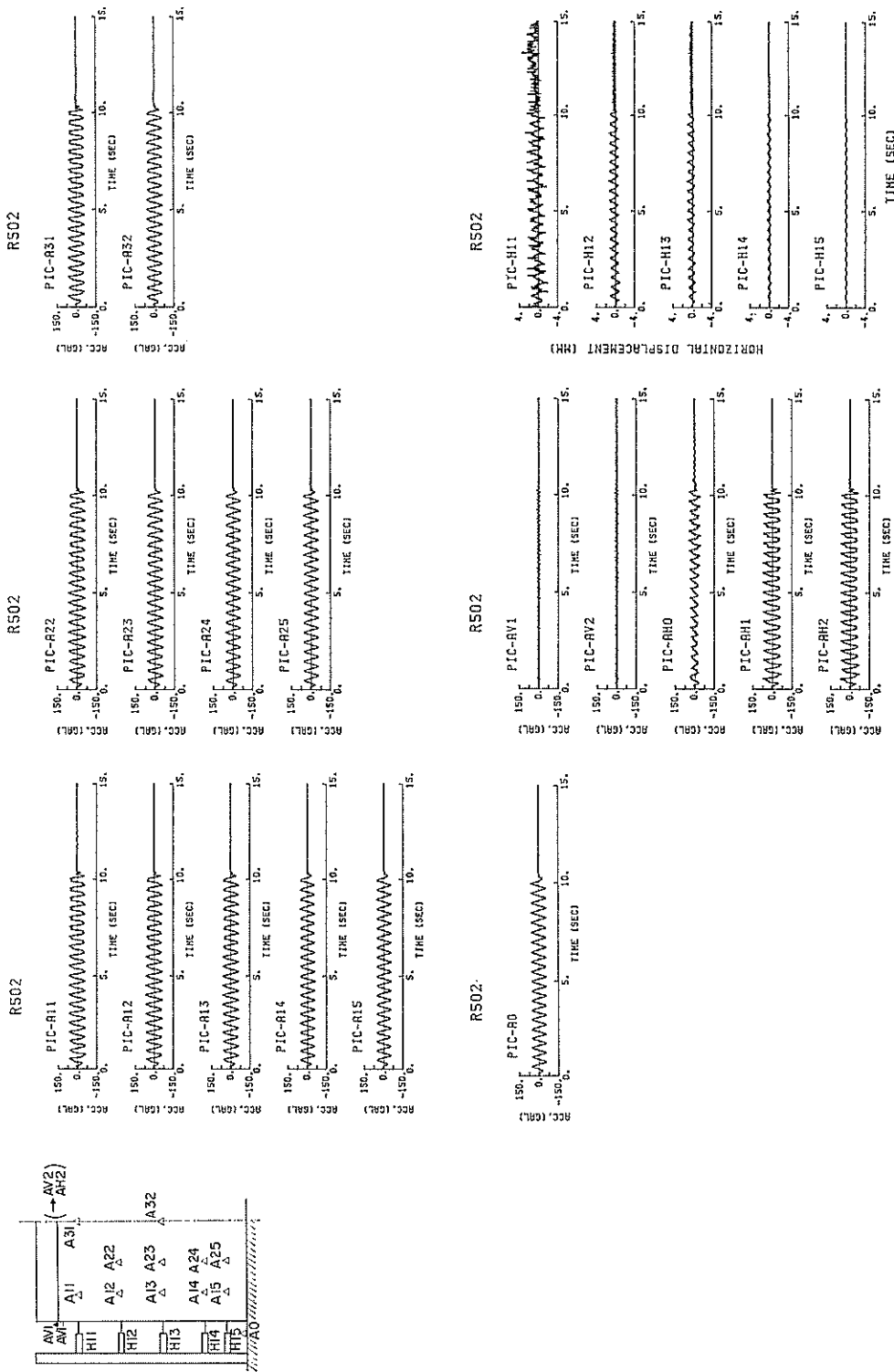
Fig. 34 Time histories of measured acceleration and displacement at Case R-402 (with a gravel drain $a/b=0.3$; maximum input acceleration 50 Gals)
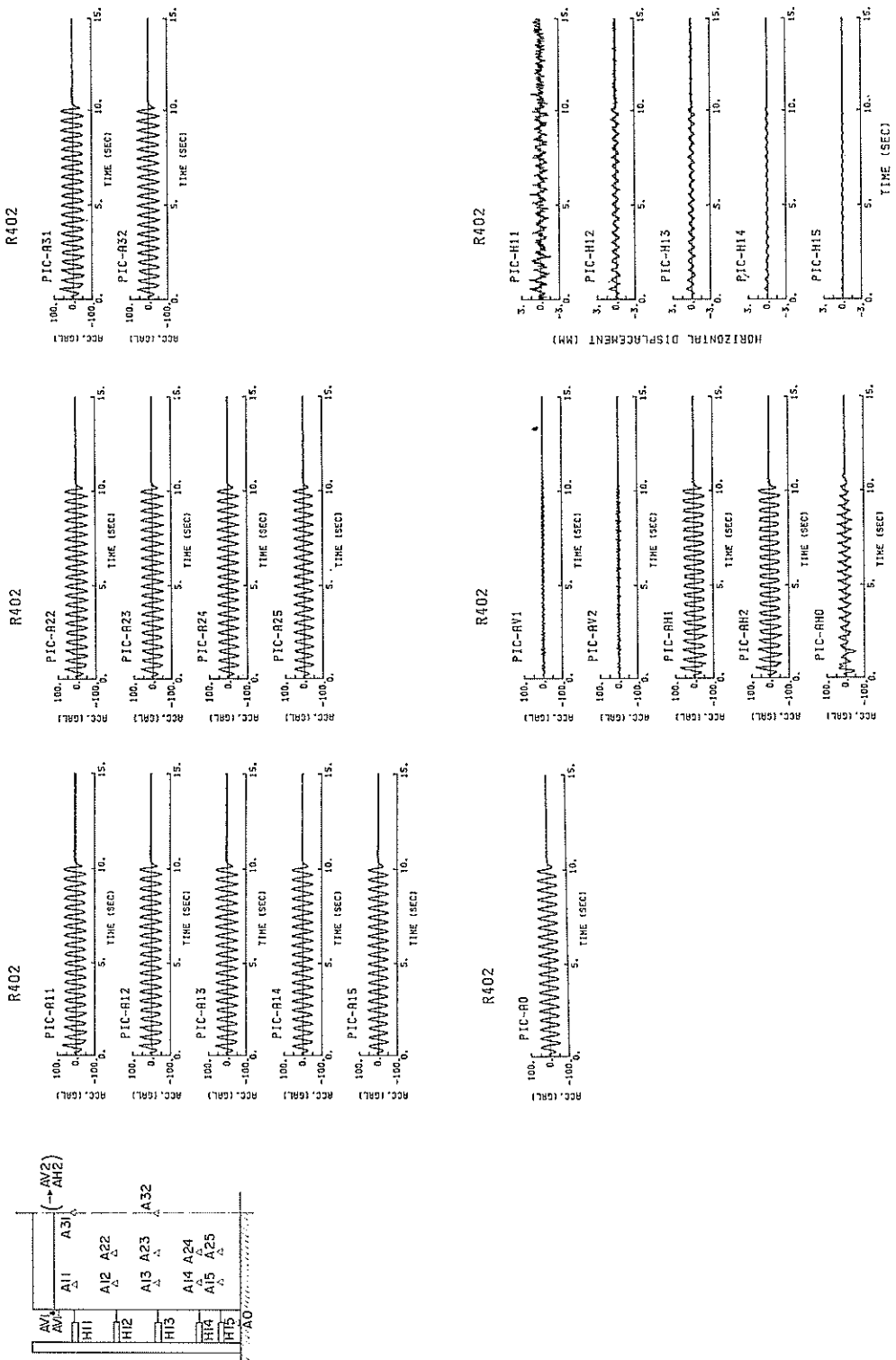
Fig. 35 Time histories of measured acceleration and displacement at Case R-502 (with a gravel drain $a/b=0.3$; maximum input acceleration 50 Gals)
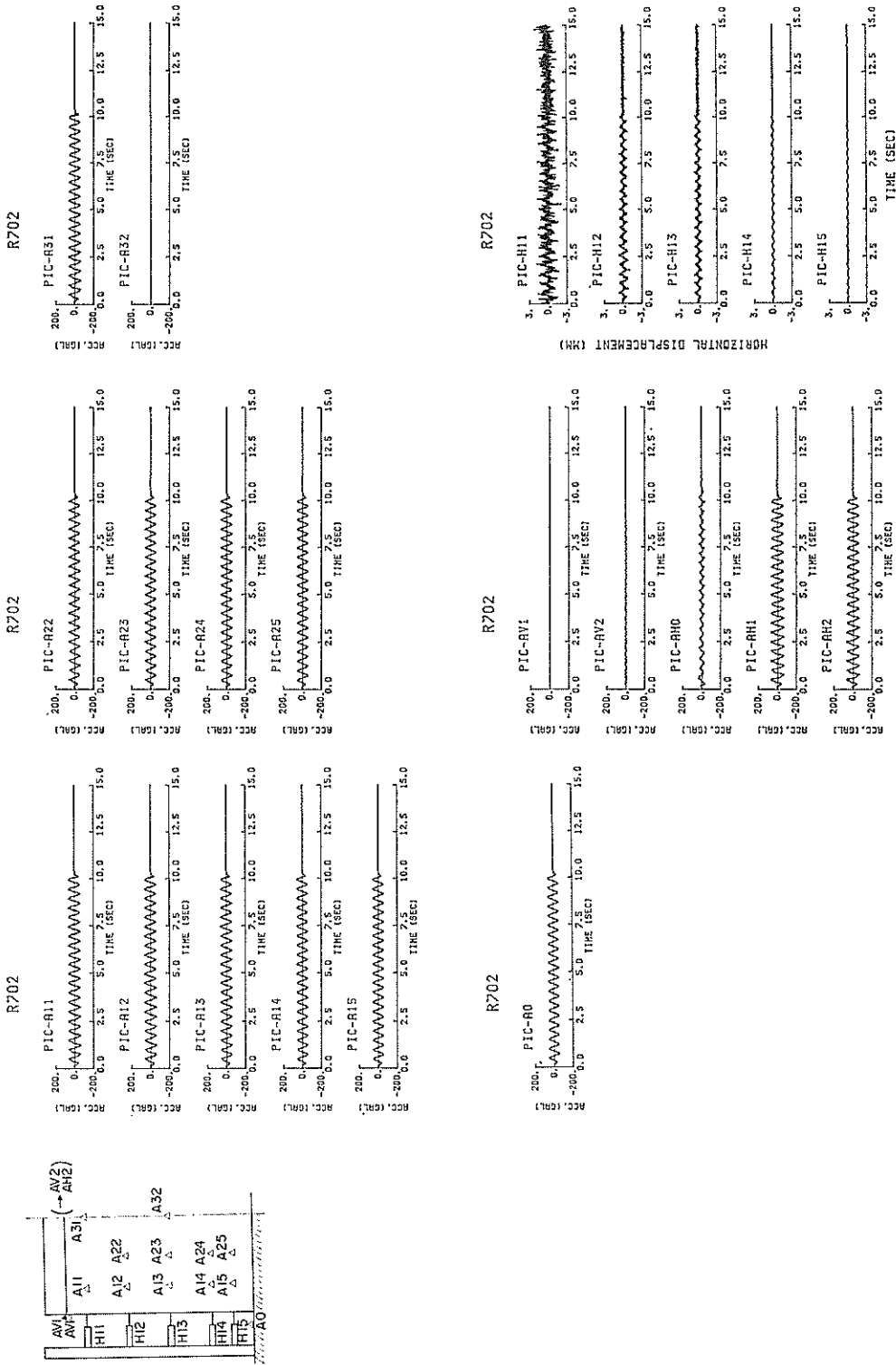
Fig. 36 Time histories of measured acceleration and displacement at Case R-702 (with a gravel drain $a/b=0.45$; maximum input acceleration 51 Gals)
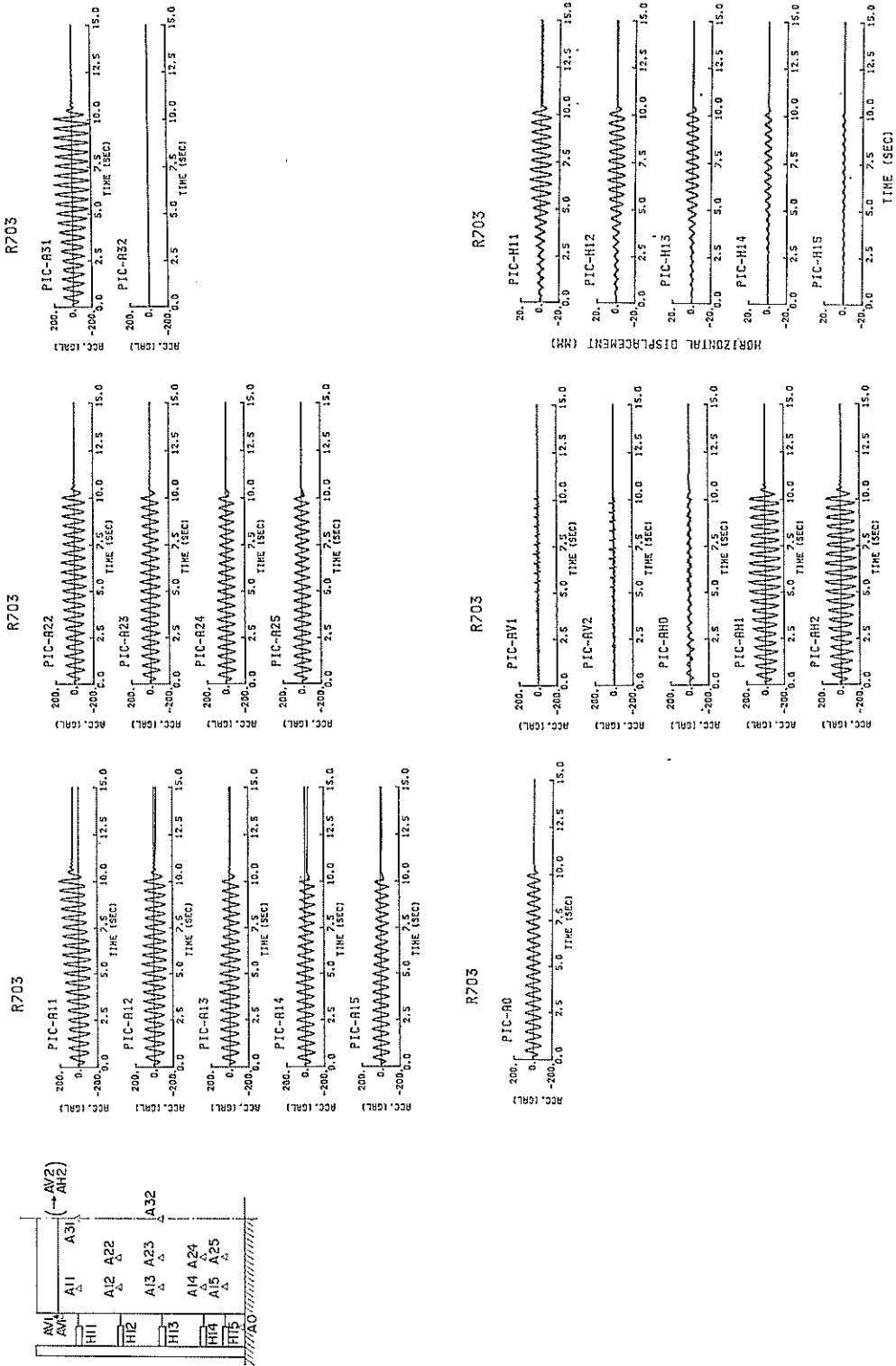
Fig. 37 Time histories of measured acceleration and displacement at Case R-703 (with a gravel drain $a/b=0.45$; maximum input acceleration 82 Gals)
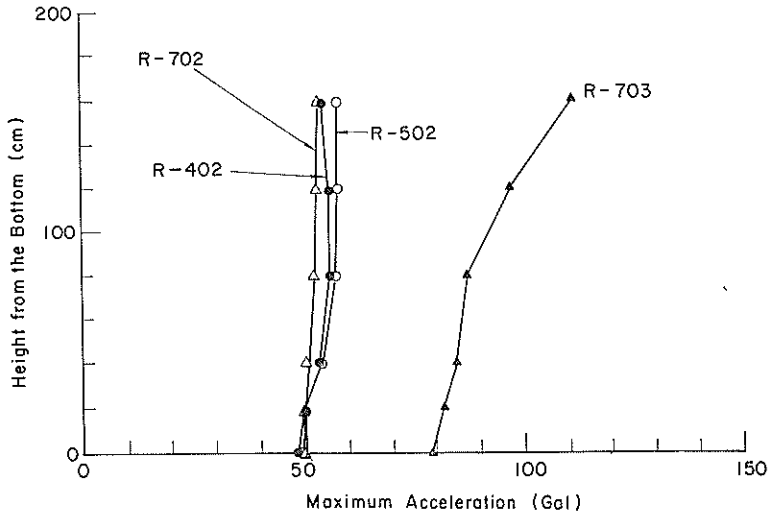
Fig. 38 Distribution of maximum acclerations at Cases R-402, R-502, R-702, and R-703 (with a gravel drain; under sinusoidal input motions)

Table 9 Settlements and drained water at the tests with a gravel drain under sinusoidal input motion

Case No.	a/b	Settlement (cm)			Drained Water (kgf)	
		S S*	S 1	S 2	L 2 (Drain)	L 3 (Sand)
R-402	0.3	0.2	0	0.1	5.3	0.1
R-502	0.3	0.5	0.6	0.2	9.2	0.3
R-702	0.45	0.2	0.2	0	0	0
R-703	0.45	3.1	1.5	1.0	69.5	14.1

* Average from SS 1~SS 6
  Locations of the instruments are as shown in Fig. 3;
     S S (at 180cm level)
     S 1 (at 120cm level)
     S 2 (at 80cm level)
     L 2 : Water drained from gravel drain
     L 3 : Water drained from the surface of sand deposit

for the analyses and, therefore, a clear and quantitative grasp of these results will eventually be given there. However, at this point, it might be worthy to obtain a clear perspective on the test results presented so far.

a) Rate of dissipation of excess pore water pressures at the sand deposit

   The excess pore water pressures at the sand deposit, as shown in **Figs. 17** (b) and 18 (b), dissipate logarithmically when the maximum excess pore water pressures attained during the shaking are less than about half of the initial vertical effective stress. Once the maximum excess pore water pressures reach the initial vertical effective stress, the rate of dissipation, as shown in **Figs. 19** (b) and **20** (b), becomes drastically low and becomes dependent on the stress or strain histories applied to the sand deposit.

b) Effect of the gravel drain on the excess pore water pressures

   When the maximum acceleration of the input motion is about 50 Gals, the gravel
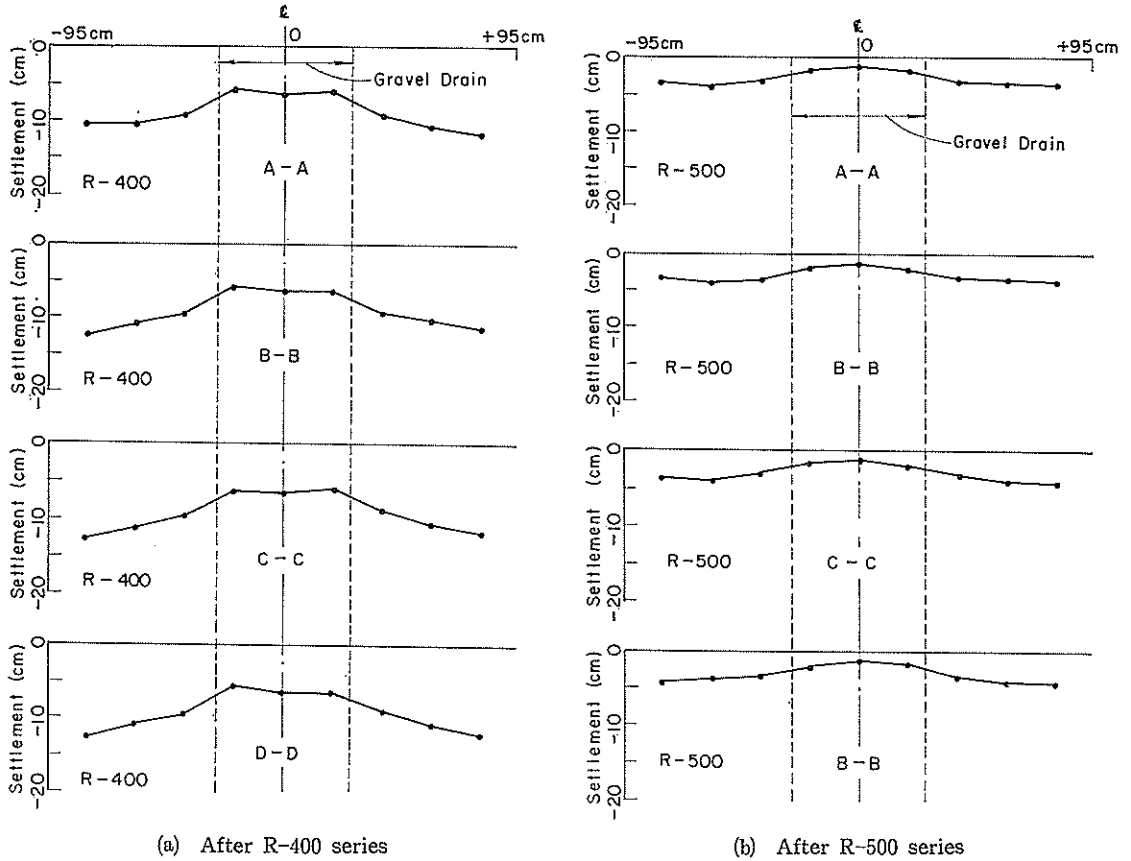
(a) After R-400 series (b) After R-500 series

Fig. 39 Settlements at the end of the series R-400, R-500, and R-700 (with a gravel drain; under sinusoidal input motions)

drain, with the spacing ratio $a/b=0.3$, is effective for reducing the maximum excess pore water pressures in the sand deposit as shown in **Fig. 40**. However, when the maximum acceleration of the input motion is leveled up to about 80 Gals, the gravel drain, even with the spacing ratio $a/b=0.45$ as shown in **Fig. 41**, failed to reduce the maximum excess pore water pressures at the outer region of the sand deposit; instantaneously liquefied at this region.

Further details on the performance of gravel drain can be understood by the time histories of the excess pore water pressures. As shown in **Fig. 42**, which are extracted from **Figs. 20** and **31**, the effect of the gravel drain is (i) to reduce the rate of increase in pore water pressures as shown in **Fig. 42 (a)** and (b), (ii) to increase the rate of dissipation in pore water pressures as shown in **Fig. 42 (c)** and (d). If the part of the sand deposit is close enough to the gravel drain, as shown in the lowest two time histories in **Fig. 42(b)**, the rate of generation in pore water pressures is balanced with the rate of dissipation at about 7.5 seconds and from there on the excess pore water pressures are kept at steady state value till the end of the shaking. On the other hand, if the part of the sand deposit is far away from the gravel drain, as shown in the uppermost three time histories in **Fig. 42(b)**, even though the gravel drain lowered the increasing rate in the excess pore water pressures, the gravel drain failed to reduce the maximum value of the excess pore water pressures in this particular case.
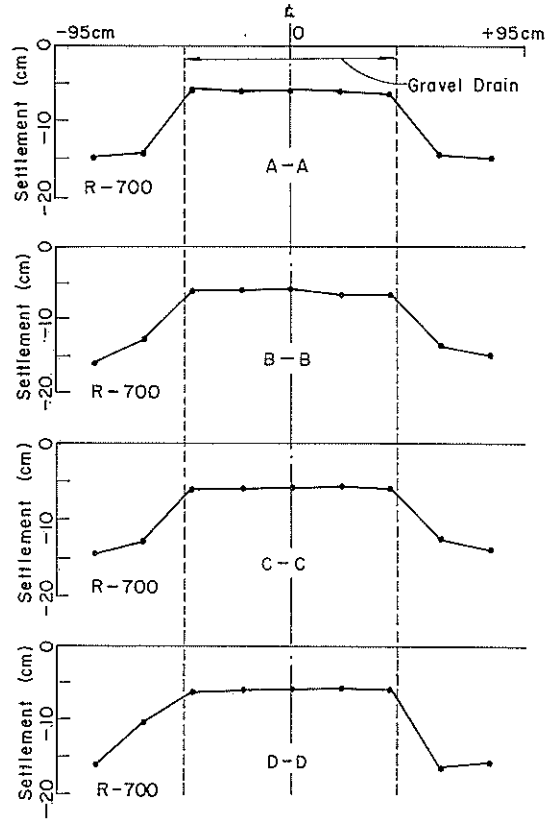
(c) After R-700 series

Fig. 39 Settlements at the end of the series R-400, R-500, and R-700 (with a gravel drain; under sinusoidal input motions)
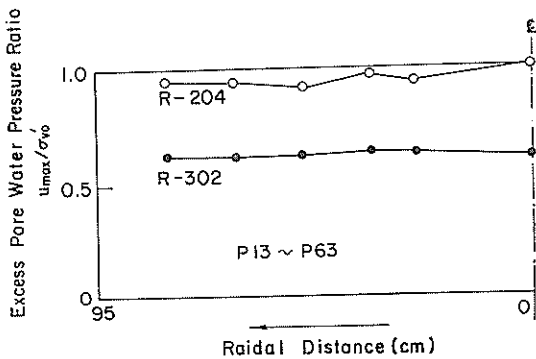
(a) without the gravel drain
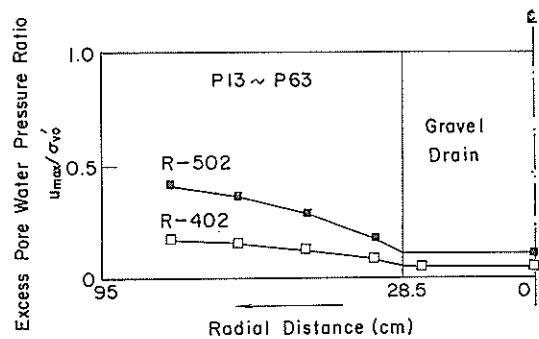
(b) with the gravel drain ($a/b=0.3$)

Fig. 40 Maximum excess pore water pressures at the tests with and without the gravel drain (under sinusoidal motion of about 50 Gals)
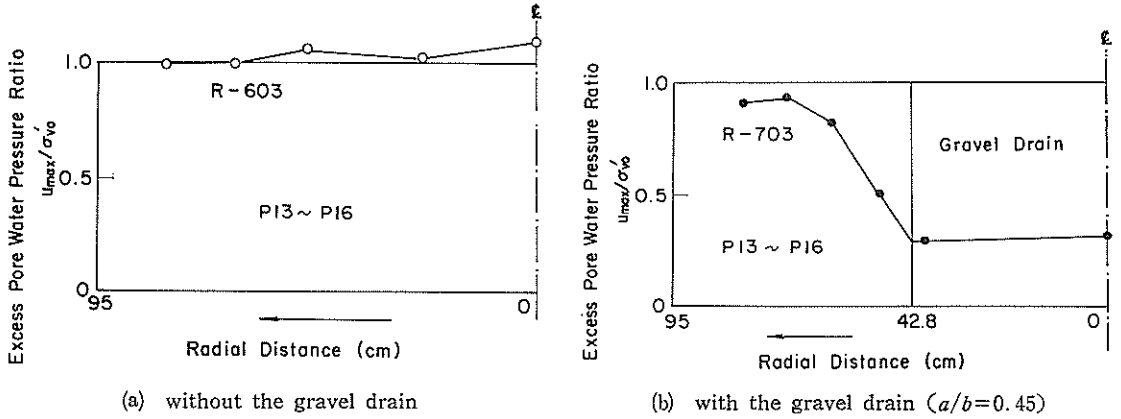
(a) without the gravel drain (b) with the gravel drain ($a/b=0.45$)

Fig. 41 Maximum excess pore water pressures at the tests with and without the gravel drain (under sinusoidal motion of about 83 Gals)
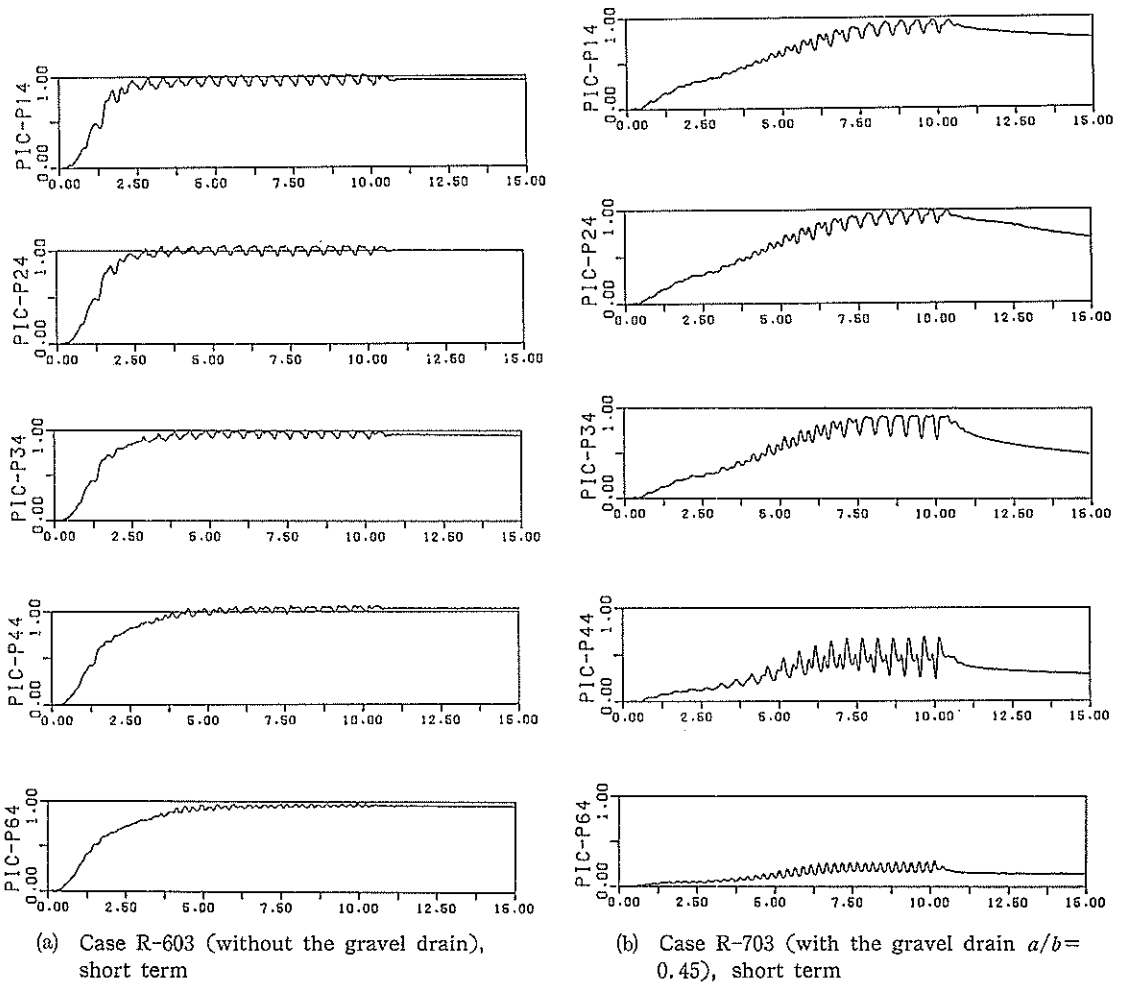
(a) Case R-603 (without the gravel drain), short term (b) Case R-703 (with the gravel drain $a/b=0.45$), short term

Fig. 42 Comparison of the time histories of excess pore water pressure with and without the gravel drain (under sinusoidal motion of about 83 Gals) (to be continued)
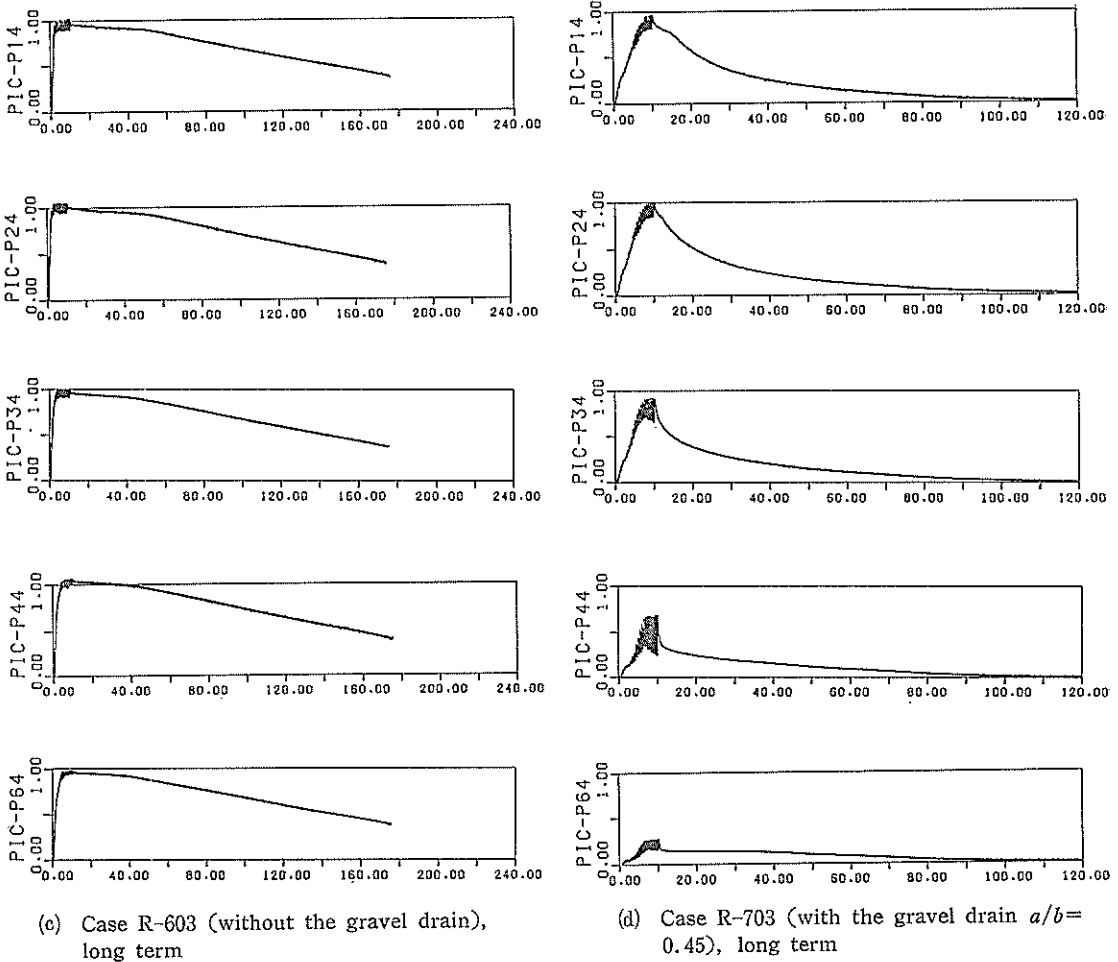
(c) Case R–603 (without the gravel drain),
long term

(d) Case R–703 (with the gravel drain $a/b=$
0.45), long term

Fig. 42 Comparison of the time histories of excess pore water pressure with and
without the gravel drain (under sinusoidal motion of about 83 Gals)

In general, whether the gravel drain succeeds in reducing the maximum value
of the excess pore water pressures depends on many factors mentioned at the
introduction. Besides, whether one part of the sand deposit is close enough to the
gravel drain or not in the above-mentioned sense depends on the same factors as
above. Analyses which will be presented in the next chapter will give some of the
conclusions on these aspects of the performance of the gravel drain.

c) Settlements

Even if the gravel drain is installed and the liquefaction is prevented, the
settlements inevitably occur in accordance with the amount of the drained water.
As shown in **Fig. 43**, measured amount of drained water and equivalent amount of
drained water computed from measured settlements at the surface of the ground
agree with each other throughout the nine series of the tests conducted for the
present study.

Settlements do occur, as shown in **Fig. 26**, not only after shaking stops when
only the dissipation takes place but also during the shaking when the dissipation as

Fig. 44 Time histories of the measured excess pore water pressure at Case R-802 (without gravel drain; under earthquake input motion; maximum input acceleration 105 Gals) (to be continued)
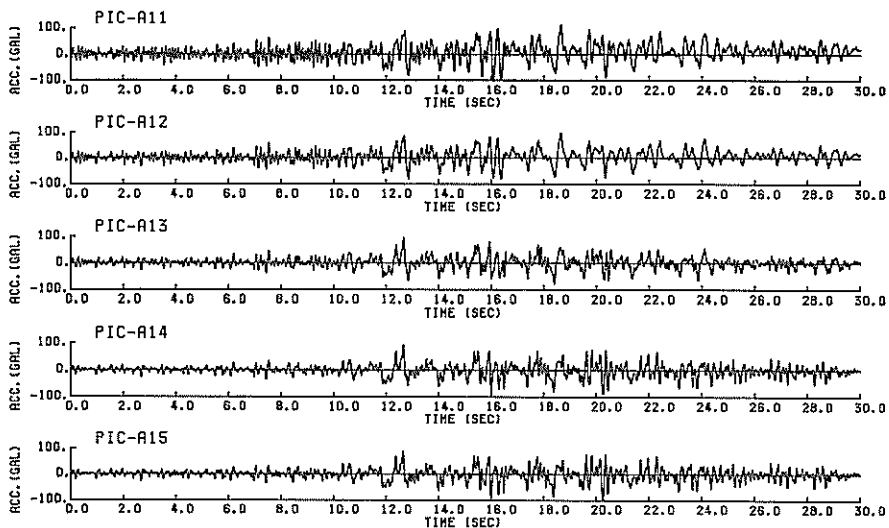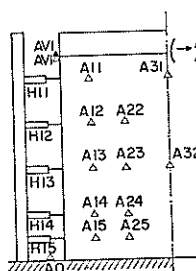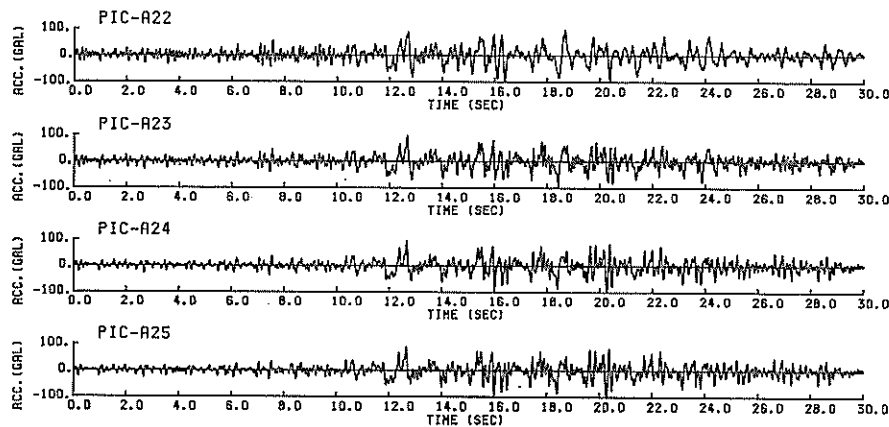
(a) short term

R802

(b) long term

Fig. 44 Time histories of the measured excess pore water pressure at Case R-802 (without gravel drain; under earthquake input motion; maximum input acceleration 105 Gals)

Fig. 45 Time histories of the accelerations and the displacements at Case R-802 (without gravel drain; maximum input acceleration 105 Gals) (to be continued)
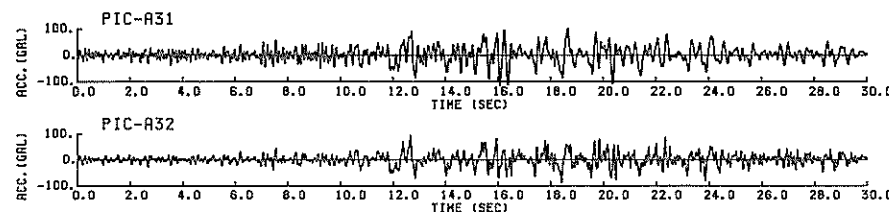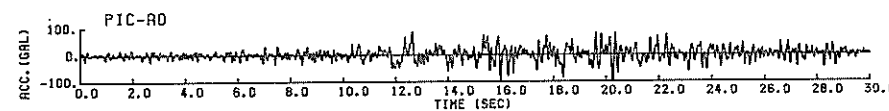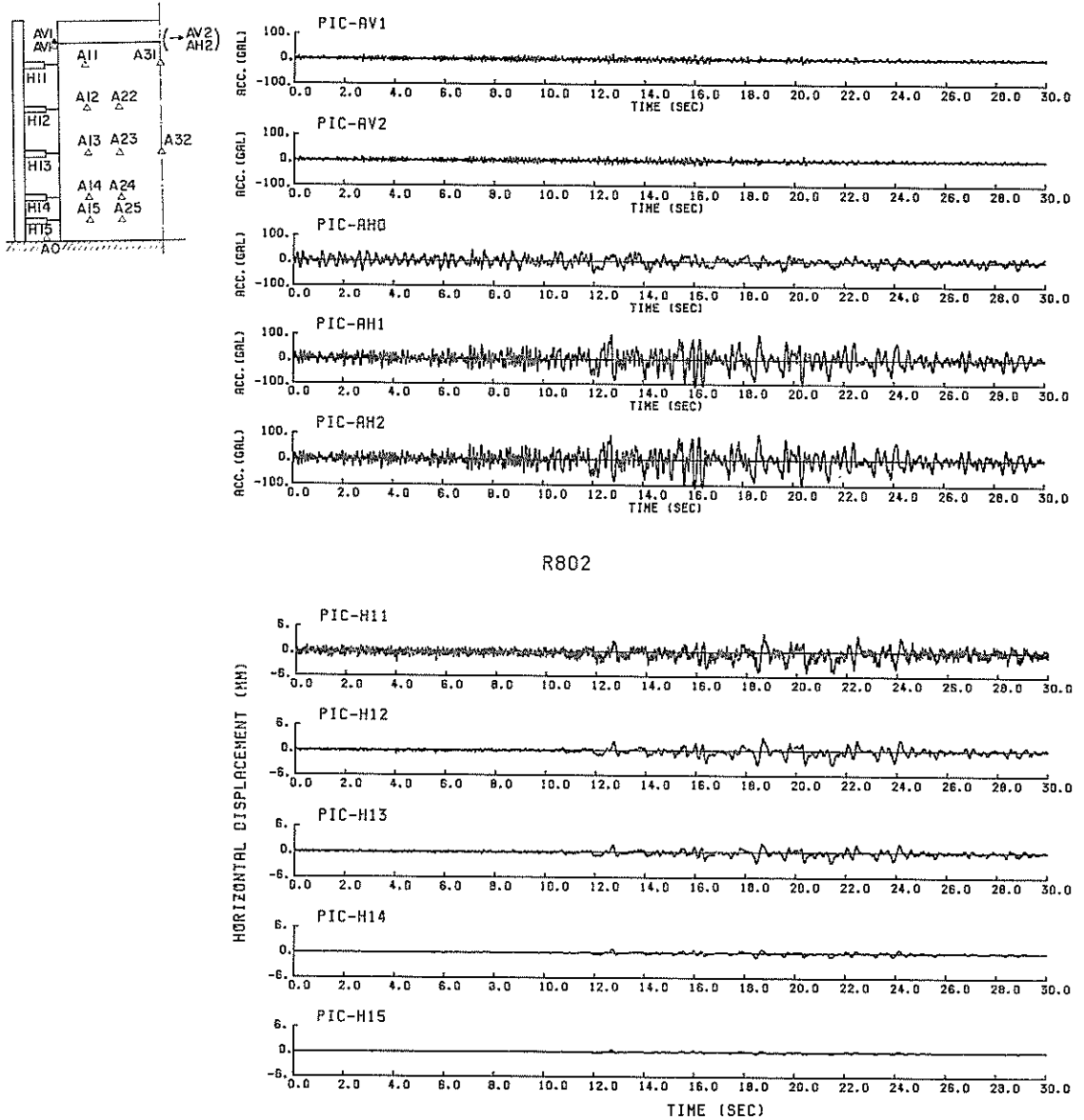
R802

R802

Fig. 45 Time histories of the accelerations and the displacements at Case R-802
(without gravel drain ; maximum input acceleration 105 Gals)

to examine whether the implications obtained from the results of the sinusoidal excitations are readily applicable to the performance of the gravel drains under earthquake excitations. With these things in mind, the tests under earthquake input motions were conducted with and without the gravel drains.

(1) The test results under earthquake input motions with and without the gravel drain (R-800 and R-900 series)

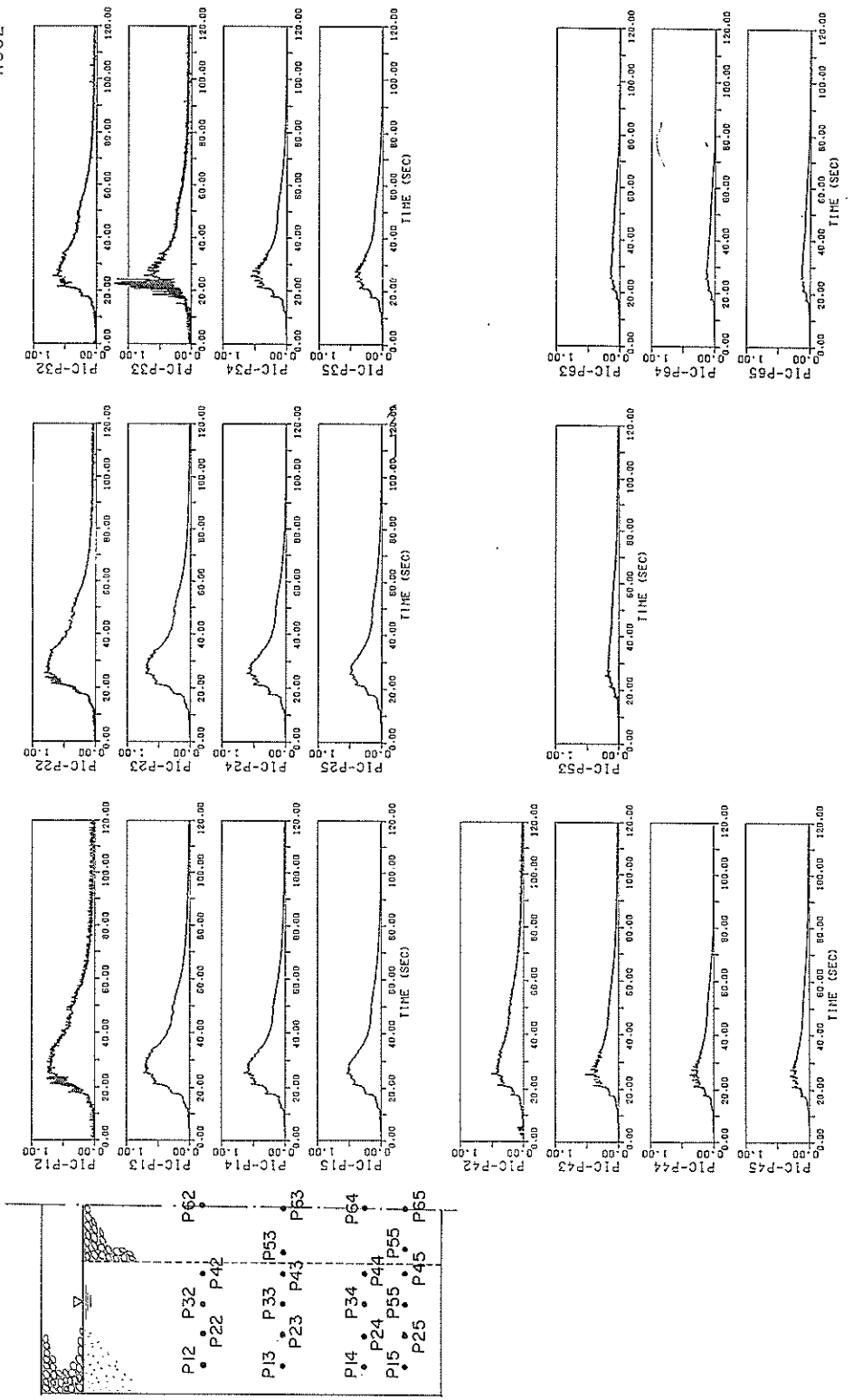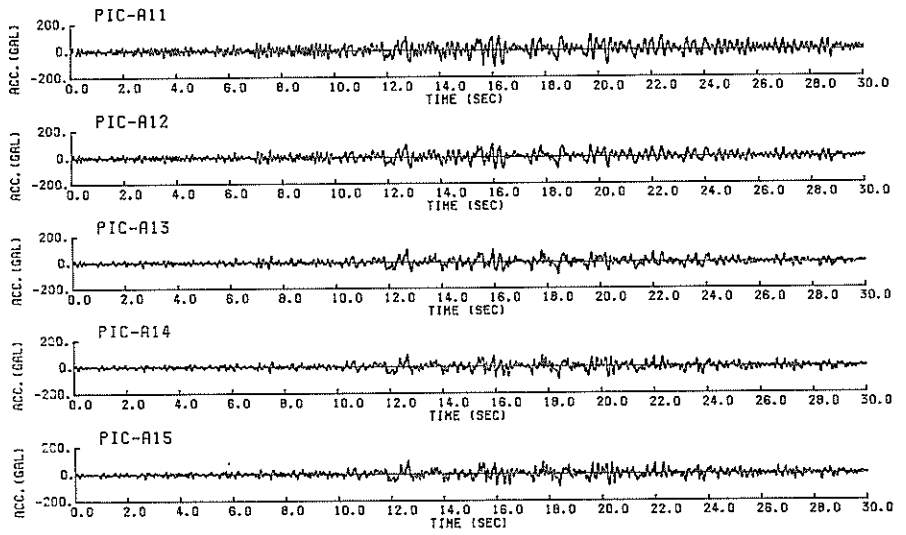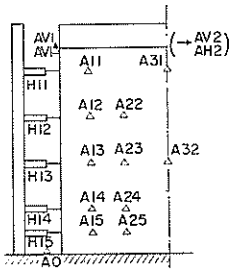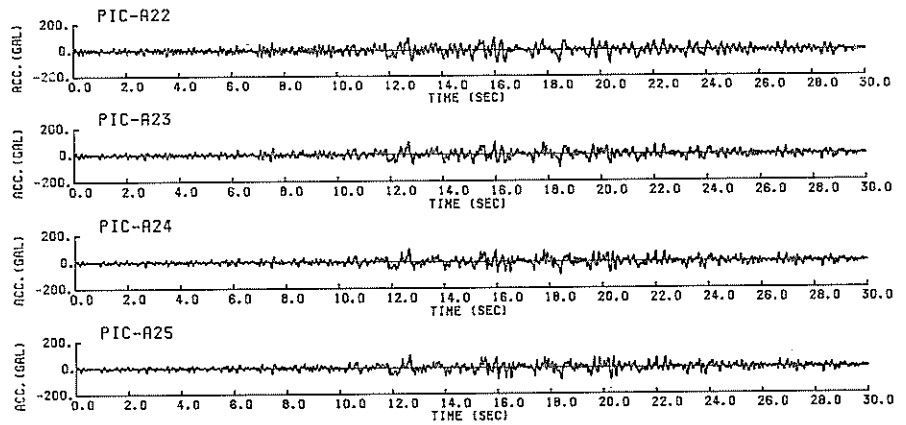As mentioned before, the sand deposit, without the gravel drain, was shaken

Fig. 46 Time histories of the measured excess pore water pressure at Case R-902 (with gravel drain; under earthquake input motion; maximum input acceleration 99 Gals)
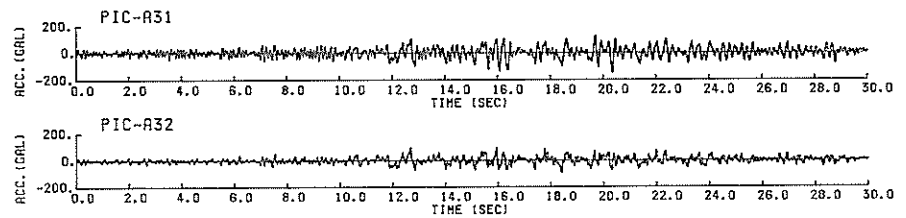
R902·

R902

R902

R902
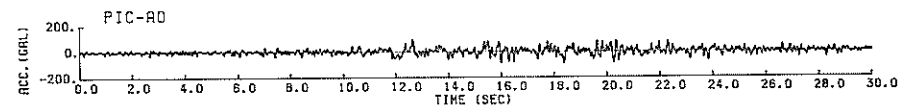
Fig. 47 Time histories of the accelerations and the displacements at Case R-902 (with gravel drain ; maximum input acceleration 99 Gals) (to be continued)
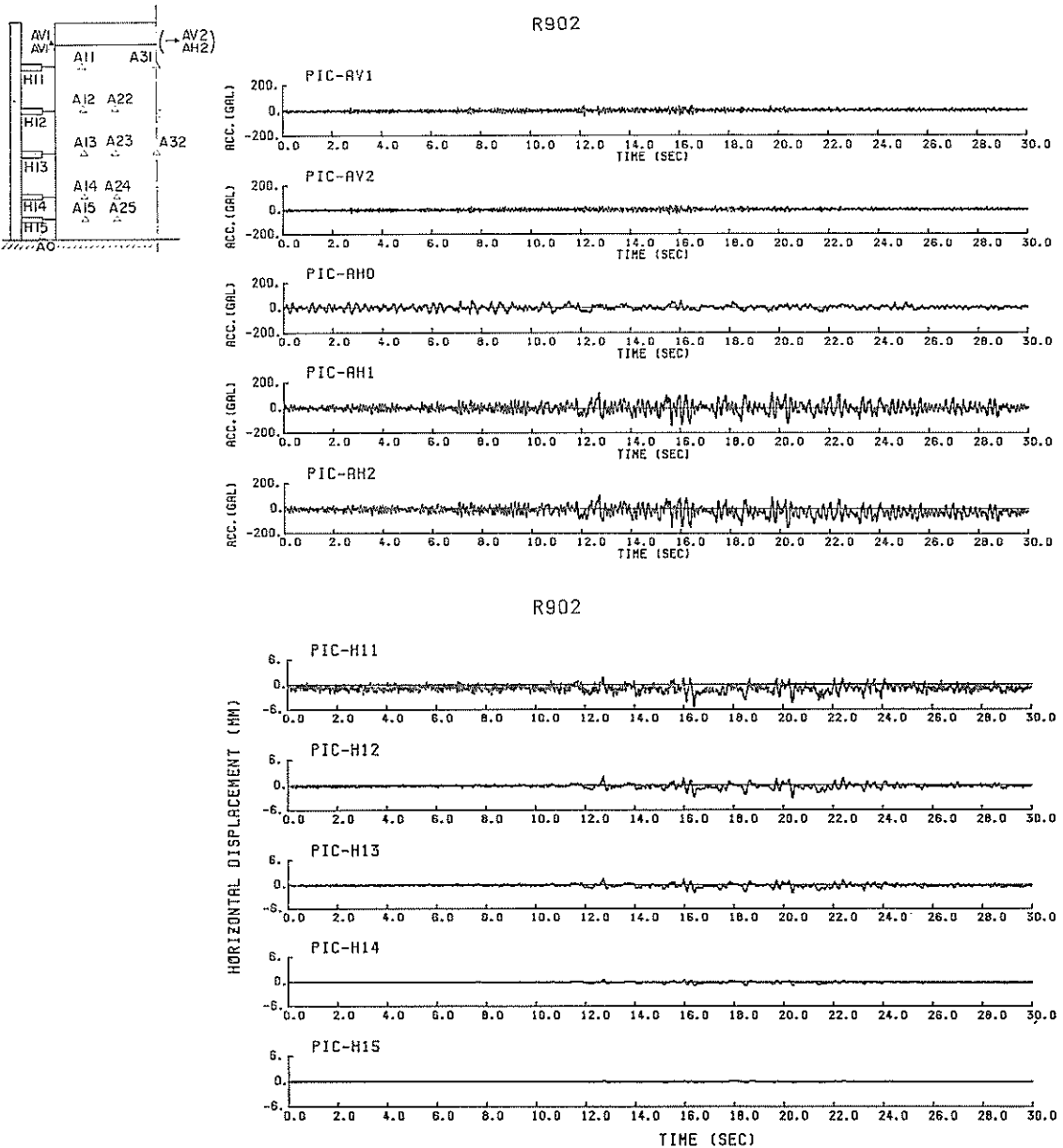
Fig. 47 Time histories of the accelerations and the displacements at Case R-902 (with gravel drain; maximum input acceleration 99 Gals)

with the earthquake input motions for the duration of 120 seconds in R-800 series. In contrast to the tests of sinusoidal excitations, excess pore water pressures in the sand deposit without gravel drain, as shown in **Fig. 44**, began to dissipate even during the shaking as soon as the level of the excitations, as shown in **Fig. 45**, became lower.

Instantaneous high rate of increase in excess pore water pressures are observed at about 18 and 22 seconds. No strong peak accelerations are observed at these times.

(a) R-802 (without gravel drain) (b) R-902 (with gravel drain)

Fig. 48 Maximum accelerations at Cases R-802 and R-902; the tests with and without the gravel drain under earthquake motion of about 100 Gals
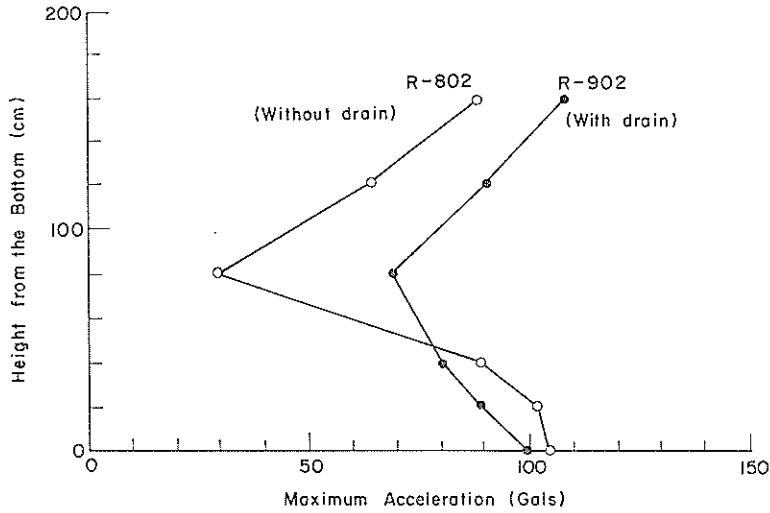
Fig. 49 Maximum accelerations at Cases R-802 and R-902; the tests with and without the gravel drain under earthquake motion of about 100 Gals

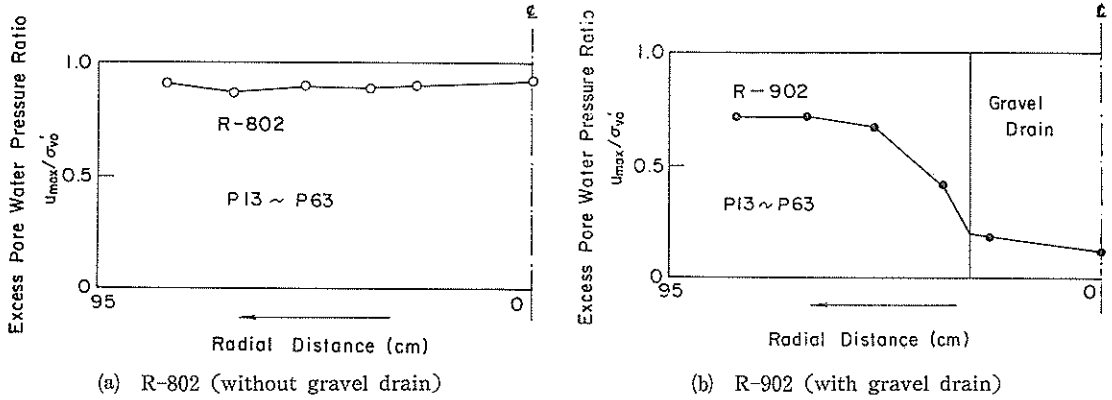However, the time histories of shear stress computed from those of the accelerations, as shown in **Appendix D**, show that the strong peak shear stresses are applied at these times.

When the gravel drain was installed for R-900 series, the rate of increase in excess pore water pressures became lower, the maximum value became lower, and the rate of the dissipation of excess pore water pressures became higher as shown in **Fig. 46**. A closer view on this figure reveals that instantaneous increases in excess pore water pressures at 18 and 22 seconds obviously were not suppressed by the effect of drainage even with the aid of the gravel drain. However, the dissipation after the instantaneous rises in the excess pore water pressures contributed to suppress the average increasing rate of the excess pore water pressures.

The accelerations and the displacements corresponding to this performance of

(a) Case R-802　　　　　　　　　(b) Case R-902

Fig. 50　Settlements at the end of the series R-800 and R-900 (under earthquake motions)

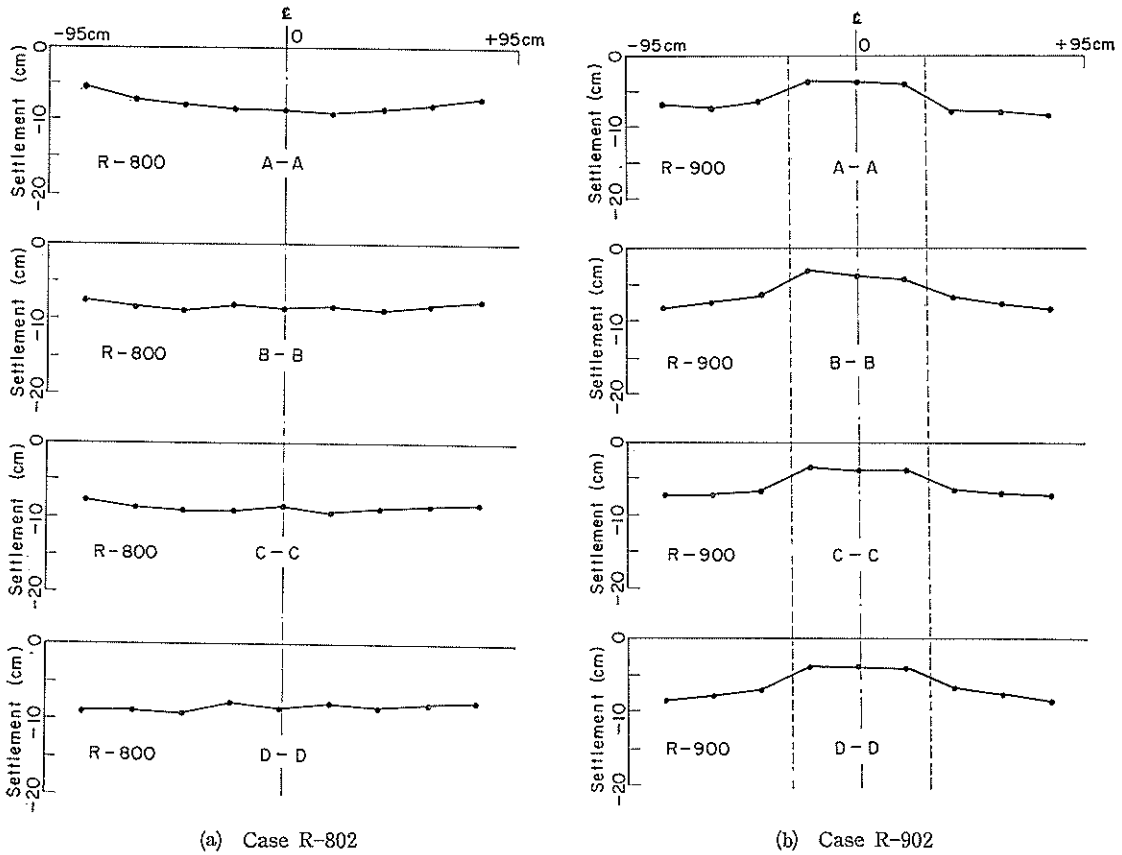the gravel drain are shown in **Fig. 47.**

The distributions of the maximum excess pore water pressures at the tests with and without the gravel drain are shown in **Fig. 48.** The maximum accelerations corresponding to these excess pore water pressures are shown in **Fig. 49.** The settlements as a result of the series of the tests with and without the gravel drain are shown in **Fig. 50** and **Table 10.**

(2)　Implications of the tests under earthquake motion

The tests under the earthquake motion have given the similar implications as the tests under sinusoidal motion. Namely, the effect of the gravel drain on the excess pore water pressures is (i) to reduce the rate of increase in excess pore water pressures, (ii) to increase the rate of dissipation in pore water pressures. One reservation to the item (i) is, at the instance when strong pulse-like shear stresses act, excess pore water pressures are, apparently, not significantly reduced. This is because, at the instance when the strong pulse-like shear stresses act, the rate of generation of excess pore water pressures is very high while the duration of time allowed for dissipation is very short. Consequently, the maximum value of the excess pore water pressures, in general, depends on the detailed feature of the earthquake motions. Therefore, it may be much more difficult to predict the exact value of the maximum excess pore water pressures under earthquake excitations than that under sinusoidal excitations.

Table 10 Settlements and drained water at the tests with and without
a gravel drain under earthquake input motion

Case No.	a/b	Settlement (cm)			Drained Water (kgf)	
		S S*	S 1	S 2	L 2 (Drain)	L 3 (Sand)
R-802	—	1.5	1.4	0.6	—	37.1
R-902	0.3	1.5	0.7	0.5	25.5	0.5

* Average from SS 1~SS 6
 Locations of the instruments are as shown in Fig. 3;
  S S (at 180cm level)
  S 1 (at 120cm level)
  S 2 (at 80cm level)
  L 2 : Water drained from gravel drain
  L 3 : Water drained from the surface of sand deposit

However, the duration of the portion during which the excess pore water pressures are close to the maximum value will be very short as shown in the time histories of the excess pore water pressures at time 18 and 22 seconds in **Fig. 46**. In general, residual deformation of soil structures or foundations due to liquefaction occurs as accumulation of small deformations rather than as instantaneous failure. Therefore, the residual deformation, in general, is not sensitive on the variation in instantaneous peak values of the excess pore water pressures. Consequently, the difficulty in predicting the exact value of the maximum excess pore water pressures is not very serious problem for designing the gravel drain.

As for the settlements, the tests under earthquake motion have given the same implications as those under sinusoidal motion. Namely, (i) the settlements do occur even if the gravel drain is installed, (ii) the pattern of the settlements is of differencial settlement; in general, whether the settlements at the gravel drain are larger than those at the sand deposit surrounding the gravel drain or vice versa depends on the densities of the sand deposit and the gravel drain.

3.4 Clogging of gravel drains

(1) Model test upon clogging of gravel drain (R-500 series)

If the materials used for the gravel drain are very coarse compared with the grain size of the sands surrounding the gravel drain, the sand particles will migrate into the pore of the gravels with the flow of pore water and eventually will clog the gravel drain. Therefore, it is necessary to select the appropriate grain size of the materials to be used for the gravel drain. R-500 series, conducted without a filter surrounding the gravel drain, are served for confirming this aspect of the performance of the gravel drain; soundness against the clogging. As shown in **Table 7** (e), R-500 series were shaken at the maximum acceleration level of 64 Gals at Case R-503 when the outer part of the surrounding sands instantly liquefied as shown in **Fig. 51**. Undergone through this test with one additional test as shown in **Table 7** (e), the gravel drain was dugged out to see whether the gravel drain was clogged with sands. The section of the gravel drain was carefully examined but there were no migrating sands. General considerations on the clogging of the gravel drain will be given later.

(2) Model test with a clogged gravel drain (R-100 series)

It is usual that the material used for the gravel drain is selected so as not to be clogged with the sands. However, it is of some interest to know how the gravel drain would perform if the gravel drain happened to have been clogged before the earthquake. R-100 series, as mentioned earlier, gives some insight on this aspect on
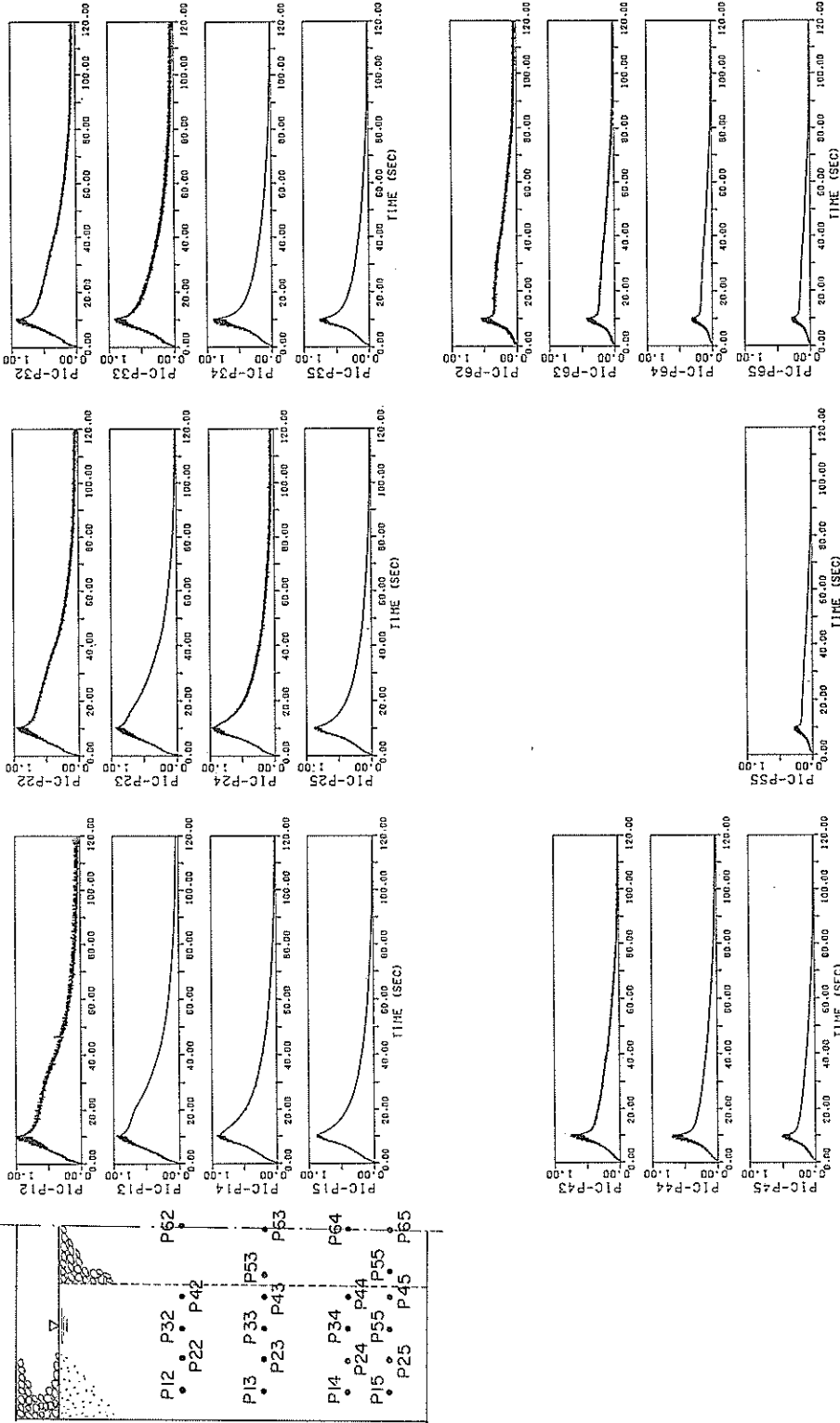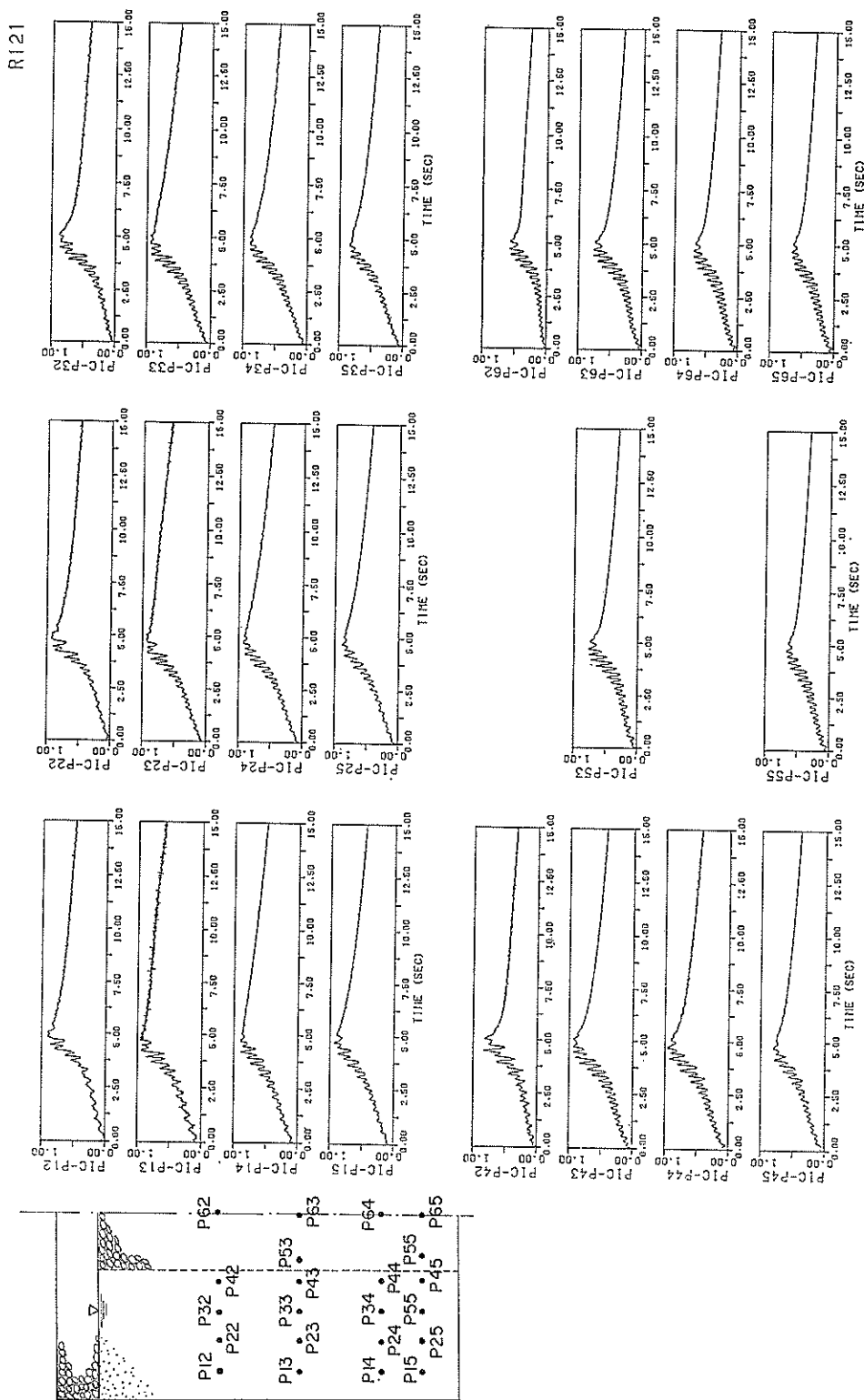
Fig. 51 Time histories of excess pore water pressure at Case R-503

Fig. 52 Time histories of excess pore water pressure at Case R-121 (with a clogged gravel drain) (to be continued)

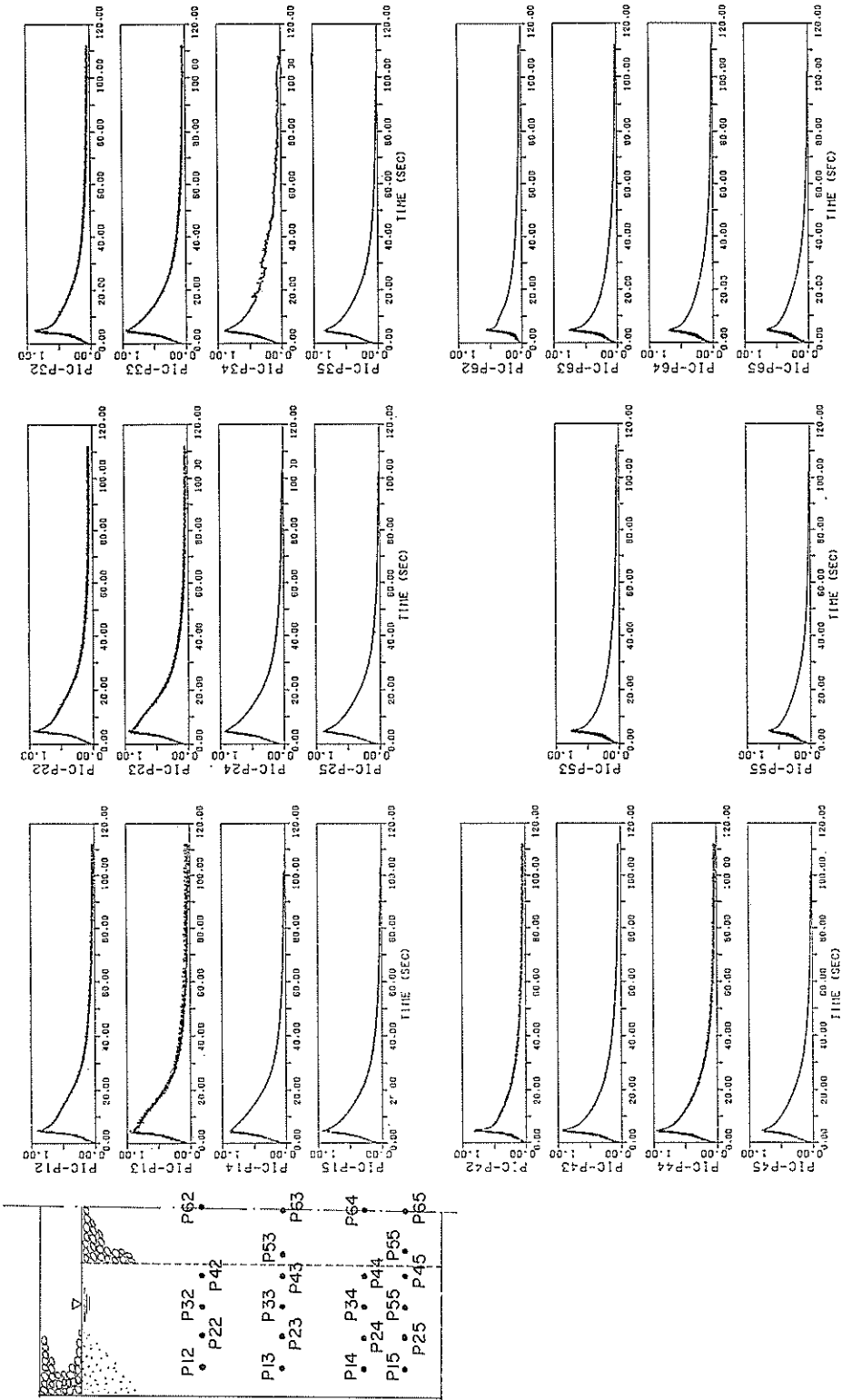(a) Short term

Fig. 52 Time histories of excess pore water pressure at Case R-121 (with a clogged gravel drain)
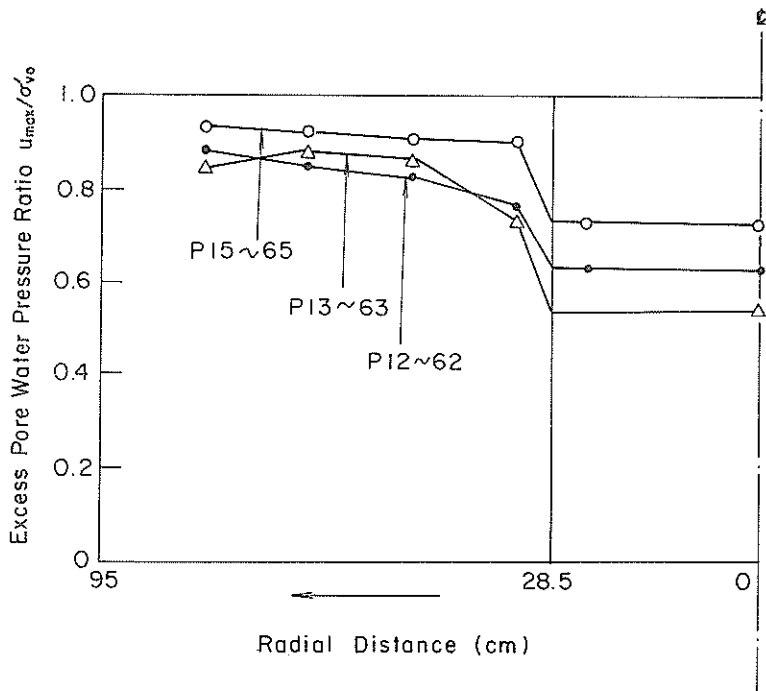
(b) long term

Fig. 53 Distribution of maximum excess pore pressure ratio at Case R–121 (with a clogged gravel drain)

the surface of the sand deposit was 6.3 kgf.

Before going to present the results of the R-100 series, let us mention two evidences which indicate that the gravel drain for R-100 series had been clogged before the shaking. One is the initial relative density of sand deposit. The initial relative density for R-100 series is unusually high, as shown in Table 5, compared with that for other series of tests. Because the procedure for pouring the sand into the water was kept unchanged through out nine series of the tests, it is probable that the gravel drain for R-100 series was clogged with the sand during the process of the sand pouring. The other evidence is that the drained water from the gravel drain contained a significant amount of the sand particles.

The clogged gravel drain for R-100 series was shaken with the sinusoidal input motion for the duration of five seconds. Excess pore water pressures were measured as shown in **Fig. 52**. The distribution of the maximum excess pore water pressures are shown in **Fig. 53**. Accelerations and displacements are shown in **Fig. 54**. Settlements at the end of the series of shakings are shown in **Fig. 55**. At Case R-121, the amount of the water drained through the gravel drain was 20.4 kgf and that from the surface of the sand deposit was 6.3 kgf.

Although the drain was completely clogged, it was remarkable that the amount of the water drained through the gravel drain was larger than that from the surface of the sand deposit. Even the hydraulic gradient towards the gravel drain, as shown in **Fig. 53**, did exist. The mechanism which can explain these facts might be as follows. The densites of the sand having migrated within the gravel drain would be lower than those at the surrounding sand deposit. The sands within the
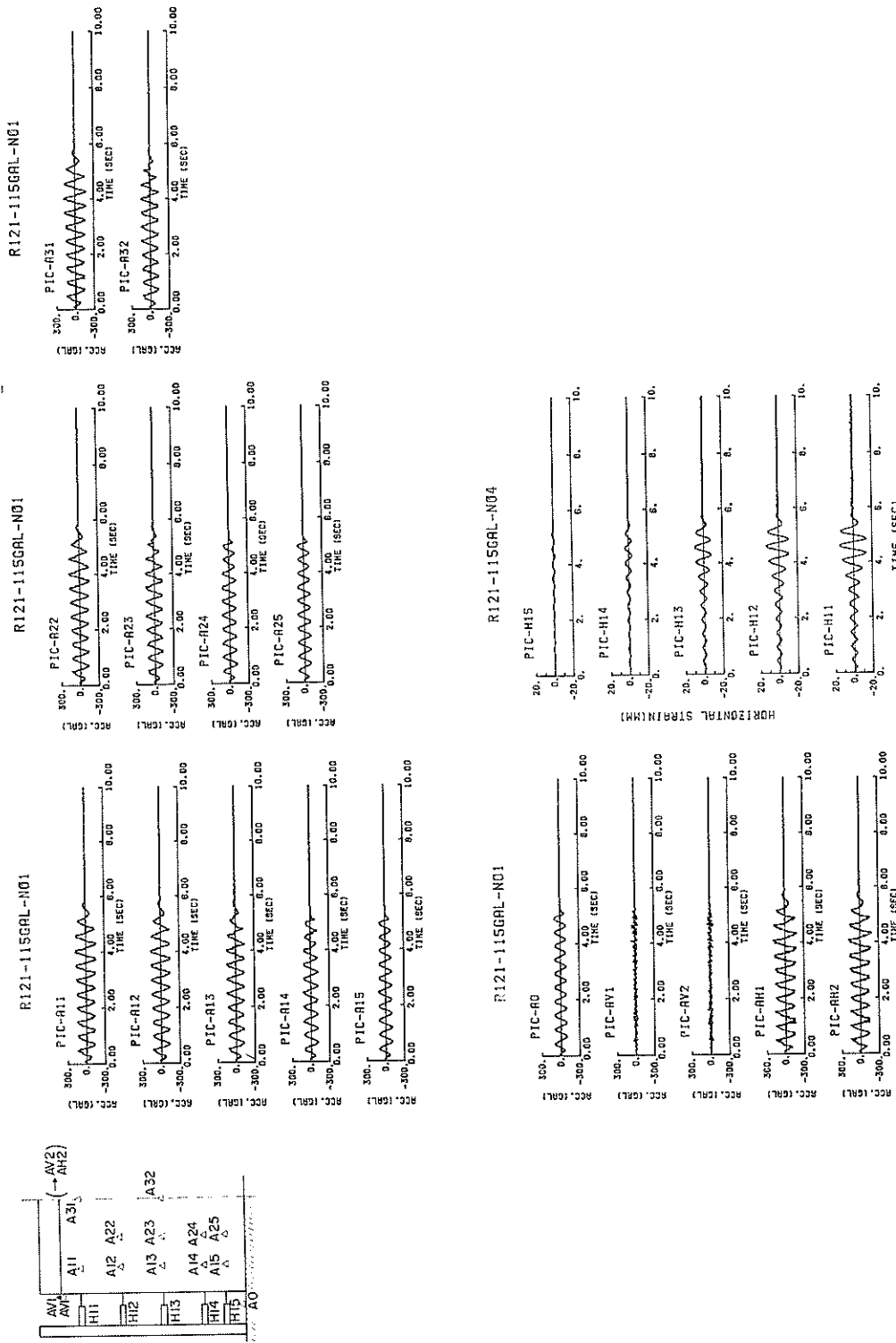
Fig. 54 Time histories of accelerations and displacements at Case R-121 (with a clogged gravel drain)
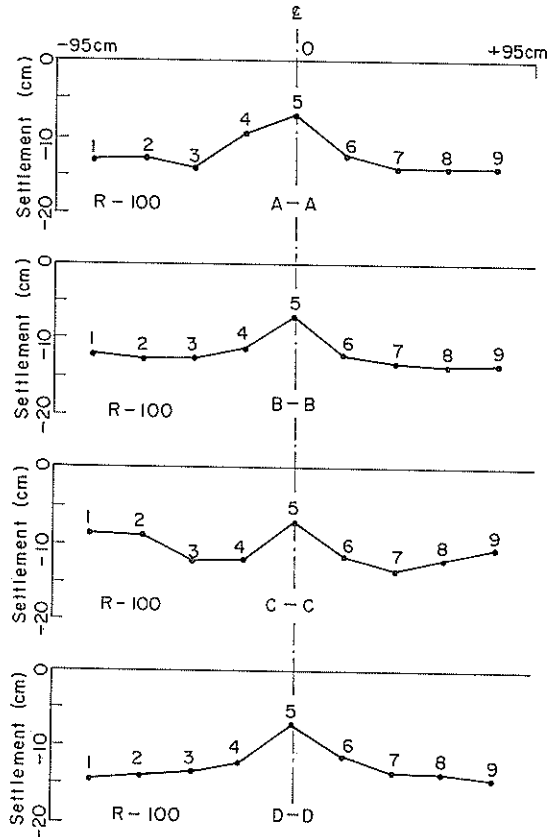
Fig. 55 Settlements at the end of R-100 series
(with a clogged gravel drain)

gravel drain, therefore, would be easier to liquefy than those at the surrounding sand deposit. During the shaking, the sands having migrated in the gravel drain would have already liquefied when the pore water started flowing into the gravel drain from the surrounding sand deposit. The apparent permeability of the gravel drain filled with liquefied sand was higher than the permeability of the sand deposit surrounding the gravel drain. As a consequence, the greater amount of drained water from the gravel drain would result.

However, once the shaking ceased, the rate of dissipation became rather poor and almost the same as that without the gravel drain. This can be understood if the results shown in **Fig. 52** (b) for Case R-121 are compared with those shown in **Fig. 18** (b) for Case R-302 which is conducted without the gravel drain. Furthermore, if the results in **Fig. 53** are compared with that in **Fig. 33**, it is understood that, even during the shaking, the hydraulic gradient towards the gravel drain is much smaller than that of the non-clogging drain.

These facts indicate that the gravel drain, even when clogged with sand, has some possibility to mitigate the liquefaction potential but, obviously, the reliability of the performance of the gravel drain, at such conditions, is poor.

(3)   Considerations on the clogging

Apart from the present study, several studies have been conducted in order to

establish the criterion for selecting appropriate filtering materials against clogging. The following conditions are proposed by these studies;

$D_{15}/d_{85}<5$ [16] (at which, D_{15}: grain size in mm, corresponding to 15% finer by weight, of filtering material used for the gravel drain; d_{85}: grain size in mm, corresponding to 85% finer by weight, of the sand deposit)

$D_{25}/d_{75}<9.5$, or $D_{15}/d_{85}<6.4$ [17]

$D_{15}/d_{85}<9$ [18] (with a judgement for the sake of safety, proposing $D_{15}/d_{85}<5$ [18])

In addition to these studies, there is a study which paid an attention to the accurate definition of clogging and the effect of the density of the sand[19].

All of those studies were conducted by using a cylinder with flow of water forced from the outside. The shaking test conducted in the present study more closely simulates the actual condition on the performance of the gravel drain against clogging during earthquakes. R-500 series shows that, with $D_{15}/d_{85}=2.85/0.255=11$, the gravel drain is not clogged. R-100 series shows that, with $D_{15}/d_{85}=11.5/0.255=45$, the gravel drain is clogged. Because the kinds of the materials used for the gravel drain are very limited, the result from the present study might have a limitation in general applicability. However, as mentioned above, the conditions satisfied in the present study are very close to those on the gravel drain in the field during the earthquakes. Therefore, the results of the present study should be of unique value concerning the clogging.

The gravel drain, even if clogged with sand, has some degree of capability to mitigate the degree of liquefaction as shown in R-100 series. However, the reliability of the performance of the clogged gravel drain is obviously poor.

4. Analyses on performance of gravel drains

The results of the model tests have been presented so far and some of the implications are obtained on the performance of the gravel drains. However, if one intends to design a gravel drain, one has to get quantitative conclusions on the performance of the gravel drains. This chapter is devoted towards this purpose.

When the composite ground made of sand deposit and gravel drains is shaken by the earthquake, its dynamic response will, in general, be influenced by the degree of the excess pore water pressures generated in the composite ground. The degree of the excess pore water pressure, in turn, will be influenced by the dynamic response of the composite ground. In short, both of the dynamic response and the degree of the excess pore water pressures are related with each other. However, in general, the dynamic response of the ground will not be greatly influenced by the excess pore water pressures if the degree of the excess pore water pressures are kept less than about half of the initial vertical effective stresses. In this case, dynamic response of the ground will be computed without the information on the degree of the excess pore water pressures. Keeping the excess pore water pressures at the low level, say less than half of the initial vertical effective stresses, is usually necessary to resist the possible failure of the foundations and soil structures during earthquakes. Consequently the dynamic response of the composite ground can be usually computed without considering the degree of the excess pore water pressures. The remaining thing necessary to consider for designing the gravel drain is, given the dynamic response of the composite ground and the porperties of the composite ground, what is the degree of the excess pore water pressures which will be generated during the earthquakes. This is the purpose of the analyses presented here.

4.1 Modelling performance of gravel drains

The excess pore water pressures once generated in the sand deposit by the earthquake excitations begin to dessipate, after the main part of the earthquake motions ceases, according to the mechanism of consolidation. Obviously, if the level of the excess pore water pressures are very high, say more than half of the initial vertical effective stresses, significant amount of sand particles will lose the contacts with each other and will float within the pore water. In this case, the mechanism of the dissipation of the excess pore water pressures will be quite different from the mechanism of the consolidation[20]. However, as mentioned earlier, it is usual that the level of the excess pore water pressures will be kept less than about half of the initial vertical effective stresses if the gravel drains are appropriately designed against the possible failure of soil structures and foundations. Therefore, the mechanism of the consolidation is considered to be applicable in most of the cases.

According to the mechanism of the consolidation, the greater the permeability and the smaller the compressibility of the sand deposit are, the greater the rate of the dissipation is. If the gravel drains are installed in the sand deposit, the rate of the dissipation in the composite ground, made of the sand deposit and the gravel drains, will become higher than of the sand deposit without the gravel drains. The rate of the dissipation in the composite ground becomes higher, if the spacing of the gravel drains are shorter and if the ability to drain is higher. The ability to drain is influenced by the permeability, the length and the radius of the gravel drains.

During the earthquake shaking, the generation as well as the dissipation of the excess pore water pressures occurs. The rate of the generation of excess pore water pressures is higher if the level of the earthquake shaking is higher, if the effective energy of the earthquake motions is concentrated in a shorter duration of the motion, and if the density of the sand deposit is smaller. The mechanism of the gravel drain for mitigating the liquefaction potential is to balance the rate of the generation with that of the dissipation of the excess pore water pressures at the low level enough to maintain the stability of the structures. In short, the performance of the gravel drains is considered to be modelled by the equation of consolidation with an additional term to generate excess pore water pressures.

It is now widely recognised that an ideal formulation for the consolidation is Biot's formulation. Biot's equations are known to be reduced to Terzaghi's consolidation equations if the rotational components of displacement due to shear deformation are not significant[21]. As mentioned earlier, the experimental results indicate that there is a difference in the settlement between the gravel drain and the sand deposit around the gravel drain. The difference in the settlements cause the rotational shear deformation at the boundary of the sand deposit and the gravel drain. Consequently, in a strict sense, Terzaghi's consolidation equations are not applicable to the performance of the the gravel drain. However, it is generally advisable to adopt the model with a small number of constants, which can reliably be obtained from the usual soil investigations. In this context, Terzaghi's formation is preferable. Besides, if the difference in the settlements are small enough, Terzaghi's formulation can give a good approximation on the behavior of the composite ground. Consequently, Terzaghi's formulation of consolidation will be adopted as basic equations for the analyses.

As for the model to generate the excess pore water pressures, several empirical formulae are proposed. Difference among them is not significant if the constants for the model are appropriately chosen. Therefore, the author takes the liberty of adopting Seed's empirical equation[22] used for the analysis of the gravel drain.

Thus the basic equations for the performance of the gravel drain will be as follows;

$$\left. \begin{array}{l} \dfrac{\partial u}{\partial t} - \dfrac{\partial u_g}{\partial t} = \dfrac{1}{m_v} \cdot \dfrac{1}{r} \cdot \dfrac{\partial}{\partial r} \cdot \left(\dfrac{k_s}{\gamma_w} \cdot r \dfrac{\partial u}{\partial r} \right) + \dfrac{1}{m_v} \cdot \dfrac{\partial}{\partial z} \left(\dfrac{k_v}{\gamma_w} \cdot \dfrac{\partial u}{\partial z} \right) \ \ (\text{if } 0 \leqq r < a) \\[3mm] \dfrac{\partial u}{\partial t} - \dfrac{\partial u_{gd}}{\partial t} = \dfrac{1}{m_{vd}} \cdot \dfrac{1}{r} \cdot \dfrac{\partial}{\partial r} \left(\dfrac{k_d}{\gamma_w} \cdot r \dfrac{\partial u}{\partial r} \right) + \dfrac{1}{m_{vd}} \cdot \dfrac{\partial}{\partial z} \left(\dfrac{k_d}{\gamma_w} \cdot \dfrac{\partial u}{\partial z} \right) \ \ (\text{if } a \leqq r \leqq b) \\[3mm] \dfrac{\partial u}{\partial r} = 0 \quad (\text{at } r=0, \ r=b, \ \text{and } z=0) \\[3mm] u = 0 \quad (\text{at } z=h) \end{array} \right\} \quad (1)$$

in which

r, z: the radial and vertical coordinates, in which r originates at the center axis of the gravel drain and points outward, and z originates at the bottom level of the gravel drain and points upward

a, b: the radii of the gravel drain and the equivalent circle of the tributary area of the sand deposit

h : water level measured from the bottom of the gravel drain

t : the time coordinate

u : the excess pore water pressure

u_g : the excess pore water pressure which will be generated by the cyclic shear under undrained condition in the sand deposit

u_{gd} : the same as u_g but in the gravel drain

k_s, k_v : the coefficients of permeabilities in the horizontal and vertical directions in the sand deposit

k_d : the coefficients of permeabilities in the gravel drain

γ_w : the unit weight of water

m_v, m_{vd}: the coefficients of volume compressibilities of the sand deposit and the gravel drain

u_g in Eq. (1) is given by the following empirical equation;

$$\frac{u_g}{\sigma_{v0}'} = \frac{2}{\pi} \cdot \arcsin\left[\left(\frac{N}{N_l} \right)^{1/2\alpha} \right] \tag{2}$$

in which

σ_{v0}' : the initial effective vertical stress

N : number of cycles of cyclic shear stress

N_l : number of cycles required to cause initial liquefaction ($u/\sigma_{v0}' = 1.0$)

α : an empirically determined constant that has a typical value of 0.7

If we note that $t = N \cdot f$ = duration of applying cyclic shear stresses the frequency of which is f Hz and $t_l = N_l \cdot f$ = duration of cyclic shear stress required to cause initial liquefaction, Eq. (2) can be rewritten as follows;
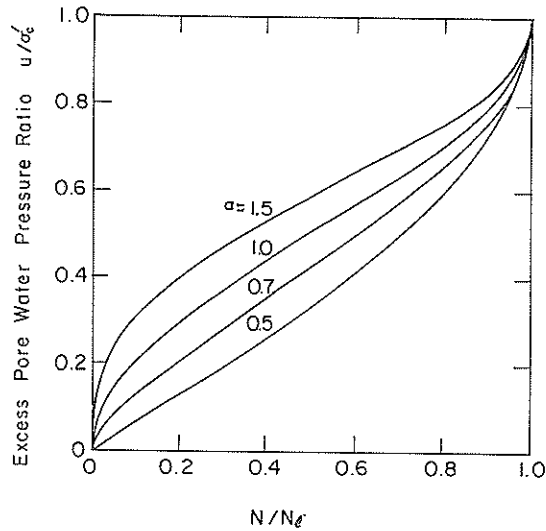
$$\frac{u_g}{\sigma_{v0}'} = \frac{2}{\pi} \cdot \arcsin\left[\left(\frac{t}{t_l} \right)^{1/2\alpha} \right] \tag{3}$$

Thus

$$\frac{\partial u_g}{\partial t} = \frac{\sigma_{v0}'}{\alpha \pi t_l} \cdot \frac{1}{\sin^{2\alpha-1}\left(\dfrac{\pi}{2} \cdot \dfrac{u}{\sigma_{v0}'} \right) \cdot \cos\left(\dfrac{\pi}{2} \cdot \dfrac{u}{\sigma_{v0}'} \right)} \tag{4}$$

The drainage of pore water influences the value of u/σ_{v0}' and thus influences the

N : Number of cyclic loadings

N$_\ell$: Number of cyclic loadings required
to cause initial liquefaction

Fig. 56 Typical excess pore water pressure generation
curves given by Eq. (2)

rate of generation of pore water pressure u_g through Eq. (4). Some examples of the relation given by Eq. (2) are illustrated in **Fig. 56**. The excess pore water pressure which will be generated by the cyclic shear under undrained condition in the gravel drain u_{gd} in Eq. (1) is given in the same manner as u_g.

As mentioned above, the formulation given by Eqs. (1) and (4) might give a good approximation on the performance of the gravel drains but has some limitations on the applicability because they are derived on the assumptions which are not necessarily valid at all conditions; the assumption of the mechanism of consolidation, the assumption of the Terzaghi's formulation, and the assumption of the empirical equation on the generation of excess pore water pressures. Therefore, the results of the model tests will be compared with the computed results by Eqs. (1) and (4) in the following sections.

4.2 Liquefaction properties of the model sand deposit
(1) Outline of the procedures to determine the properties

In order to analyse the performance of the gravel drain by Eqs. (1) and (4), properties of the sand deposit are necessary; the material properties related to the dissipation and the generation of excess pore water pressures. One approach to obtain these material properties is to conduct laboratory tests on sand specimen. The cyclic triaxial test is one example. A difficulty, however, exists in this approach because material properties under very low confining pressures have to be obtained. The author, therefore, abandoned this approach and, instead, adopted the other approach; to regard the shaking table tests of sand deposit without the gravel drain as index tests, which present data relevent to the properties of the sand deposit on the dissipation as well as the generation of excess pore water pressures. The test results under sinusoidal input motions (i.e., R-200, R-300, and R-600 series) were

used for this purpose because, in these tests, the part representing the dissipation and the other part representing the generation of the excess pore water pressures were easily recognized. Basic procedures to obtain the properties from these test results are as follows:

(a) Properties on the dissipation of excess pore water pressures

The time histories of the excess pore water pressures after the shaking are used for obtaining the properties on the dissipation in the sand deposit. Among the constants which govern the dissipation of excess pore water pressures, the coefficient of permeability has been given by the test as in **Fig. 9**. Therefore, the coefficient of volume compressibility is the only unknown constant which governs the dissipation in the sand deposit. The coefficient of volume compressibility is obtained by back-fitting technique.

Strictly speaking, the coefficient of permeability becomes dependent on the hydraulic gradient if the hydraulic gradient becomes high enough to violate the assumption of laminar flow. However, the sand used for the present study is so fine, i.e. $D_{10}=0.1$ mm, that the assumption of laminar flow is considered valid at almost any condition on the hydraulic gradient which is relevant in this study.

(b) Properties on the generation of excess pore water pressures

The time histories of the excess pore water pressures during the shaking are used for obtaining the properties on the generation of excess pore water pressures in the sand deposit. The generation of excess pore water pressures is governed by two factors; the applied shear stress and the liquefaction strength of the sand deposit. Among these factors, the time histories of shear stresses are computed from the measured time histories of accelerations. By using the time histories of the shear stresses thus obtained, the liquefaction strengths of the sand deposit are obtained by back-fitting technique. Obviously, even during the shaking, the excess pore water pressures partly dissipate. Therefore, the properties on the dissipation are also used for the back-fitting.

(2) Coefficient of volume compressibility of the sand deposit

As mentioned earlier, the coefficient of volume compressibility must be obtained in order to determine the properties of the dissipation in the sand deposit. Two factors have to be considered upon the coefficient of volume compressibility of the sand deposit; influence of the excess pore water pressure ratios and influence of the initial confining pressures. These factors will be considered step-by-step.

(a) Influence of excess pore water pressure ratio

As the first step, it is assumed that the coefficient of volume compressibility does not depend on the initial confining pressures. The rate of dissipation at the tests of R-200, R-300, and R-600 series give, as shown in **Fig. 57**, the coefficient of volume compressibility of about 0.02 cm²/kgf when the maximum excess pore water pressure ratio attained before the dissipation is less than 0.5. The coefficient of volume compressibility becomes dependent upon the maximum excess pore water pressure ratio if the ratio becomes greater than 0.5. When the ratio exceeds 0.95, the coefficient of volume compressibility determined from the rate of dissipation ranges from 0.05 to 0.35 cm²/kgf and cannot be reliably determined from the value of the maximum excess pore water pressure ratio. Moreover, once the ratio exceeds 0.95, the coefficient of compressibility changes through out the dissipation as shown in **Fig. 57** by open squares.

These results indicate the following facts. When the maximum excess pore water pressure ratio attained before the beginning of the dissipation is less than 0.5, influence of the ratio on the compressibility is minor and mechanism of the
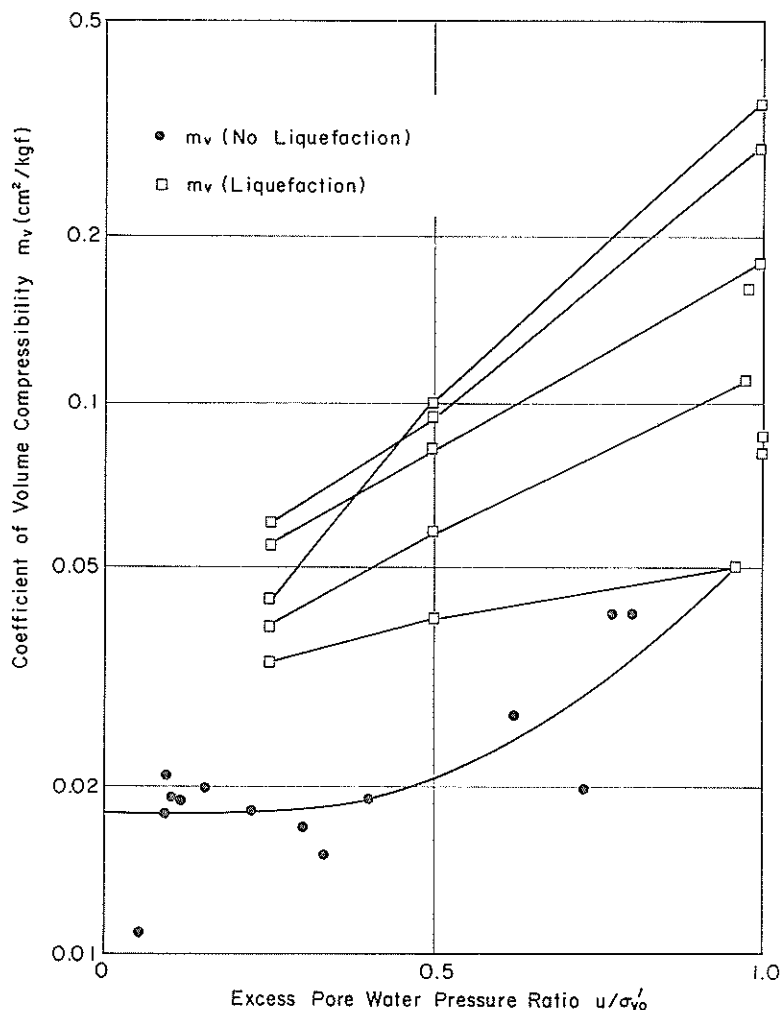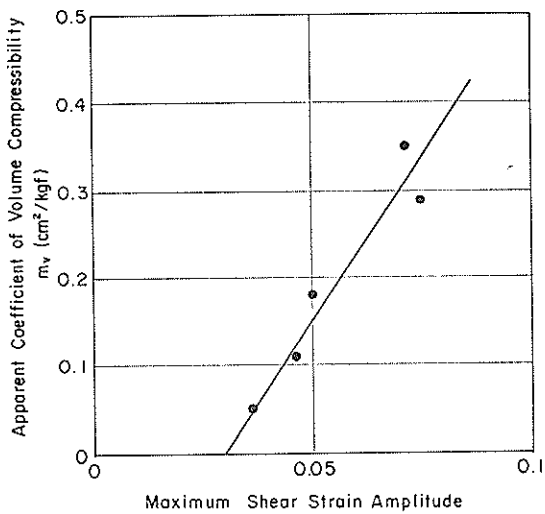
Fig. 57 Measured coefficient of volume compressibility during dissipation of excess pore water pressures

dissipation of excess pore water can be well approximated by the Terzaghi's consolidation equation. Apparently, the mechanism of the dissipation can still be approximated by the Terzaghi's consolidation equation even when the excess pore water pressure ratio becomes greater than 0.5 but less than 0.95. In this case, however, the coefficient of volume compressibility should be given as a function of the maximum excess pore water pressure ratio attained before the dissipation. Once the maximum excess pore water pressure ratio exceeds 0.95, most of the contacts between the sand particles will be lost. Strictly speaking, the mechanism of the consolidation can not be adopted to this state of liquefaction. However, if the coefficient of apparent volume compressibility is given as a function of some additional parameters, the characteristics of the dissipation of excess pore water pressures can still be simulated within the framework of the Terzaghi's consolidation equation.

Three or four candidates are taken as the additional parameters; (i) duration of shaking or number of cyclic loadings after excess pore water pressure ratio exceeds
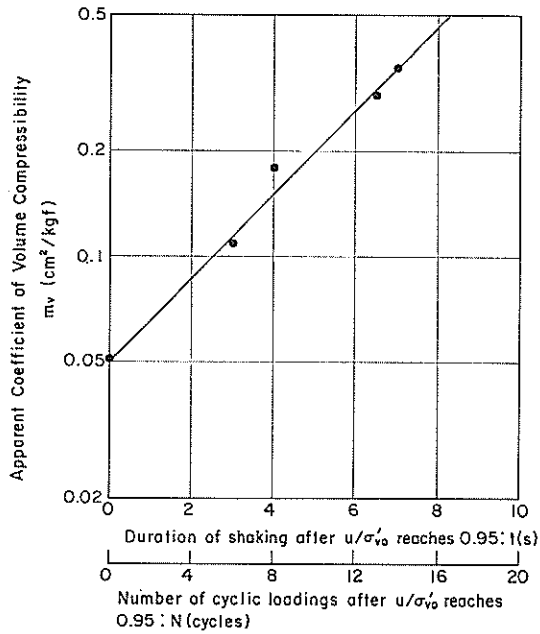
(a) Relation with duration of shaking or number of cyclic loadings after liquefaction

(b) Relation with maximum shear strain amplitude
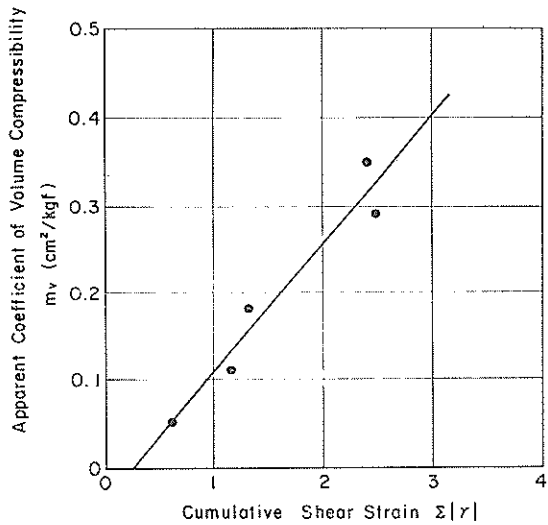
(c) Relation with cumulative shear strain

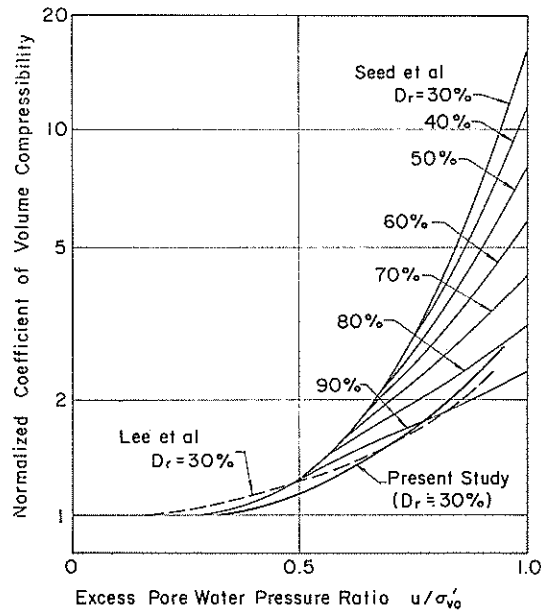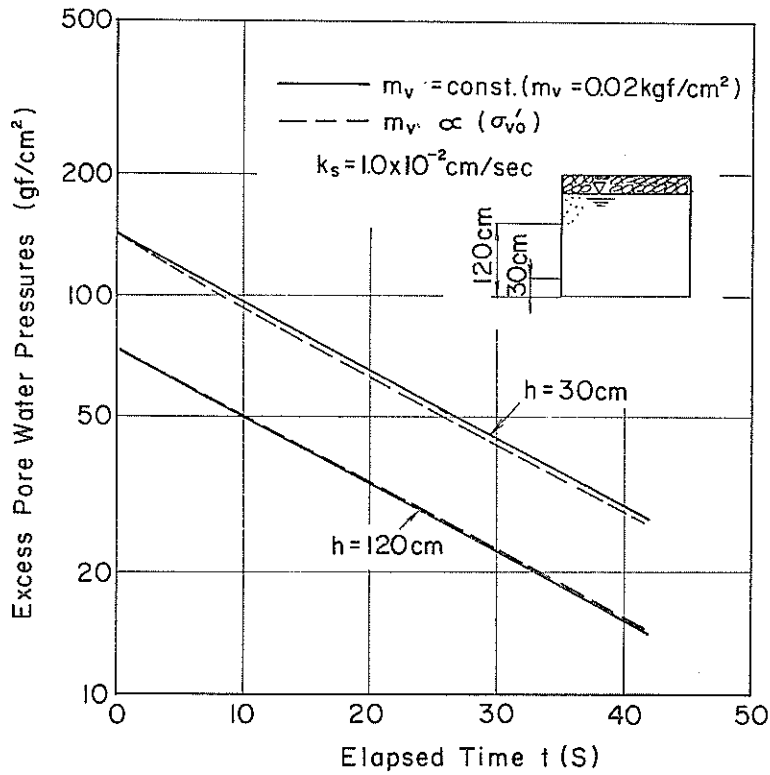**Fig. 58** Emperical relations on the apparent coefficient of volume compressibility after liquefaction

Fig. 59 Comparison of compressibility with those proposed by other studies

(a) Without the gravel drain

Fig. 60 Effect of confining pressure dependent compressibility on the dissipation of excess pore water pressures during the model tests) (to be continued)
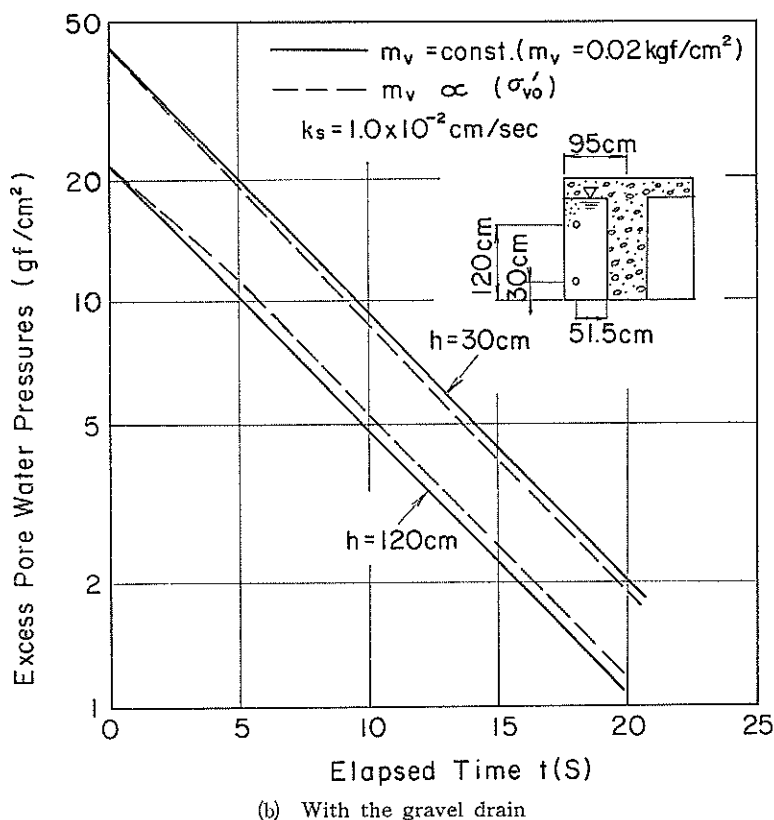
(b) With the gravel drain

Fig. 60 Effect of confining pressure dependent compressibility on the dissipation of excess pore water pressures during the model tests

0.95, (ii) maximum shear strain amplitude, (iii) cumulative shear strain amplitude. Empirical relations on the apparent coefficient of volume compressibility just after the liquefaction are obtained as shown in **Fig. 58**. Apparently good correlations are obtained for all the parameters.

As mentioned previously, once the excess pore water pressure ratio exceeds 0.95, the apparent compressibility changes throughout the dissipation. The coefficient apparently reduces towards the value of 0.33 cm²/kgf at $u/\sigma'_{v0}=0$ along a straight line in the semi-log scale as shown in **Fig. 57**.

Among the results obtained here, the dependency upon the excess pore water pressure ratio has been studied by several researchers.[23][24] As shown in **Fig. 59**, the result obtained by the present study is consistent with the result by Lee and Albaisa (1974)[23].

(b) Influence of the initial confining pressure

In the previous step for studying the influence of the excess pore water pressure ratio, the compressibility was, as mentioned earlier, assumed to be independent of the initial confining pressures. As the next step, the influence of the initial confining pressure will be studied here.

As a comparison, the coefficient of volume compressibility is assumed constant at one case and inversely proportional to the initial confining pressure at the other case. The results of the simulation for the model sand deposit indicate, as shown

Table 11 Constants used fon the simulation for studying the influence
of initial confining pressure upon the generation and the
dissipation of excess pore water pressures

$$a = 0.3 \text{ m}$$
$$b = 1.0 \text{ m}$$
$$h = 20 \text{ m}$$
$$k_s = 10^{-2} \text{ cm/s}$$
$$k_d = 20 \text{ cm/s}$$
$$m_v = 0.02 \text{ cm}^2/\text{kgf} \quad (\text{at } z = 10 \text{ m})$$
$$m_{vd} = 0.006 \text{ cm}^2/\text{kgf} \quad (\text{const})$$
$$t_l = 10 \text{ s}$$
$$f = 2 \text{ Hz}$$
$$\gamma_{sat} = 2.0 \text{ tf/cm}^3$$

a : radius of gravel drain
b : radius of effective circle for tributary area
h : depth of gravel drain
k_s : coefficient of permeability of sand
k_d : coefficient of permeability of gravel
m_v : coefficient of volume compressibility of sand
m_{vd} : coefficient of volume compressibility of gravel
t_l : duration of shaking required to cause initial liquefaction
f : frequency of shaking
γ_{sat} : saturated unit weight of sand and gravel

in **Fig. 60** (a), that the influence of the initial confining pressure is negligibly small upon the dissipation of excess pore water pressures in the model sand deposit. This result justifies the assumption made previously for studying the influence of the excess pore water pressure ratio.

In the sand deposit without gravel drain, path lengths of the seepage towards the surface is obviously dependent on the depth from which the seepage initiates; the deeper the location is, the longer the path length becomes. In general, the longer the path length is, the slower the dissipation is. If the gravel drain is installed in the sand deposit, path lengths of the water flow towards the gravel drain becomes independent of the depth. Therefore, the influence of the initial confining pressure might be more remarkable when the gravel drain exists. The results of the simulation for the model composite ground indicate, as shown in **Fig. 60** (b), that rate of the dissipation is indeed higher at the part which has smaller coefficient of volume compressibility. However, the results also indicate that the influence of the initial confining pressure is still negligibly small upon the dissipation of excess pore water pressures. Consequently, the influence of the initial confining pressure can be neglected for the analyses of the model tests in the present study.

It may be of some value to study, at this point, whether the above conclusion is also valid in the case of full scale gravel drains in the field. Conditions given for the simulation are shown in **Table 11**. The ground water level was assumed to be the same as the ground surface level. The results indicate, as shown in **Fig. 61,** that, except for the part very close to the ground surface, the influence of the initial confining pressure is minor.

(c) Modelling the coefficient of volume compressibility
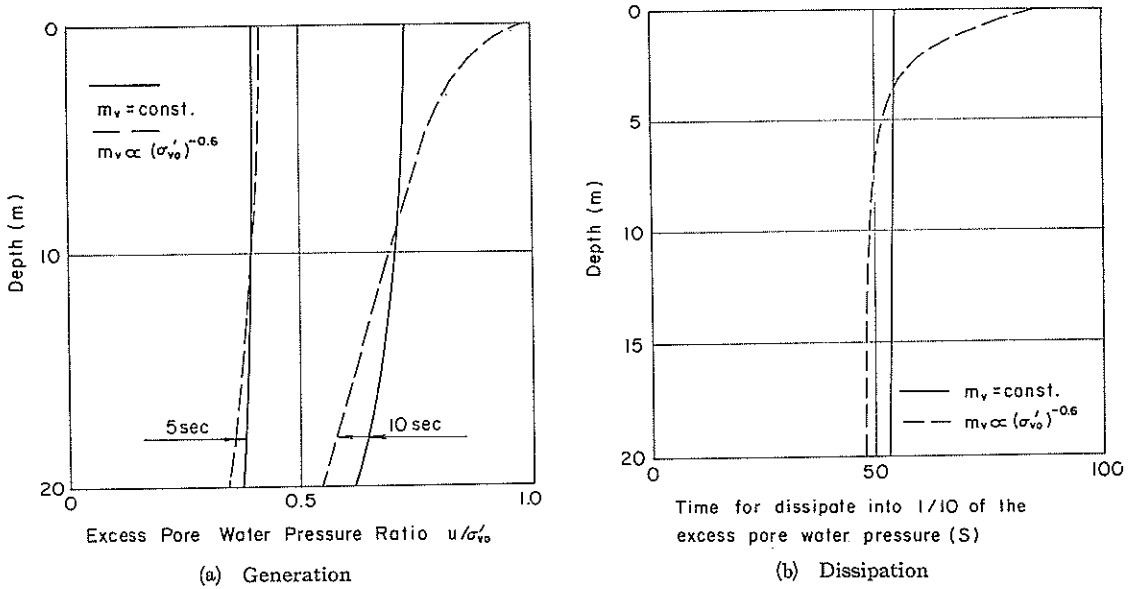Based upon the above findings, the coefficient of volume compressibility of the

(a) Generation (b) Dissipation

Fig. 61 Effect of confining pressure dependent compressibility on the generation and dissipation of excess pore water pressures at the typical field conditions

model sand deposit will be given by the following rules for the present study.

(i)   The coefficient of volume compressibility is given as a function of the excess pore water pressure ratio indicated by solid lines in **Fig. 57**.

(ii)   Once the excess pore water pressure ratio exceeds 0.95, the coefficient will be given as a function of duration of time for shaking, as shown in **Fig. 58(a)**, after liquefaction.

(iii)   Whenever the excess pore water pressure ratio exceeds 0.75, which corresponds to the coefficient of volume compressibility of 0.03 cm²/kgf, the change in the coefficient of volume compressibility during the dissipation is given by the straight lines in the semi-logarithmic plotting figure shown in **Fig. 57**. The straight line is directed to the coefficient of volume compressibility of 0.03 cm²/kgf at $u/\sigma'_{v0}=0$.

(3)   Properties on the generation of excess pore water pressures

Eq. (4) shows that there are obviously only two constants which govern the generation of excess pore water pressures; the duration of shaking required to cause initial liquefaction: t_l, and a parameter for specifying the pore pressure generation curve: α. The parameter α has a typical value of 0.7 and this value is adopted in the present study. The constant t_l, however, is not necessarily simple to determine. The constant t_l is governed by two factors: the applied shear stress and the liquefaction strength of the sand deposit. The procedure to determine these factors is as follows:

(a)   Time histories of shear stresses

Let us imagine that the model sand deposit is composed of many disk-like thin elements. Let us denote the element at the top of the sand deposit as the first element, the element next to the first element as the second element, etc. The balance of the forces acting on the i-th element of sand deposit gives,
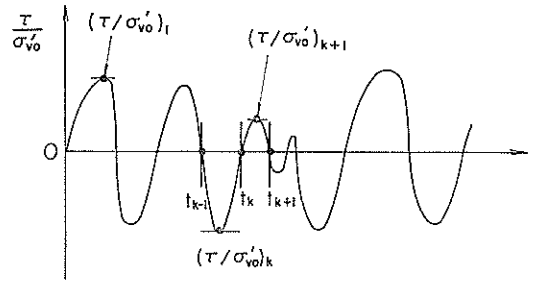
(a) Time history of shear stress ratio
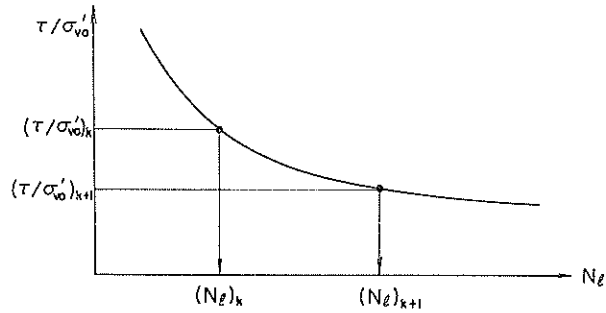
(b) Liquefaction strength curve

Fig. 62 Schematic figure for simulation of excess pore water
pressure generation

$$\tau_i = \tau_{i-1} + \frac{w_i \cdot \ddot{x}_i}{A \cdot g} \qquad\qquad (5)$$

in which

τ_i :   shear stress acting on the lower boundary of i-th element
τ_{i-1} :   shear stress acting on the upper boundary of i-th element
W_i :   weight of i-th element
$\ddot{x}_i$:   acceleration of the i-th element
g :   acceleration of gravity
A :   horizontal sectional area of the element

By applying Eq. (5) at instantaneous values of the accelerations, the time histories
of shear stress at specified depths are obtained. Small acceleration of the dead
weight, which was put on the container for suppressing the rocking motion, was also
taken into the computation of shear stress. In order to enhance the reliability of the
acceleration data, average was taken over the values measured at the same level of
the sand deposit, such as those measured at A11 and A31 in **Fig. 3**, wherever possible.
Time histories of shear stresses obtained in this way are shown in **Appendix D**.
(b) Instantaneous value of t_l
    In order to obtain the instantaneous value of t_l, it is necessary to make a guess,
in a trial and error basis, a liquefaction strength curve such as shown in **Fig. 62 (b)**,
which shows a relationship between the shear stress ratio of cyclic loadings under
undrained condition and the number of cyclic loadings at which liquefaction initiates.
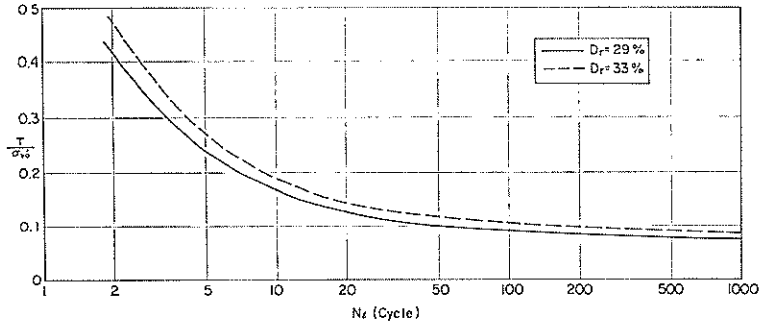
Fig. 63 Liquefaction strength curves obtained by back fitting
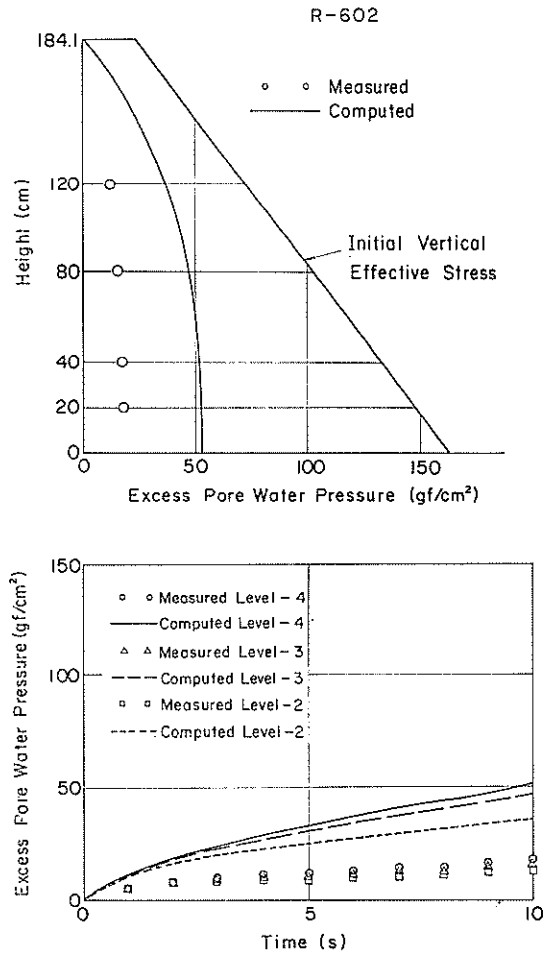
Fig. 64 Measured and computed excess pore water
pressures for Case R-602 (without gravel
drain, sinusoidal input motion

Let us suppose that time histories of the shear stress ratio is obtained as shown in
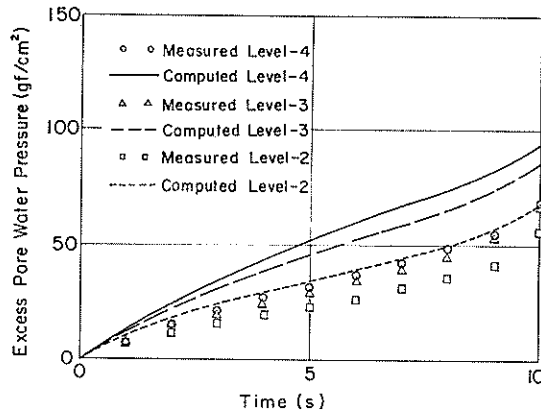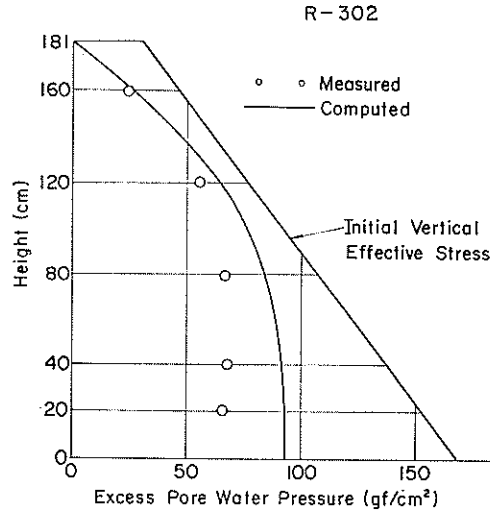Fig. 62 (a). For the k-th half cycle which starts at t_{k-1} and ends at t_k, if we recall
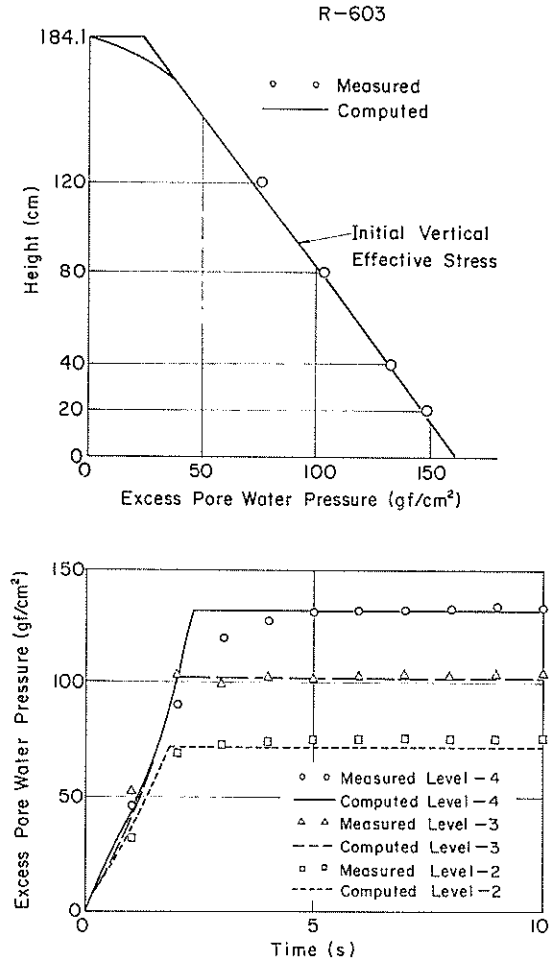
R‒302

Fig. 65 Measured and computed excess pore water pressures for Case R‒302 (without gravel drain, sinusoidal input motion, maximum input acceleration 50 Gals)

that $t_l = N_l \cdot f$, the instantaneous value of t_l is given by,

$$t_l = (N_l)_k \cdot 0.5/(t_k - t_{k-1}) \qquad \text{for } t_{k-1} < t < t_k \tag{6}$$

in which definitions of the variables are, as shown in Fig. 62;

$(N_l)_k$: number of cycles required to cause initial liquefaction by the cyclic loadings of which amplitude is the same as that of the k-th half cycle

t_{k-1} : the time from which the k-th half cycle of shear stress wave starts

t_k : the time at which the k-th half cycle of shear stress wave ends

(c) Simulation by Eqs. (1) and (4)

By using t_l thus obtained, the excess pore water pressures for R-200, R-300, and R-600 series are computed by using finite element method.
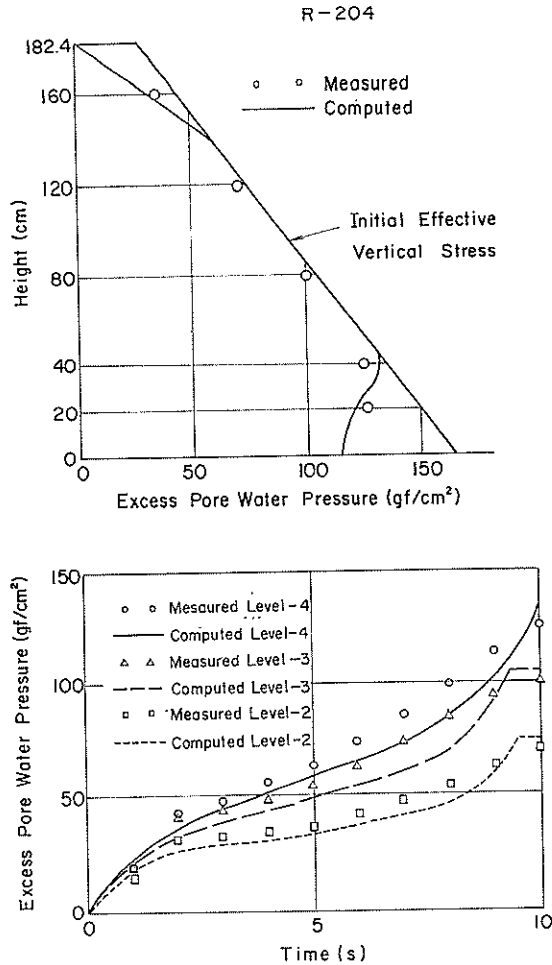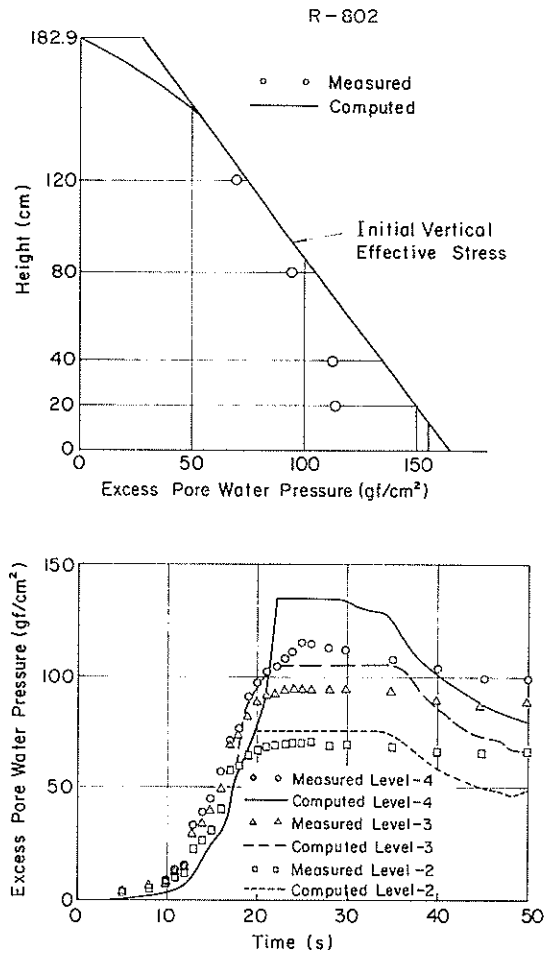
R-204

Fig. 66 Measured and computed excess pore water
pressures for Case R-204(without gravel drain,
sinusoidal input motion, maximum input
acceleration 43 Gals)

(d) Evaluation of the results

Compare the computed results with the test results. If the agreement is not
satisfactory, go back to the step (b) with corrections on the assumed liquefaction
strength curve.

After several trials, the above-mentioned procedure gave the liquefaction
strength curve shown by solid line in **Fig. 63**. The computed results by using this
curve are shown together with the test results in **Figs. 64** through **67**. Distribution
of the maximum values, shown in the upper section, and time histories at several
levels, shown in the lower section, are compared in these figures. Levels-2 through 4
at the lower section in these figures denote, as defined earlier, the level of the pore
water pressure meters; i.e. Level-2 corresponds to P12 through P62, Level-3 to P13
through P63, etc. The measured values plotted in these figures are obtained by

Fig. 67 Measured and computed excess pore water
pressures for Case R-603(without gravel drain,
sinusoidal input motion, maximum input
acceleration 84 Gals)

taking the average over the values measured at the same level. The simulation
over-estimates the excess pore water prssures at Cases R-602 and R-302 but under-
estimates them at Case R-204. At R-603, the simulation gives consistent result
with the test result. It was not possible to get better results with further refine-
ments. Therefore, the author accepted the liquefaction strength curve obtained
by the above-mentioned procedure as the best approximation.

The consistencies between the computed and measured results in **Figs. 64**
through **67** are, in a sense, trivial because the liquefaction strength curve is
obtained by the back-fitting to those data. Whether the liquefaction strength curve
will give a consistent result with the other data is still to be known. Case R-802,
which was conducted without gravel drain under earthquake motions, is used in this
context. The results, as shown in **Fig. 68**, indicate that the simulation gives a good
approximation on the test result.

— 124 —

Fig. 68 Measured and computed excess pore water
pressures for Case R–802(without gravel drain,
earthquake input motion, maximum input
acceleration 105 Gals)

Consequently, the liquefaction strength curves shown in **Fig. 63** together with
the above-mentioned procedure for generation of excess pore water prssures will be
considered as the bases for analysing the performance of the gravel drain hereafter.

The relative density of the model sand deposits was, as mentioned previously,
about 29%. However, the relative density of the model composite ground, made of
the sand deposit and the gravel drain, was about 33%. Therefore, a correction is
applied for taking the difference of the relative densities into account; the lique-
faction strength is scaled up in proportion to the relative density. The liquefaction
strength curve shown by a broken line in **Fig. 63** is the result of the correction.

4.3 Increase of excess pore water pressures

By using the liquefaction properties of the sand deposit thus obtained, the
performances of the composite grounds, made of the sand deposit and the gravel
drain, were simulated by the formulation with Eqs. (1) and (4).
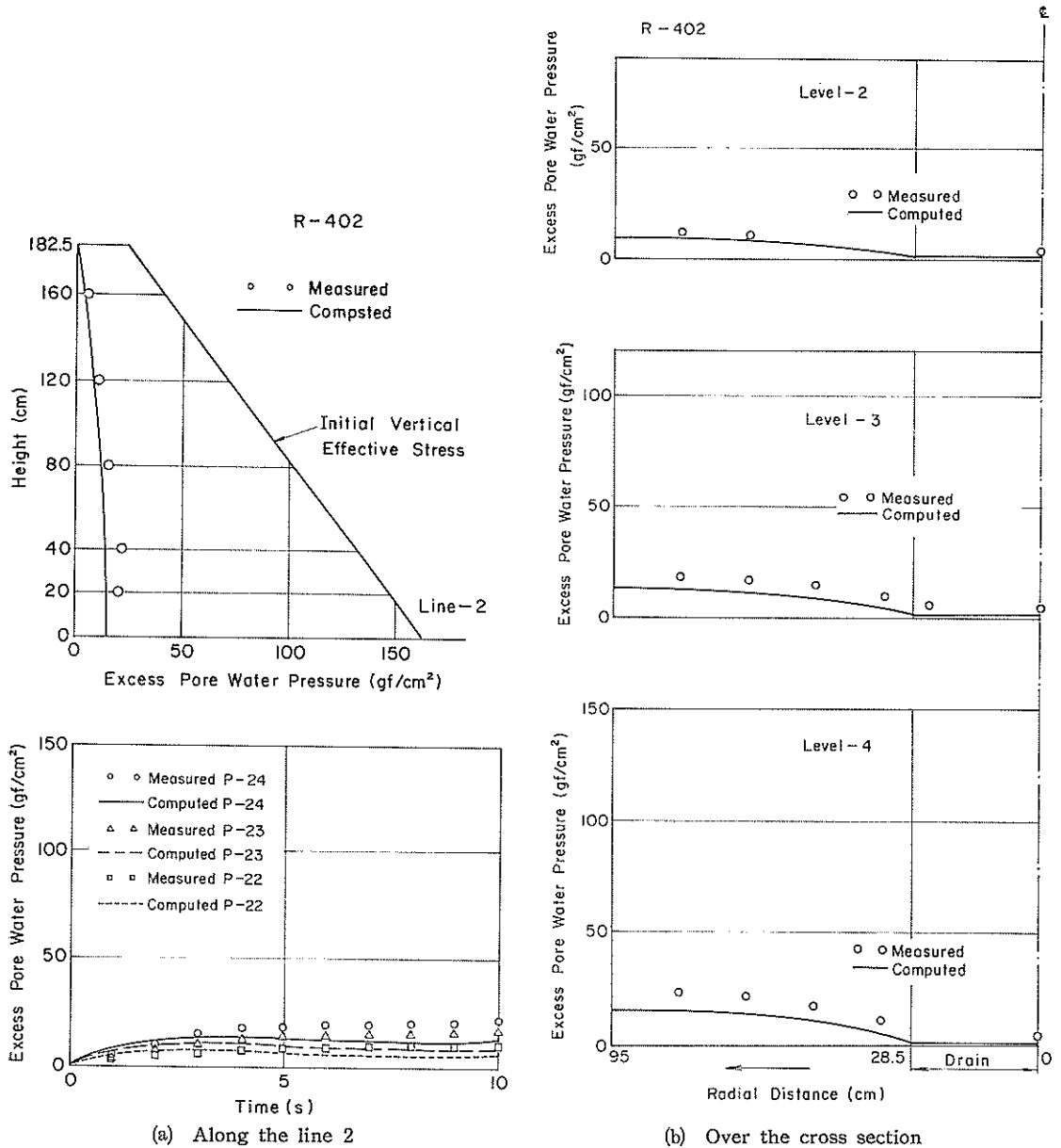
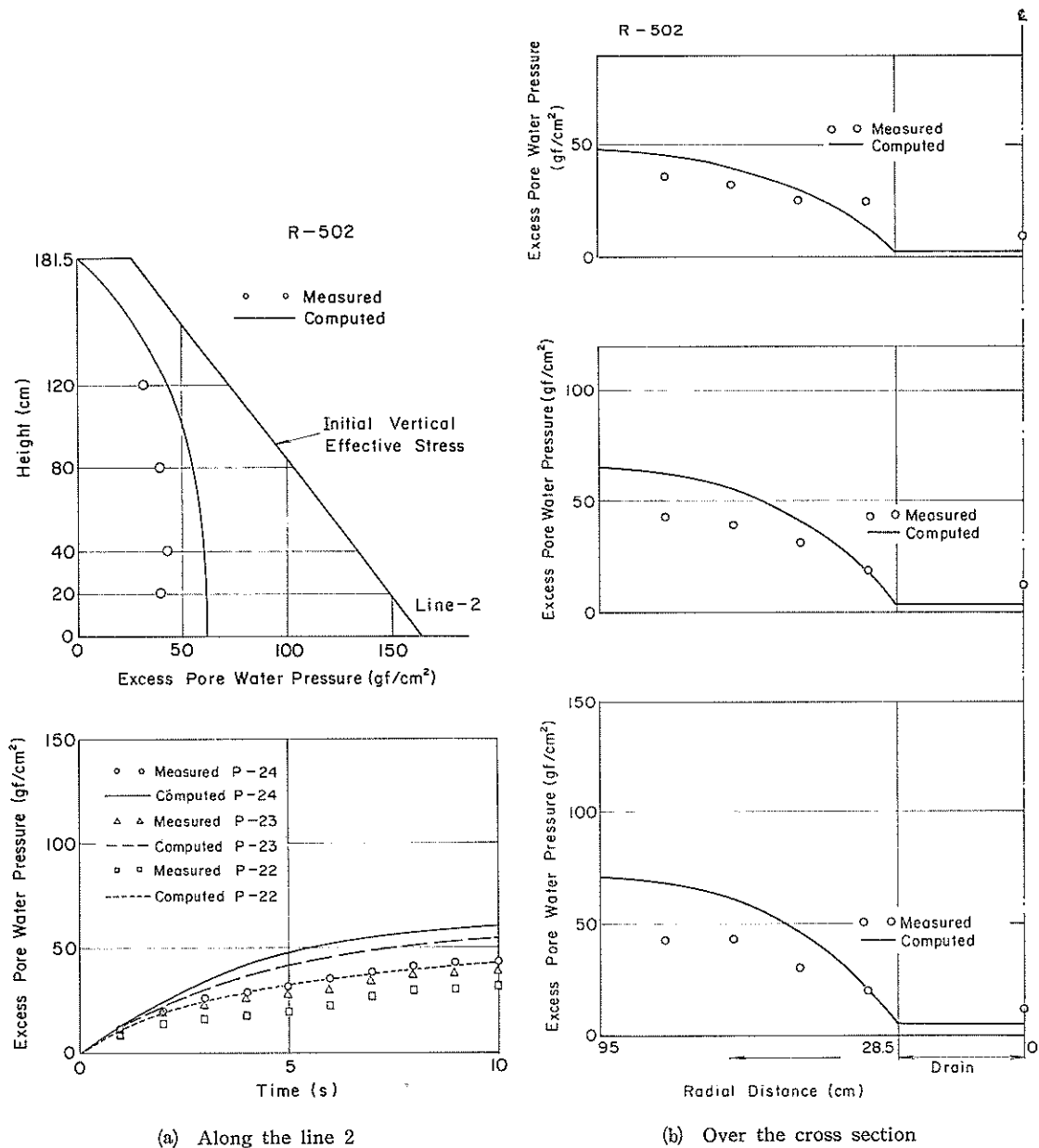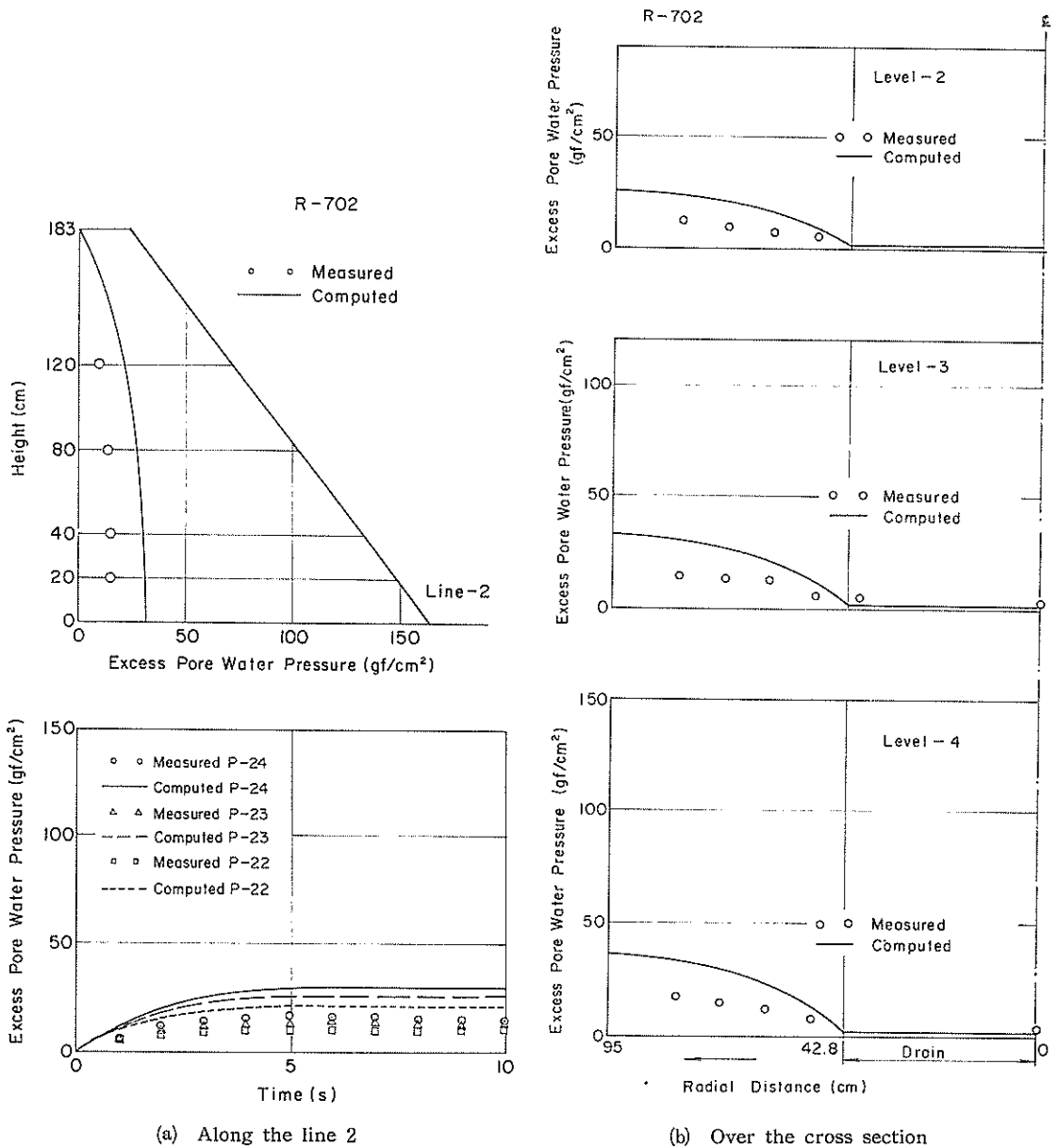**Fig. 69** Measured and computed excess pore water water pressures for Case R-402 (with gravel drain a/b=0.3, sinusoidal input motion, maximum input acceleration 50 Gals)

In addition to the properties of the sand deposit, properties of the gravel drain should be given for the simulation; i.e. the coefficient of permeability, the coefficient of volume compressibility, and the properties on the generation of excess pore water pressures of the gravel drain. The coefficient of permeability of the gravel drain depends on the hydraulic gradient as shown in **Fig. 12**. For simplicity, a representative value of 5 cm/s was used for the simulations conducted in this section.

As for the compressibility of the crushed stones, there is no measurement.
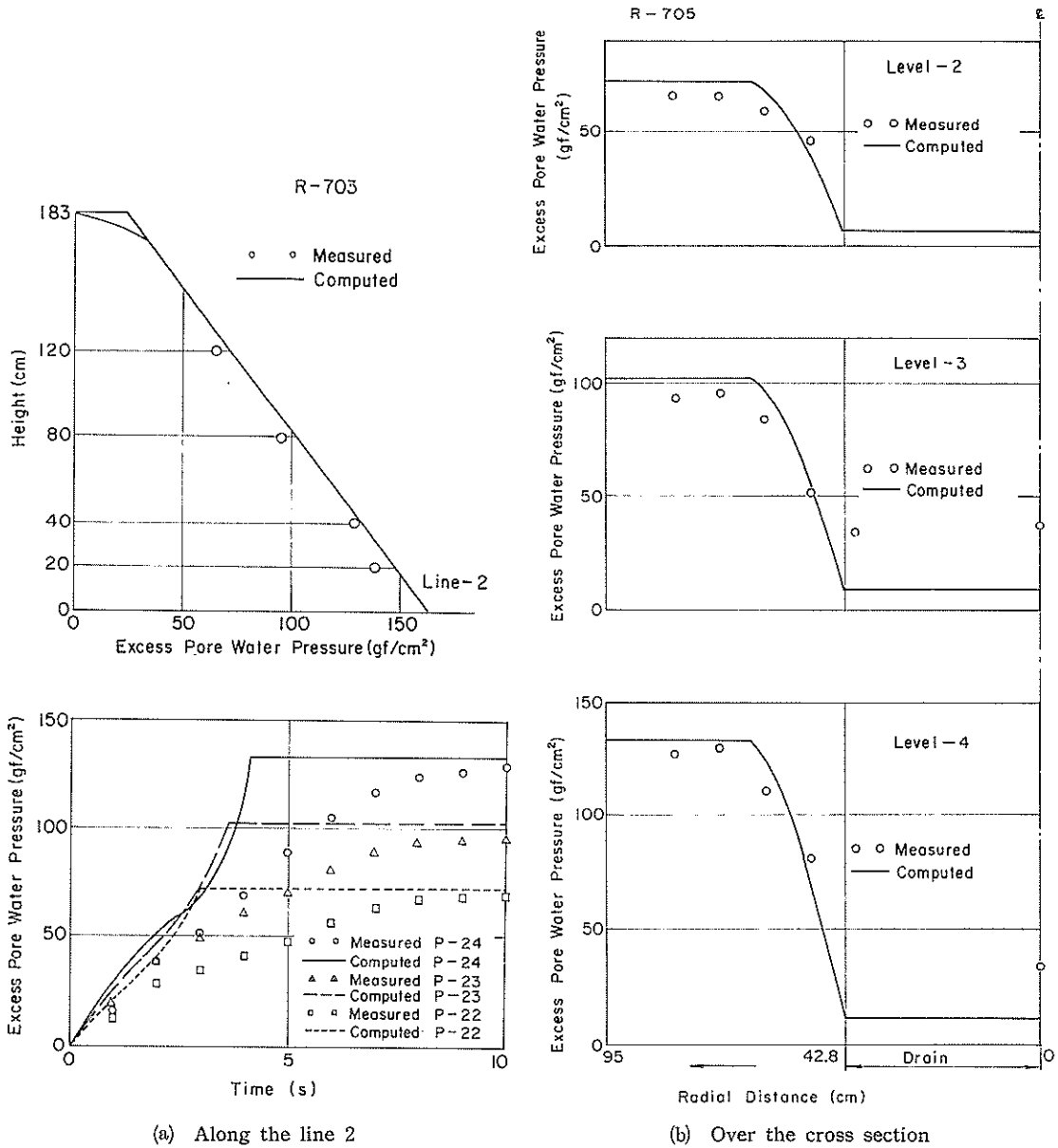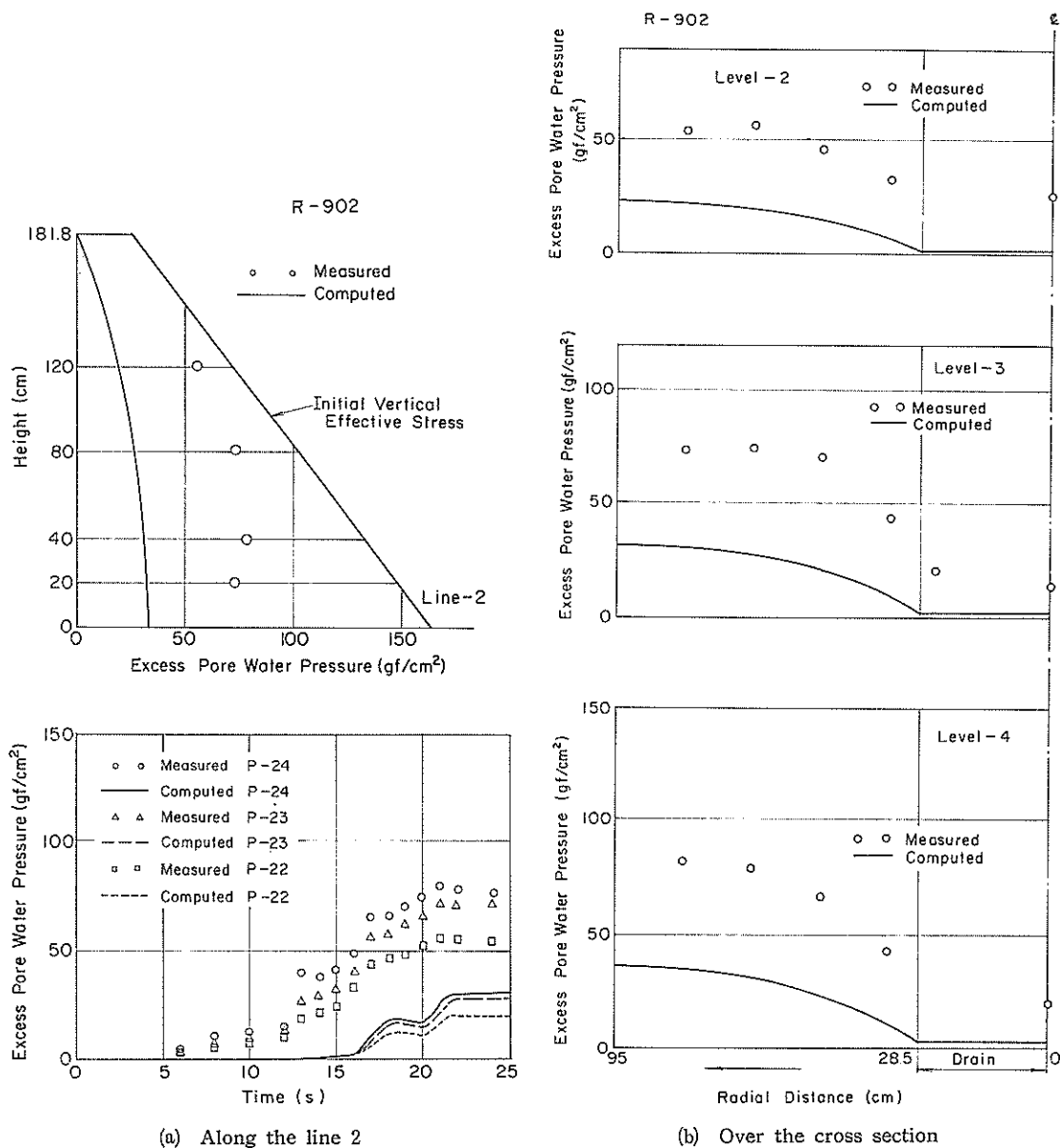
(a) Along the line 2

(b) Over the cross section

Fig. 70 Measured and computed excess pore water pressures for Case R-502 (with gravel drain a/b=0.3, sinusoidal input motion, maximum input acceleration 50 Gals)

Therefore, the value should be given from other sources. Lee and Albeisa (1974)[23] gave a correlation between the coefficient of volume compressibility and D_{50}. According to this correlation, No. 7 crushed stones with $D_{50}=3.4$ mm has $m_v=6.6\times10^{-3}$ cm²/kgf. This correlation is, however, obtained under the confining pressure of 1 kgf/cm², which is quite different from the confining pressure at the model tests conducted in the present study. The influence of difference in the confining pressures can be corrected if the result of the coefficient of volume compressibility of the sand is

Fig. 71 Measured and computed excess pore water pressures for Case R-702 (with gravel drain a/b=0.45, sinusoidal input motion, maximum input acceleration 51 Gals)

taken into account; i.e. the coefficient of valume compressibility at the shaking table tests shown in **Fig. 57** is about five times as great as that obtained by the triaxial test conducted under the confining pressure of 1 kgf/cm² as shown in **Appendix B**. Therefore, the same factor, i.e. about five, is used as a correction of confining pressures, giving the coefficient of volume compressibility of the crushed stone as 0.03 cm²/kgf.

The properties on the generation of excess pore water pressures for the crushed

(a) Along the line 2   (b) Over the cross section

Fig. 72 Measured and computed excess pore water pressures for Case R-703 (with gravel drain a/b=0.45, sinusoidal input motion, maximum input acceleration 82 Gals)

stones should also be given. The result of the settlement, as shown in **Fig. 39**, indicates that the settlements do occur at the gravel drain. Therefore, some amount of the excess pore water pressure is considered to have been generated in the crushed stones. For simplicity, however, the generation of excess pore water pressures from the gravel drain is assumed to be none for the present study.

Having determined thus all the properties necessary for the simulation, the performances of the composite ground are simulated by using finite element method

Susumu IAI

(a) Along the line 2

(b) Over the cross section

Fig. 73 Measured and computed excess pore water pressures for Case R-902 (with gravel drain
a/b=0.3, earthquake input motion, maximum input acceleration 99 Gals)

under the formulation of Eqs. (1) and (4). Comparisons with the test results are
shown in **Figs. 69** through **73**. In these figures, Line-2 indicated in the upper section
in (a) denotes, as defined earlier, the measured values at P21-P25 in **Fig. 3**. The
meaning of the Level-2, etc. in (b) is the same as mentioned in the previous section.
The results shown in **Figs. 69** through **73** indicate, except for Case R-902, the simula-
tion slightly over-estimates the excess pore water pressures in the sand deposit.
However, the simulation slightly under-estimates them in the gravel drain. In Case

— 130 —
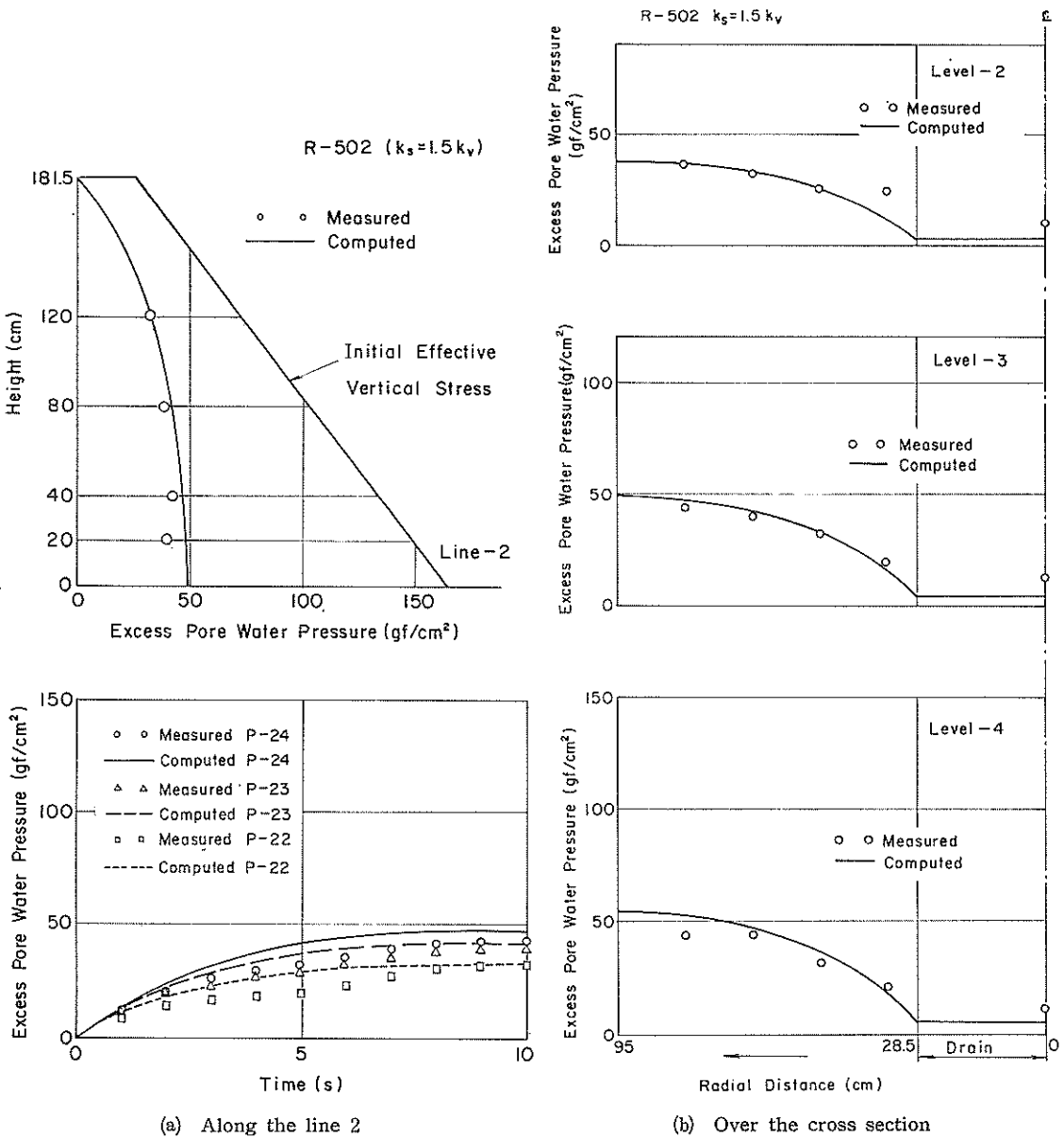
Fig. 74 Measured and computed, with modified permeability, excess pore water pressures for Case R–502 (with gravel drain a/b=0.3, sinusoidal input motion, maximum input acceleration 50 Gals)

R-902, which was conducted under the earthquake motion, the simulation under-estimates the excess pore water pressures in the sand to the factor of two. Moreover, the simulation significantly under-estimates them in the gravel drain.

As a trial for correcting the over-estimation in Cases R-502 and 703, the coefficient of the permeability of the sand deposit in the horizontal direction was taken 1.5 times as great as that in the vertical direction. However, the results, as shown in
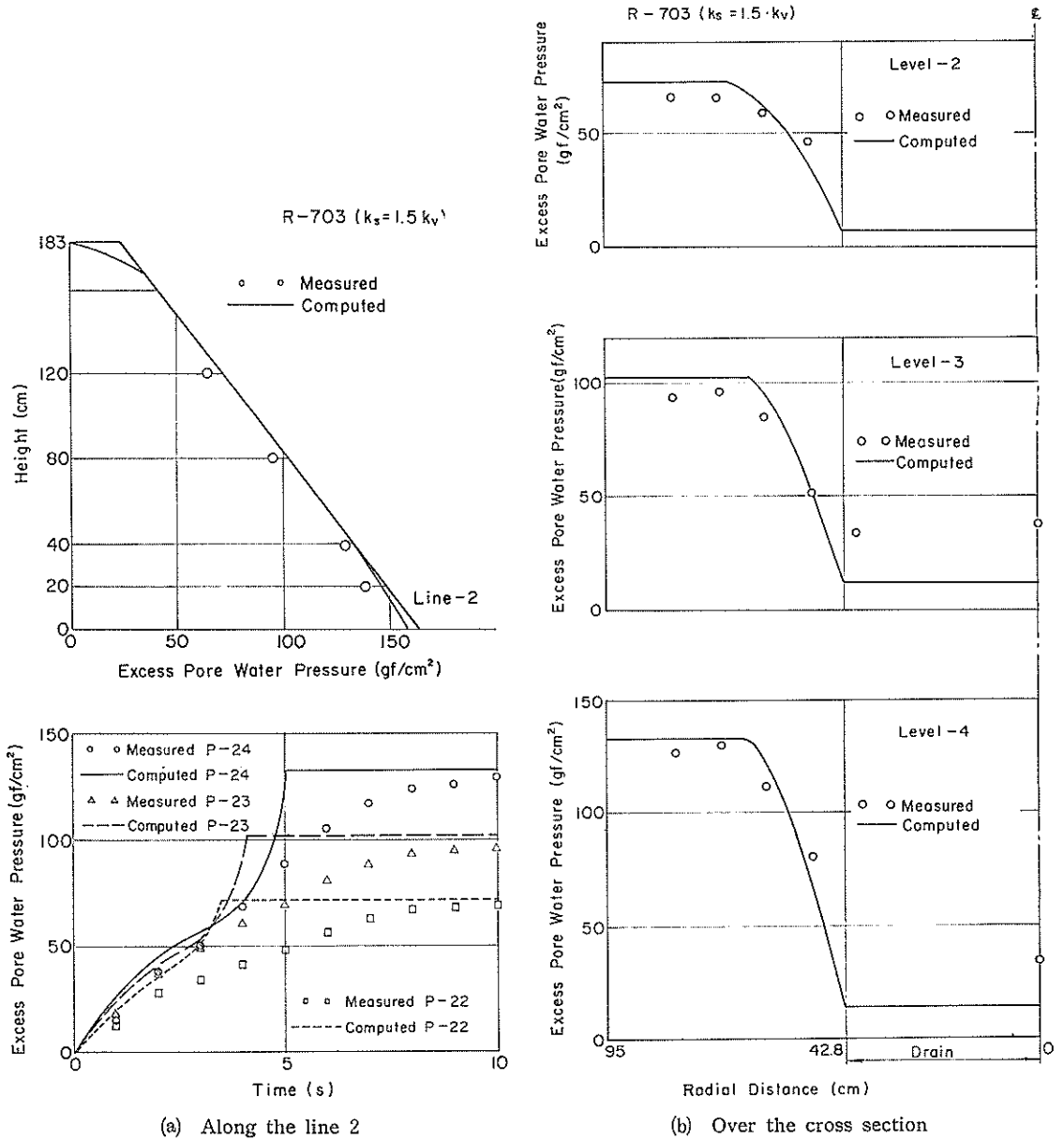
Fig. 75 Measured and computed, with modified permeability, excess pore water pressures for Case R-703 (with gravel drain a/b=0.45, sinusoidal input motion, maximum input acceleration 82 Gals)

Figs. 74 and 75, did not significantly improved.

There may be several reasons which can explain the differences between the computed and the measured results. The author suspects that the negligence on the excess pore water pressure generation from the gravel drain itself might be a major reason. Indeed, as mentioned previously, the excess pore water pressures in the gravel drain are under-estimated at all the tests. Besides, the settlements were
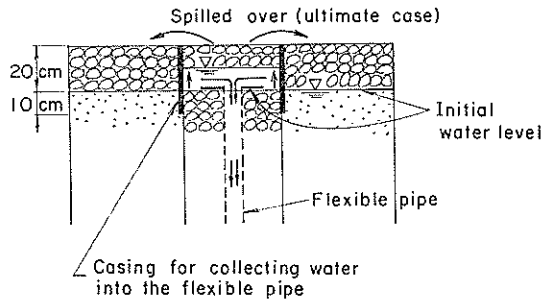
Fig. 76 Schematic figure for the influence of casing for collecting water into the flexible pipe
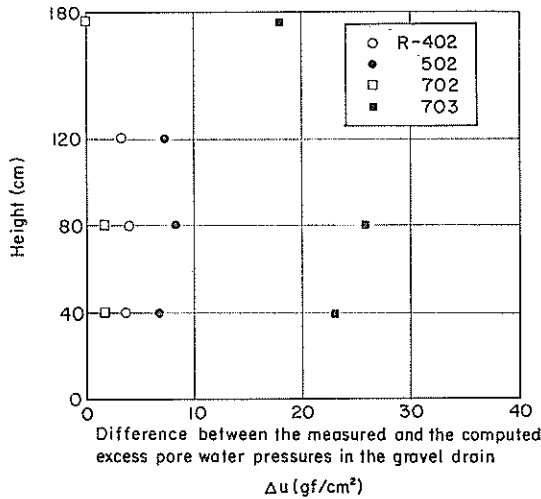
Fig. 77 Difference between the measured and the computed excess pore water pressures in the gravel drain

observed at the gravel drain as well as at the sand deposit surrounding the gravel drain. Apart from the generation of excess pore water pressures, it is also suspected that the casing, shown in **Fig. 76**, which is used for collecting the drained water towards the flexible pipe, might be a cause for the higher excess pore water pressures observed in the gravel drain. If the rate of the flow from the gravel drain is too high to drain out the water through the flexible pipe, the level of the water within the casing might rise to a certain level. The vertical distributions of the excess pore water pressures suggest, as shown in **Fig. 77**, that this is probable because the difference between the computed and the measured excess pore water pressures does not vary along the depth.

With the limited information presently available on the model tests, however, it is not possible to draw a definitive conclusion upon the inconsistencies between the computed and measured data. Consequently, the author draws the conclusion from these results that the formulation with Eqs. (1) and (4) gives a good approximation on the performance of the composite ground if we allow the safety factor of
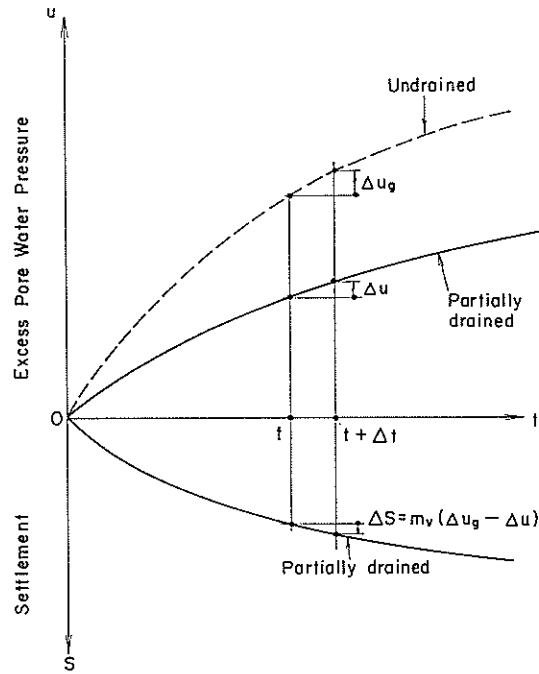
**Fig. 78** Schematic figure for the settlements under partially drained conditions
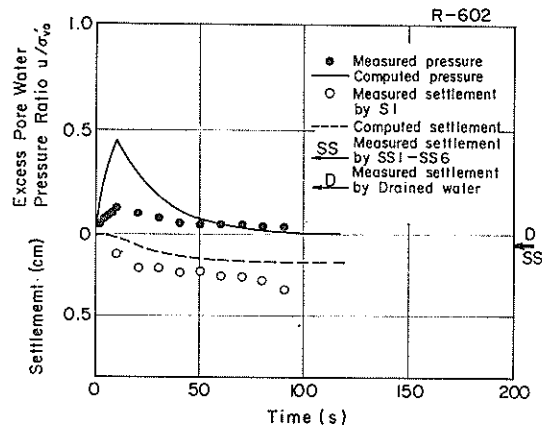
Fig. 79 Measured and computed excess pore water pressures, in long term, and settlements for Case R-602 (without gravel drain, sinusoidal input motion, maximum input acceleration 30 Gals)

about two on the value of the excess pore water pressures. In the meantime, it is advisable that the density of the gravel drain be higher enough to prevent the generation of excess pore water pressures from the gravel drain itself or, equivalently, to prevent the settlement of the gravel drain itself.
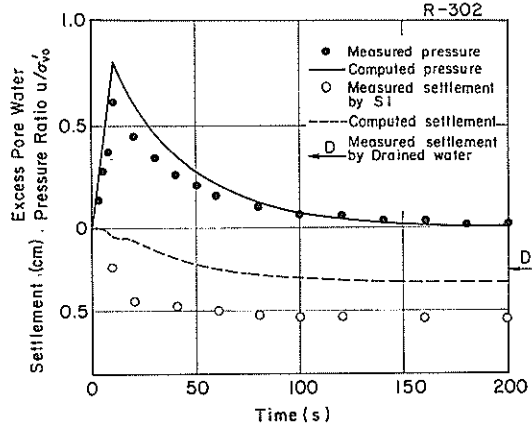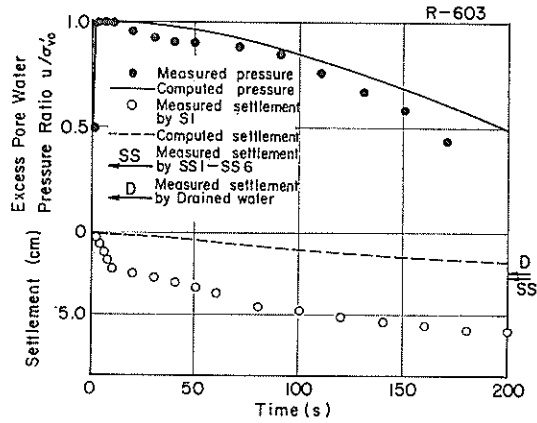
Fig. 80 Measured and computed excess pore water pressures, in long term, and settlements for Case R-302 (without gravel drain, sinusoidal input motion, maximum input acceleration 50 Gals)
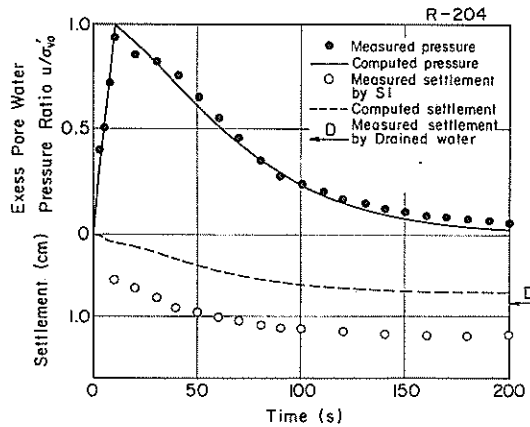
Fig. 81 Measured and computed excess pore water pressures, in long term, and settlemenns for Case R-204 (without gravel drain, sinusoidal input motion, maximum input acceleration 43 Gals)

4.4 Dissipation of excess pore water pressures and settlements

In the previous section, only the increase in the excess pore water pressures in the composite ground was studied. In this section, the performance of the gravel drain in the longer term will be studied so that dissipation of excess pore water pressures and settlements will be better understood. Before going into the comparison between the computed and the measured results, there are two items which should be explained here upon the simulation conducted in this section; one being the modified coefficient of permeability in the gravel drain and the other being the procedure to compute the settlements.

In the previous section, the coefficient of the permeability of the gravel drain

Fig. 82 Measured and computed excess pore water pressures, in long term, and settlements for Case R–603 (without gravel drain, sinusoidal input motion, maximum input acceleration 84 Gals)
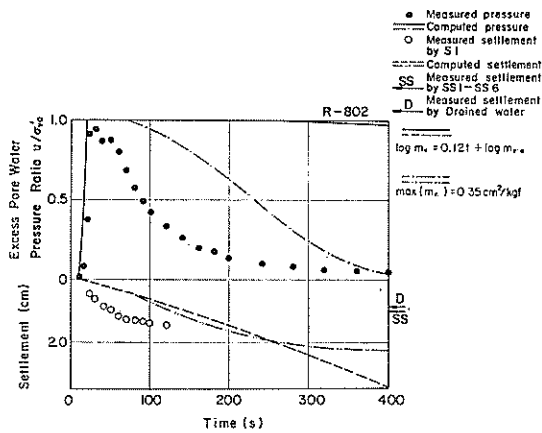

Fig. 83 Measured and computed excess pore water pressures, in long term, and settlements for Case R–802 (without gravel drain, earthquake input motion, maximum input acceleration 105 Gals)

was fixed to the value of 5 cm/s for simplicity. In this section, the coefficient of the permeability of the gravel drain is given as a function of hydraulic gradient, density of the gravel drain, and temperature of water. The function of hydraulic gradient used for the present study is given in **Fig. 12**.

The procedure to compute the settlement during and after the shaking is as follows. As schematically illustrated in **Fig. 78**, u_g given by Eq. (4) will not be the same as the excess pore water pressures u during the process under the partially drained conditions, as in the sand deposit surrounding the gravel drain. Partially drained water obviously causes settlement during or after the shaking. The increment of the settlement Δs during the time interval Δt is, as indicated by Eq. (1),
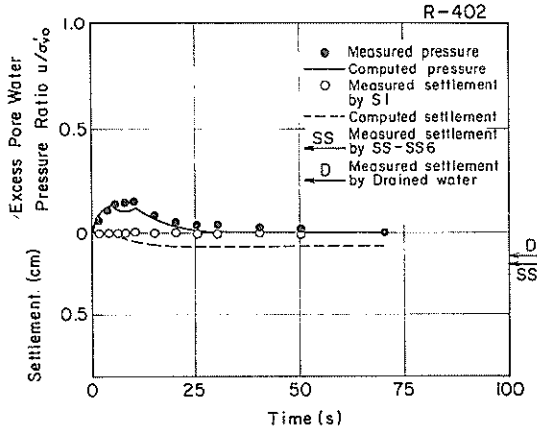
Fig. 84 Measured and computed excess pore water
pressures, in long term, and settlements for
Case R-402 (with gravel drain a/b=0.3,
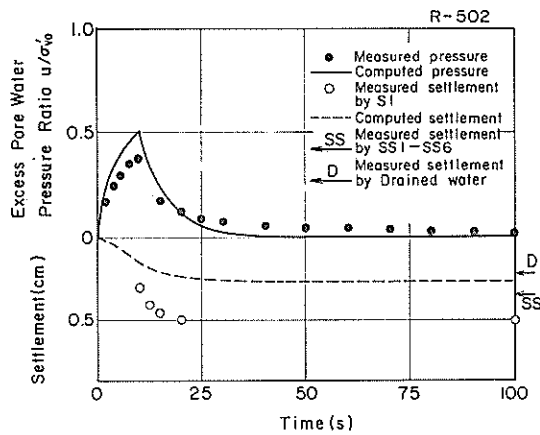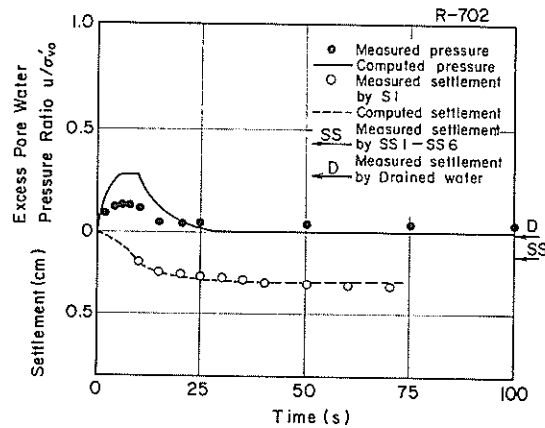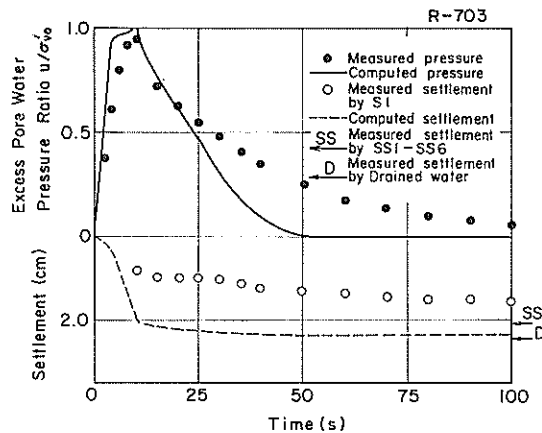sinusoidal input motion, maximum input
acceleration 50 Gals)

Fig. 85 Measured and computed excess pore water
pressures, in long term, and settlements for
Case R-502 (with gravel drain a/b=0.3,
sinusoidal input motion, maximum input
acceleration 50 Gals)

given by the following equation:

$$\Delta s = m_v (\Delta u_0 - \Delta u) \tag{7}$$

in which

Δs : increment of the settlement

m_v : coefficient of volume compressibility

Δu_0 : increment of the excess pore water pressures under undrained condition

Δu : increment of the excess pore water pressures

The settlements as well as the excess pore water pressures during and after

— 137 —

Fig. 86 Measured and computed excess pore water
pressures, in long term, and settlements for
Case R–702 (with gravel drain a/b=0.45,
sinusoidal input motion, maximum input
acceleration 51 Gals)

Fig. 87 Measured and computed excess pore water
pressures, in long term, and settlements for
Case R–703 (with gravel drain a/b=0.45,
sinusoidal input motion, maximum input
acceleration 82 Gals)

the shaking are thus computed and are shown in **Figs. 79** through **88** together with
the results of the model tests. In these figures, settlements are obtained or con-
verted at the level of 120 cm in the sand deposit. The white circles shown in these
figures are the data obtained by the settlement gauge S1 in Fig. 3. The drifting
errors contained in the values measured by this gauge are, as mentioned before,
about 1 mm/min. The residual settlements are measured, in addition to those
measured by the settlement gauge S1, by the settlement gauges SS1 through SS6
placed on the surface of the sand deposit. Furthermore, the residual settlements
are also obtained by the measured amount of the drained water. Three kinds of
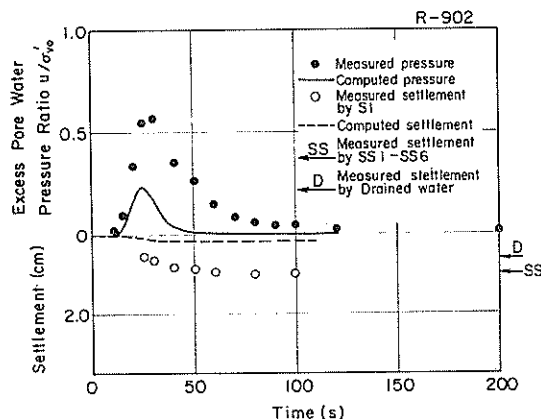settlements obtained by these methods are sometimes turned out to be inconsistent

Fig. 88 Measured and computed excess pore water pressures, in long term, and settlements for Case R-902 (with gravel drain a/b=0.3, earthquake input motion, maximum input acceleration 99 Gals)

with each other as shown in **Figs. 79** through **88**. It was not possible which value was most reliable. Therefore, when the computed settlements are within the range of the measured values by the three kinds of methods, it will be determined that the computed and the measured values are consistent with each other within the order of the discrepancy between the measured settlements.

The result of each case, shown in **Figs. 79** through **88**, is summarized as follows:

(a) Case R-602 (without the gravel drain, under sinusoidal motion, maximum input acceleration 30 Gals)

The simulation over-estimated the excess pore water pressures as shown in **Fig. 79**. However, the simulation gave a reasonable approximation on the settlements within the order of the discrepancy between the measured settlements.

(b) Case R-302 (without the gravel drain, under sinusoidal motion, maximum input acceleration 50 Gals)

The simulation gave a reasonable approximation on the excess pore water pressures as shown in **Fig. 80**. The simulation also gave a reasonable approximation on the settlements within the order of the discrepancy between the measured settlements.

(c) Case R-204 (without the gravel drain, under sinusoidal motion, maximum input acceleration 43 Gals)

The simulation gave a reasonable approximation on the excess pore water pressures as shown in **Fig. 81**. However, the simulation slightly under-estimated the settlements.

(d) Case R-603 (without the gravel drain, under sinusoidal motion, maximum input acceleration 84 Gals)

The simulation gave a reasonable approximation on the excess pore water pressures as shown in **Fig. 82**. However, the simulation slightly under-estimated the settlements.

(e) Case R-802 (without the gravel drain, under earthquake motion, maximum input acceleration 105 Gals)

Susumu IAI

The simulation gave a good approximation on the rate of increase in the excess pore water pressures. However, the empirical equation for the coefficient of volume compressibility after liquefaction, indicated in **Fig. 83**, could not give a good approximation to the longer term behaviour under earthquake motions. As a trial, the maximum value of the coefficient of compressibility was limited to the value of 0.35 cm²/kgf, which was the maximum value obtained at the case of sinusoidal input motions as shown in **Fig. 57**. The computed results, as shown in **Fig. 83**, were not improved very much.

(f) Case R-402 (with the gravel drain, the spacing ratio $a/b=0.3$, under sinusoidal input motion, maximum input acceleration 50 Gals)

The simulation gave a reasonable approximation on the excess pore water pressures as shown in **Fig. 84**. The simulation also gave a reasonable approximation on the settlements within the order of the discrepancy between the measured settlements.

(g) Case R-502 (with the gravel drain, the spacing ratio $a/b=0.3$, under sinusoidal input motion, maximum input acceleration 50 Gals)

The simulation gave a reasonable approximation on the excess pore water pressures as shown in **Fig. 85**. The simulation also gave a reasonable approximation on the settlements within the order of the discrepancy between the measured settlements.

(h) Case R-702 (with the gravel drain, the spacing ratio $a/b=0.45$, under sinusoidal input motion, maximum input acceleration 51 Gals)

The simulation over-estimated the excess pore water pressures as shown in **Fig. 86**. The simulation slightly over-estimated the settlements.

(i) Case R-703 (with the gravel drain, the spacing ratio $a/b=0.45$, under sinusoidal input motion, maximum input acceleration 82 Gals)

The simulation over-estimated the rate of increase in the excess pore water pressures as shown in **Fig. 87**. The simulation also over-estimated the rate of dissipation in the excess pore water pressures. The lower rate in the measured dissipation of excess pore water pressures might be partly due to the rise of the water level within the casing for collecting the drained water as shown in **Fig. 76**. The simulation slightly over-estimated the settlements within the order of discrepancy between the measured settlements.

(j) Case R-902 (with the gravel drain, the spacing ratio $a/b=0.3$, under earthquake input motion, maximum input acceleration 99 Gals)

The simulation under-estimated the excess pore water pressures as shown in **Fig. 88**. The simulation also under-estimated the settlements.

All the over- or under-estimations revealed in these results are of the order of factor two. As a conclusion drawn from the above results, the simulation with Eqs. (1) and (4) gives a reasonable approximation on the performance of the gravel drain if we allow the safety factor of about two on the excess pore water pressures and the settlements. It is also suggested from the above results that the dissipation of excess pore water pressures at the high excess pore water pressure ratios, especially after liquefaction, needs further study. These conclusions suggest that the maximum excess pore water pressure ratios which will be allowed at the design of the gravel drain should not be very high even if the stability analysis happens to allow higher values on the excess pore water pressure ratios.

4.5 General applicability of the model

In the present study, the maximum effort has been paid for obtaining the reliable data on the performance of the gravel drain. These data comfirm that the simple model, i.e. Eqs. (1) and (4), gives a reasonable approximation on the performance of the gravel drain if we allow the safety factor of about two on the excess pore water

pressures and the settlements.

Obviously, the conditions on the sand deposit, the gravel drain, and the input motion given for designing the gravel drain will not be, in general, the same as the ones which have been covered in the present study. Besides, a definitive comfirmation on the applicability of the model should wait the in-situ measurement on the performance of the gravel drain during the earthquakes. However, it may require many years to acquire the necessary data. In the meantime, the simple model, i.e. Eqs. (1) and (4), is considered a useful tool to provide a guideline for designing the gravel drain, especially for providing the approximations on the increasing and decreasing rate of excess pore water pressures, the maximum excess pore water pressures, and the residual settlements.

When the simple model is used in designing the gravel drain, one thing has to be reminded; the sensitivity of the performance of the gravel drain. As shown in the results of the experiments and the analyses, the maximum values of the excess pore water pressures are very sensitive to the slight variations in the properties of the sand deposit and the intensity levels and other properties of the input motions. Besides, the properties in the dissipation of excess pore water pressures and those in the settlements drastically change once the sand deposit liquefies. Therefore, as mentioned earlier, the maximum excess pore water pressures which will be allowed at the design of the gravel drain should not be very high even if the stability analysis of the sand deposit allows high value.

5. Conclusions

Nine series of the shaking table tests were conducted by using large scale models of sand deposit with and without a gravel drain; dimensions of the model were about two meters in diameter and two meters in height. The tests were conducted under sinusoidal and earthquake input motions. The results of the tests are analysed by using a model of consolidation with an additional term for generating excess pore water pressures. The following conclusions are obtained from the present study;

(1)   The excess pore water pressures at the sand deposit dissipate according to the mechanism of consolidation if the maximum excess pore water pressures attained during the shaking is less than about half of the initial vertical effective stress. Once the maximum excess pore water pressures go beyond this limit, the rate of the dissipation becomes slower as the maximum excess pore water pressures becomes greater. Especially, once the maximum excess pore water pressures reach the initial vertical effective stress, the rate of dissipation becomes drastically low and becomes dependent on the stress or strain histories applied to the sand deposit.

(2)   The effect of the gravel drain is (i) to reduce the rate of increase in pore water pressures and (ii) to increase the rate of dissipation in pore water pressures. The maximum excess pore water pressures are sensitive to the slight variations in the properties of the sand deposit and the intensity level and other properties of the input motions.

(3)   The settlements are inevitable even if the gravel drain is installed. The pattern of the settlements is of differencial settlement; the settlements at the gravel drain were smaller than those at the sand deposit surrounding the gravel drain. In general, whether the settlements at the gravel drain are smaller than those at the sand deposit or vice vesa depends on the properties of the gravels and the sands. Once the excess pore water pressures reach the value of the initial vertical effective stress, the order of the settlements becomes drastically large.

(4) The simple model based on the mechanism of consolidation with an additional term for generating the excess pore water pressures provides a reasonable approximation on the increasing and the decreasing rates of the excess pore water pressures, the maximum excess pore water pressures, and the settlements within the range of the safety factor of two.

(5) The performance of the gravel drain against the clogging was demonstrated under the conditions similar to those in the field during the earthquakes.

(Received on June 28, 1988)

Acknowledgement

References

1) TSUCHIDA, H., NODA, S., INATOMI, T., UWABE, T., IAI, S., OHNEDA, H., and TOYAMA, S.: Damage to port structures by the 1983 Nihonkai-Chubu Earthquake, *Technical Note of the Port and Harbour Research Institute*, No. 511, March 1985, 447 p. *(in Japanese)*.

2) TSUCHIDA, H., INATOMI, T., NODA, S., YAGYU, T., TABATA, T., TOKUNAGA, S., OTSUKI, Y., and HIRANO, T.: Damage to port structures by the 1978 Miyagi-ken-oki Earthquake, *Technical Note of the Port and Harbour Research Institute*, No. 325, September 1979, 175 p. *(in Japanese)*.

3) ISHIHARA, K., KAWASE, Y., and NAKAJIMA, M.: Liquefaction characteristics of sand deposits at an oil tank site during the 1978 Miyagiken-oki Earthquake, *Soils and Foundations*, Vol. 20, No. 2, June 1980, pp. 97–111.

4) MIZUNO, Y., SUEMATSU, N., and OKUYAMA, K.: Design method of sand compaction pile for sandy soils containing fines, *Tsuchi-to-kiso*, Vol. 35, No. 5, The Japanese Society of Soil Mechanics and Foundation Engineering, May 1987, pp. 21–26 (*in Japanese*).

5) IAI, S., KOIZUMI, K., and KURATA, K.: Basic consideration for designing the area of the ground compaction as a remedial measure against liquefaction, *Technical Note of the Port and Harbour Research Institute*, No. 590, June 1987, 66 p. (*in Japanese*).

6) SEED, H. B. and BOOKER, J. R.: Stabilization of potentially liquefiable sand deposits using gravel drains, *Journal of Geotechnical Engineering Division*, ASCE, Vol. 103, No. GT7, July 1977, pp. 757–768.

7) TOKIMATSU, K. and YOSHIMI, Y.: Effects of vertical drains on the bearing capacity of saturated sand during earthquakes, *International conference on engineering for protection from natural disasters*, Asian Institute of Technology, January 1980, pp. 643–655.

8) TANAKA, Y., KOKUSHO, T., ESASHI, Y., and MATSUI, I.: On preventing liquefaction of level ground using gravel piles, *Proceedings of the Japan Society of Civil Engineers*, No. 352/III-2, December 1984, pp. 89–98 (*in Japanese*).

9) ISHIHARA, K., SAITO, A., and ARIMA, H.: Applying crushed stone piles as a solution to liquefaction problem of revetment, *Tsuchi-to-kiso*, Vol. 28, No. 4, The Japanese Society of Soil Mechanics and Foundation Engineering, April 1980, pp. 9–15 (*in Japanese*).

10) MIYAMAE, S., MATSUSHITA, Y., and TAKANO, J.: On in-situ experiments on the performance of gravel piles as remedial measures against liquefaction, *Proceedings of the Hokkaido Technical Committee in the Japanese Society of Soil Mechanics and Foundation Engineering*, No. 25, February 1985, pp. 77–86 (*in Japanese*).

11) ONOUE, A., MORI, N., and TAKANO, J.: In-situ experiment and analysis on well resistance of gravel drains, *Soils and Foundations*, Vol. 27, No. 2, June 1987, pp. 42–60.

12) TANAKA, Y. and TAKANO, J.: Verification of calculating methods for gravel piles using in-situ liquefaction tests results, *Proceedings of the Japan Society of Civil Engineers*, No. 388/III-8, December 1987, pp. 33–42 (*in Japanese*).

13) IAI, S. and KOIZUMI, K.: Estimation of earthquake induced excess pore water pressure for gravel drains, *Proceedings of the Seventh Japan Earthquake Engineering Symposium*, December 1986, pp. 679–684.

14) IAI, S., KOIZUMI, K., NODA, S., and TSUCHIDA, H.: Large scale model tests and analysis of gravel drains, *19th UJNR (19th Joint Meeting, U.S.-Japan Panel on Wind and Seismic Effects)*, May 1987, 14 p.

15) THE JAPANESE SOCIETY OF SOIL MECHANICS AND FOUNDATION ENGINEERING: Methods for testing soils, pp. 25–188 (*in Japanese*).

16) JAPAN COMMITTEE FOR LARGE DAMS: Design Standard for Dams (Second version), Chapter 5, 1978 (*in Japanese*).

17) OHNO, Y., ITO, K., MINAMIKAWA, Y., and OHKITA, Y.: Short term clogging limit of gravel drain, *Proceedings of the 19th Japan National Conference on Soil Mechanics and Foundation Engineering*, June 1984, pp. 191–192 (*in Japanese*).

18) SHERARD, J., DUNNIGAN, L. P., and TALBOT, J. R.: Basic properties of sand and gravel filters, *Journal of Geotechnical Division*, ASCE, Vol. 110, No. GT6, June 1984, pp. 684–700.

19) ZEN, K., OHNEDA, H., and IRISAWA, K.: Laboratory tests on the clogging of the material used for gravel drains, *Technical Note of the Port and Harbour Research Institute*, No. 534, September 1985, 20 p. (*in Japanese*).

20) SCOTT, R. F.: Solidification and consolidation of a liquefied sand column, *Soils and Foundations*, Vol. 26, No. 4, pp. 23–31.

21) YOSHIKUNI, H. and NAKANODO, H.: Consolidation of soils by vertical drain wells with finite permeability, *Soils and Foundations*, Vol. 14, No. 2, June 1974, pp. 35–46.

22) the same as 6).

23) LEE, K. L. and ALBAISA, A.: Earthquake induced settlements in saturated sand, *Journal of Geotechnical Engineering Division*, ASCE, Vol. 100, No. GT4, April 1974, pp. 387–406.

24) SEED, H. B., MARTIN, P. P., and LYSMER, J.: Pore-water pressure changes during soil liquefaction, *Journal of the Geotechnical Engineering*, ASCE, Vol. 102, No. GT4, April 1976, pp. 323–346.

List of Symbols

A : horizontal sectional area of the element

a : radius of the gravel drain

b : radius of the equivalent circle of the tributary area of the gravel drain

D_{15} : grain size in mm, corresponding to 15% finer by weight, of filtering material used for the gravel drain

d_{85} : grain size in mm, corresponding to 85% finer by weight, of the sand deposit

Dr : relative density

e : void ratio

$e_{\max}$: maximum void ratio

$e_{\min}$: minimum void ratio

f : frequency of shaking

G_0 : shear modulus at small strain level

G_s : specific gravity

g : acceleration of gravity

$H1$: height of top of the gravel layer of the model ground

$H2$: height of top of the sand deposit of the model ground

h : depth of gravel drain

k_s : coefficient of permeability in the horizontal direction in the sand deposit

k_v : coefficient of permeability in the vertical direction in the sand deposit

k_d : coefficient of permeability of the gravel drain

k_{15} : coefficient of permeability of sand deposit at 15°C

m_v : coefficient of volume compressibility of the sand deposit

m_{vd} : coefficient of volume compressibility of the gravel drain

N : number of cycles of cyclic shear stress

N_l : number of cycles required to cause initial liquefaction

$(N_l)_k$: number of cycles required to cause initial liquefaction by the cyclic loadings of which amplitude is the same as that of the k-th half cycle

r : radial coordinate which originates at the center axis of the gravel drain and points outward

Δs : increment of the settlement
t : time coordinate
t_k : time at which the k-th half cycle of shear stress wave ends
t_l : duration of cylic shear stress required to cause initial liquefaction
U_c : coefficient of uniformity
u : excess pore water pressure
u_g : excess pore water pressure which will be generated by the cyclic shear under undrained condition in the sand deposit
u_{gd} : excess pore water pressure which will be generated by cyclic shear under undrained condition in the gravel drain
u_{max} : maximum excess pore water pressure
Δu : increment of the excess pore water pressures
Δu_g : increment of the excess pore water pressures under undrained condition
W_i : weight of i-th element
$\ddot{x}_i$: acceleration of the i-th element
z : vertical coordinate which originates at the bottom level of the gravel drain and points upward
α : an empirically determined constant, which is used in the equation for excess pore water pressure generation (a typical value is 0.7)
α_{max} : maximum input acceleration
ε_a : axial strain in the undrained triaxial test
τ_D : shear stress amplitude at the undrained triaxial test
τ_i : shear stress acting on the lower boundary of i-th element
σ'_c : initial confining pressure at the undrained triaxial test
σ'_{vo} : initial effective vertical stress
γ_{sat} : saturated unit weight of sand
γ_w : unit weight of water

Appendix A   Impulse test and resonant test

The impulse test was conducted by hitting the shaking table with a wooden hammer in the horizontal direction. The upward propagation of impulse wave was clearly observed as shown in **Fig. A1**. In this figure, A0 is the accelerometer at the shaking table and A11-A15 are the accelerometers within the sand deposit located at the heights of 160 cm, 120 cm, 80 cm, 40 cm, and 20 cm as shown in **Fig. 3**. The time marker is inserted at every 0.01 seconds in **Fig. A1**. By reversing the directions of the hits with the wooden hammer, the phase of the initial impulse was confirmed as of a shear wave.

The resonant test was conducted by applying 10 cycles of sinusoidal waves starting from 1 Hz up to 30 Hz. The amplitude of the input motion was less than 5 Gals. The resonant frequency was obtained by using the transfer function between the response of the sand deposit and the input motion. The example of the transfer function is shown in **Fig. A2**. There is a small peak and the corresponding phase shift at about 3 Hz. This pseudo resonance was identified, by using the pair of accelerometers AV1 and AV2 in **Fig. 3** measuring the vertical components, as of the rocking motion of the whole system. The resonant frequency identified as of the shear response was 8.5 Hz in the case shown in **Fig. A2**.
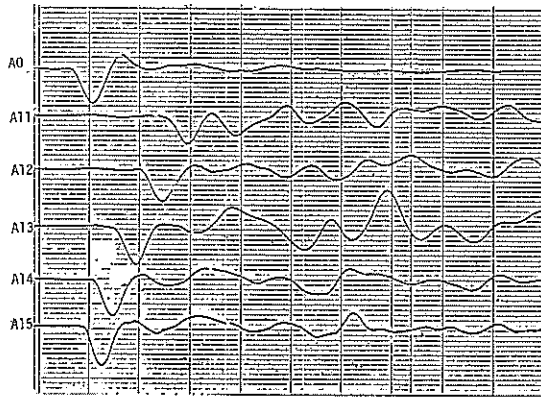
Fig. 1 Result of an impulse test
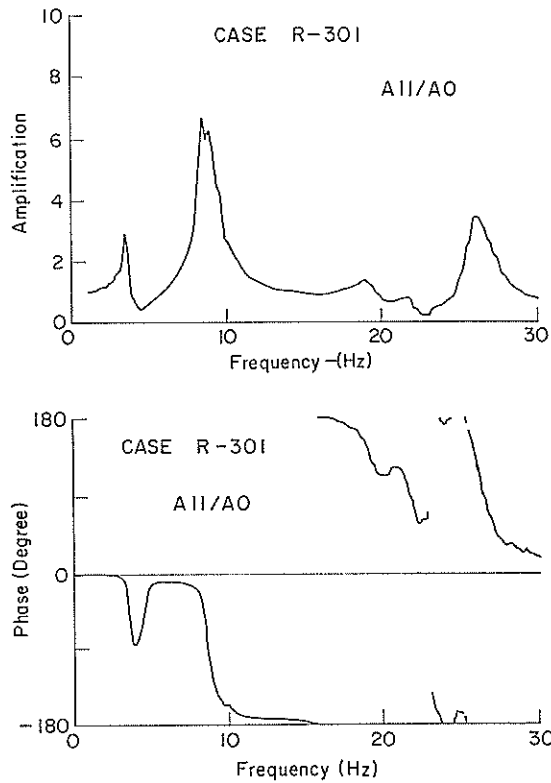
Fig. A2 Result of a resonant test

Appendix B   Properties of the sand obtained by triaxial test

The sand used for the present study was tested with a trixial test apparatus by Mr. K. Irisawa, Member of Soil Dynamics Laboratory. Unfortunately the sand used for the trixial test was not exactly the same as the sand used for the shaking tests conducted in the present study; fines in the amount of less than 5% are contained in the sand used for the triaxial test while the fines were completely washed out for the sand used for the shaking tests. e_{max} and e_{min} for the sand used for the triaxial test were 1.300 and 0.793, which are slightly different from the values obtained for the sand used for the shaking tests. However, the relative densities were calculated using the values obtained for the sand used for the shaking tests.

The results of the undrained triaxial cyclic loading tests are shown in **Figs. B1** and **B2**. The initial confining pressure used for the tests was 1.0 kgf/cm². The coefficients of volume compressibility were obtained by measuring the amount of the drained water after the undrained triaxial cyclic loadings. The same initial confining pressure was used. The results are presented in **Fig. B3**.
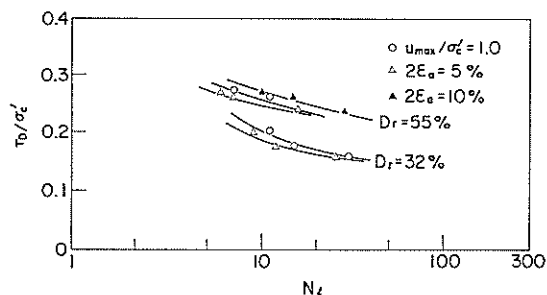
Fig. B1   Results of the undrained cyclic triaxial tests

(a)   Dr=32%   (b)   Dr=55%
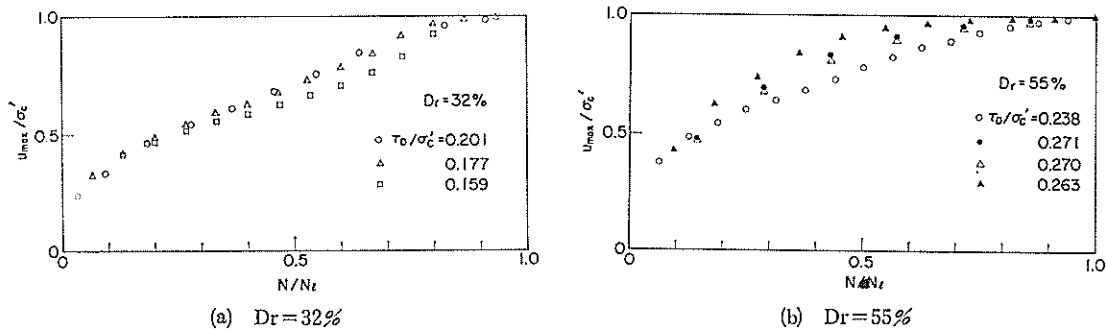
Fig. B2   Pore water pressure generation curves

(a) Dr＝30—35%

(b) Dr＝35—40%
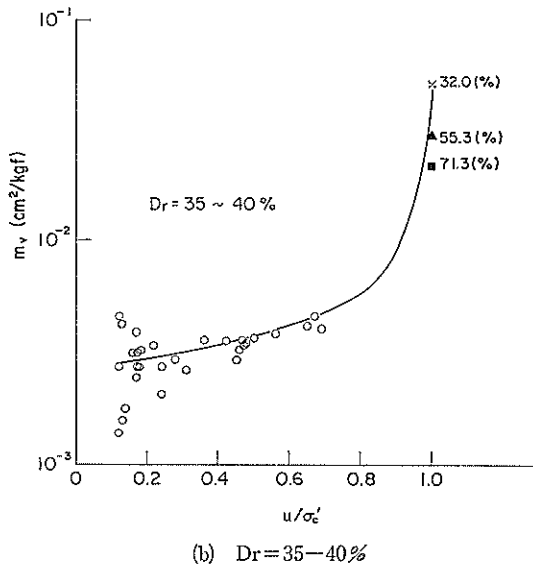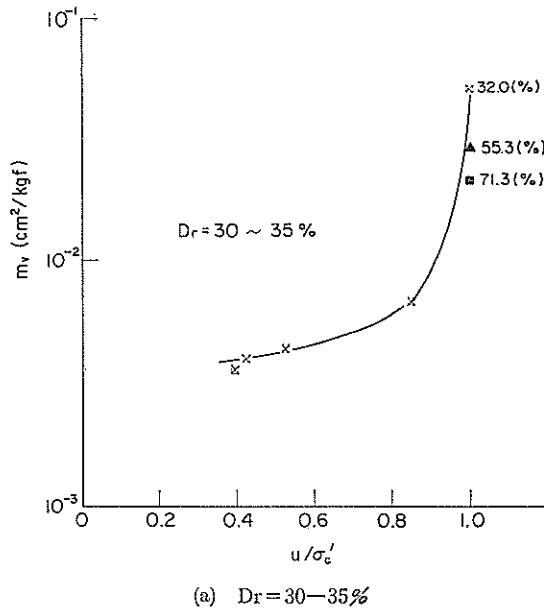
Fig. B 3 Coefficient of compressbility after excess
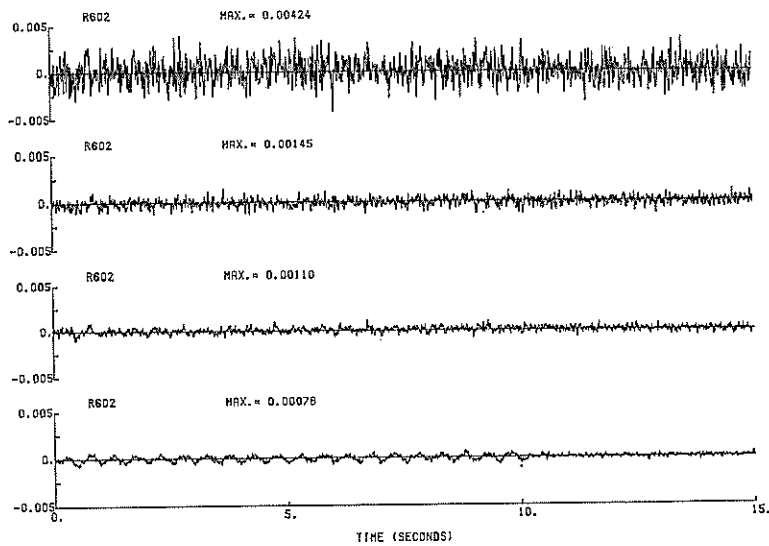pore pressure rise (to be continued)
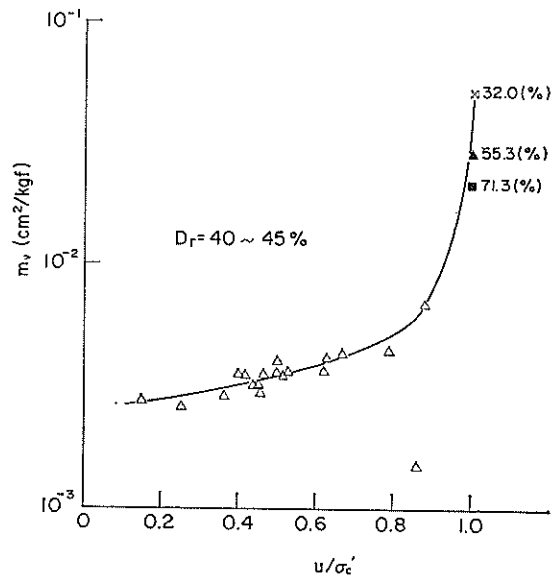
(c) Dr＝40—45%

Fig. B3 Coefficient of compressibility after excess
pore pressure rise

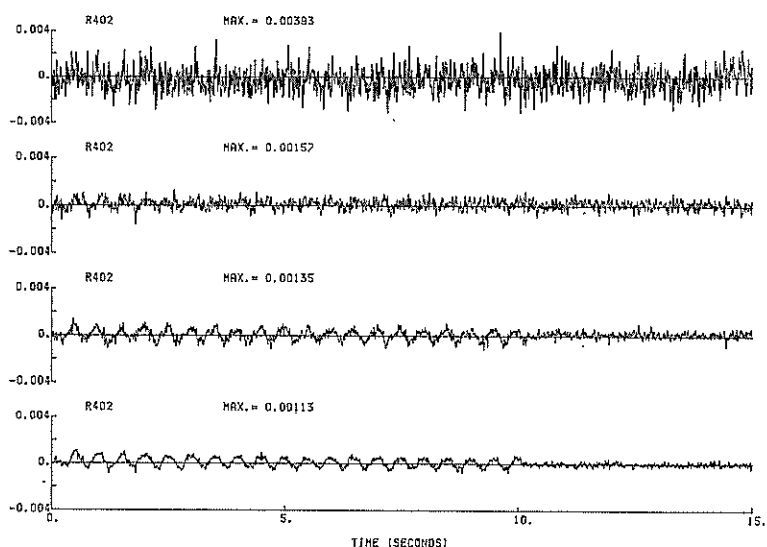## Appendix C   Time histories of the shear strains

The time histories of the shear strains were obtained from the measured displacements. The results are shown in **Fig. C1**.
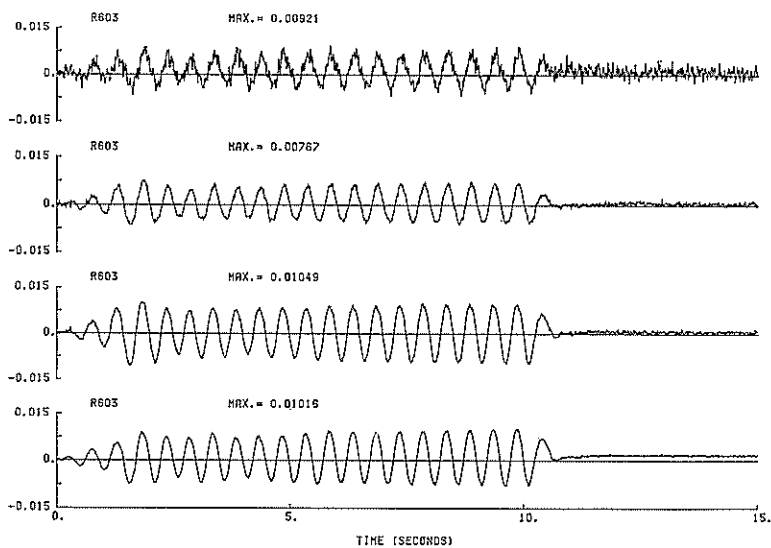

(a)   Case R—602 (without gravel drain, sinusoidal input motion, maximum acceleration 30 Gals)

Fig. C1   Time histories of the shear strains at the height of, from the upper most row, 140cm, 100cm 40cm, and 30cm obtained from measured displacements by H11–H15
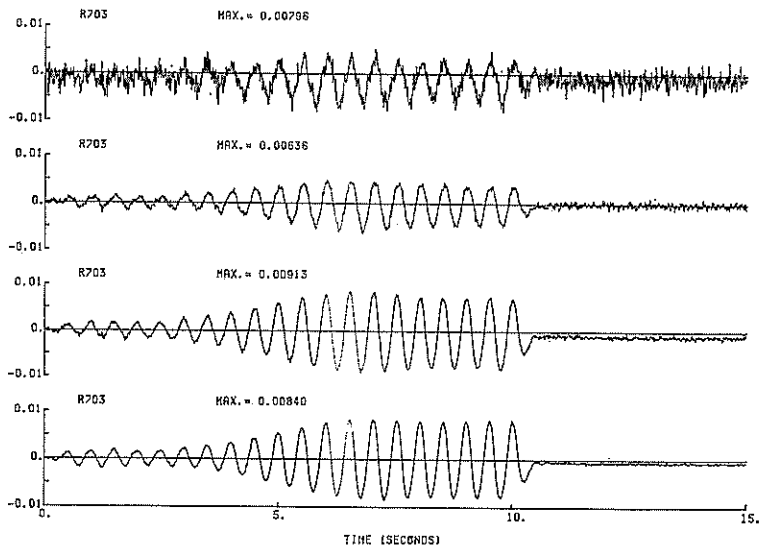(to be continued)

(b) Case R—204 (without gravel drain, sinusoidal input motion, maximum acceleration 43 Gals)

(c) Case R—603 (without gravel drain, sinusoidal input motion, maximum acceleration 84 Gals)

Fig. C1 Time histories of the shear strains at the height of, from the upper most row, 140cm, 100cm 40cm, and 30cm obtained from measured displacements by H11–H15
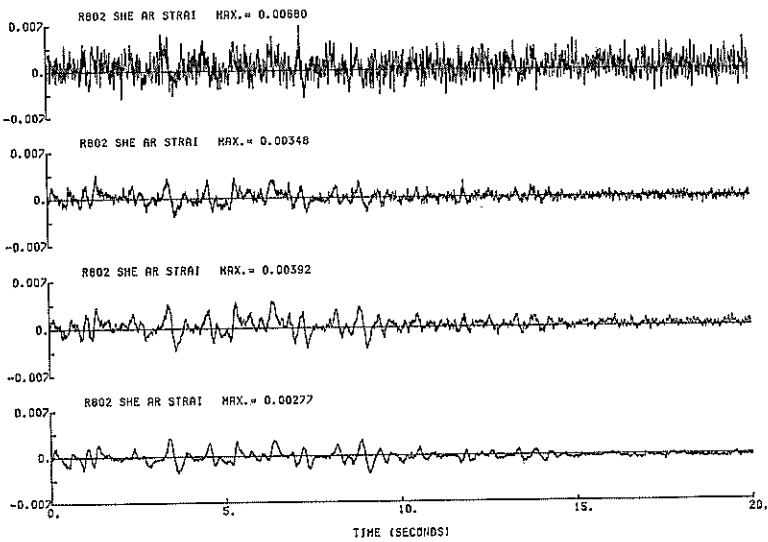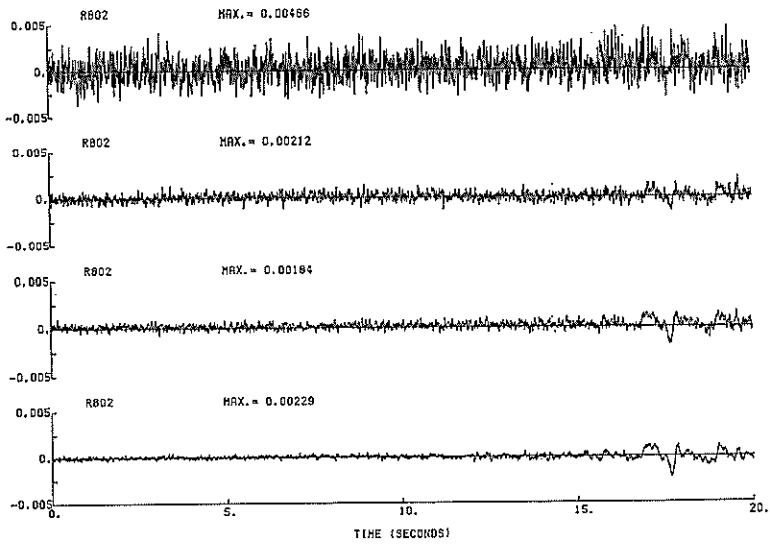
(to be continued)
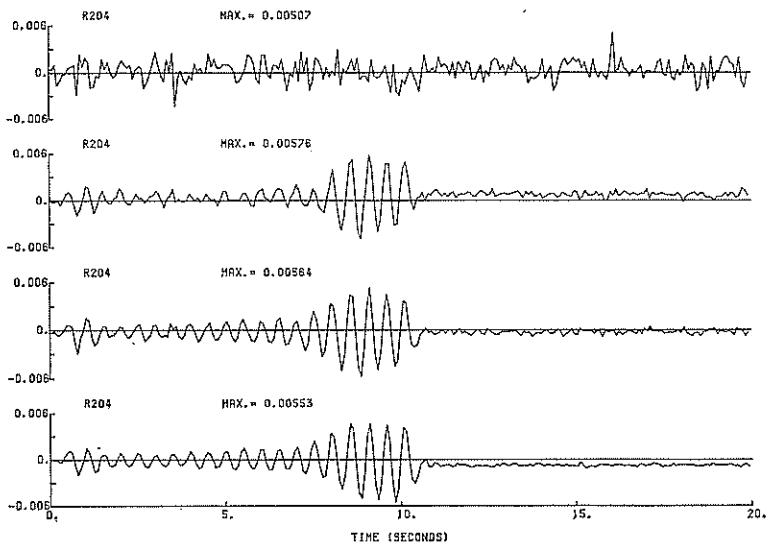
(d) Case R—603 (with gravel drain a/b=0.3, sinusoidal input
motion, maximum acceleration 50 Gals)
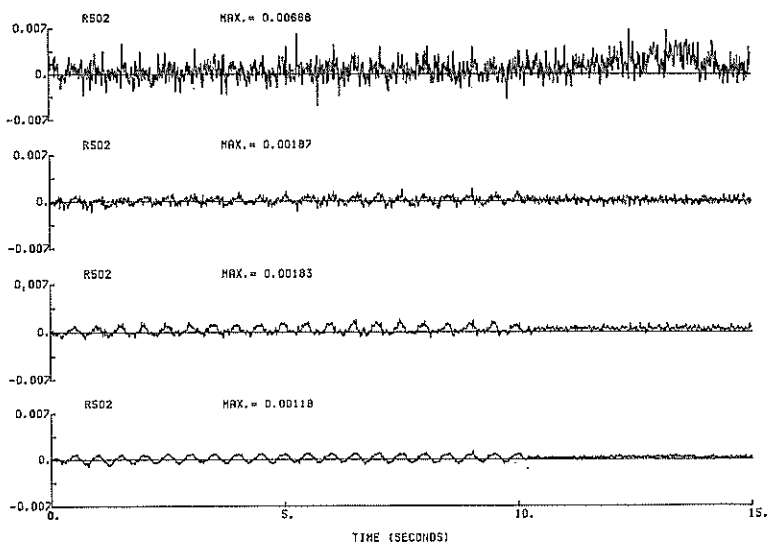
(e) Case R—502 (with gravel drain a/b=0.3, sinusoidal input
motion, maximum acceleration 50 Gals)

Fig. C1 Time histories of the shear strains at the height of,
from the upper most row, 140cm, 100cm 40cm, and
30cm obtained from measured displacements by H11–H15
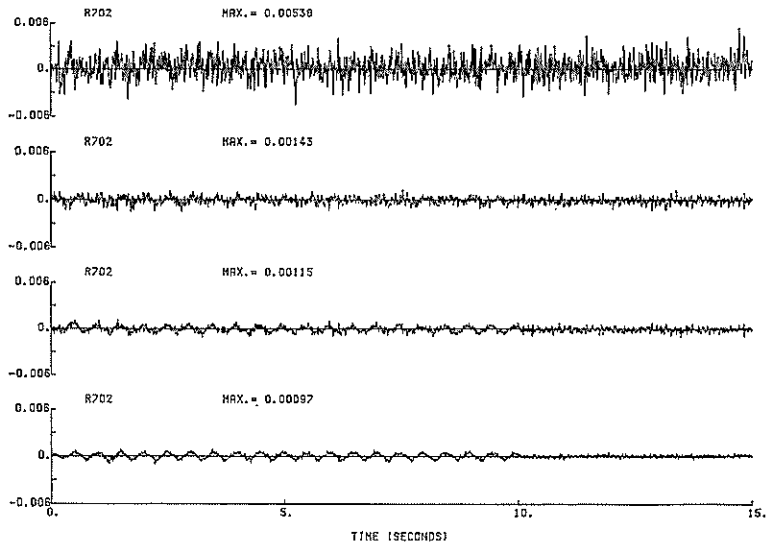
(f) Case R—702 (with gravel drain a/b=0.45, sinusoidal input motion, maximum acceleration 51 Gals)

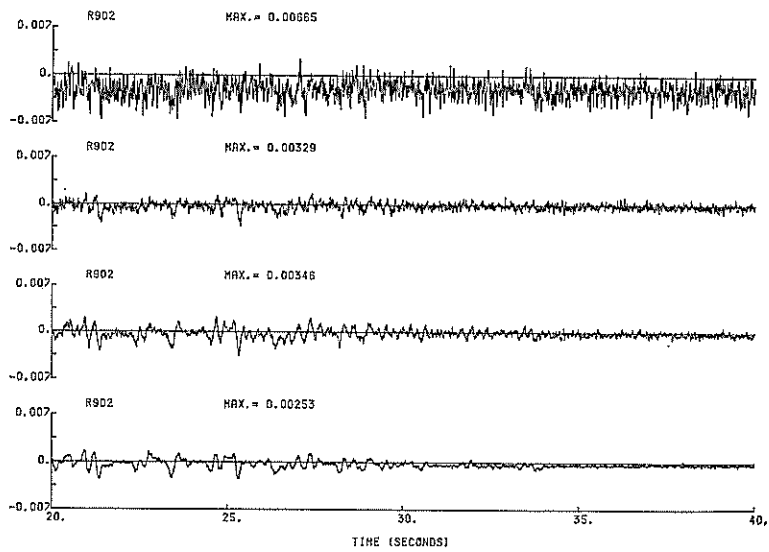(g) Case R—703 (with gravel drain a/b=0.45, sinusoidal input motion, maximum acceleration 82 Gals)
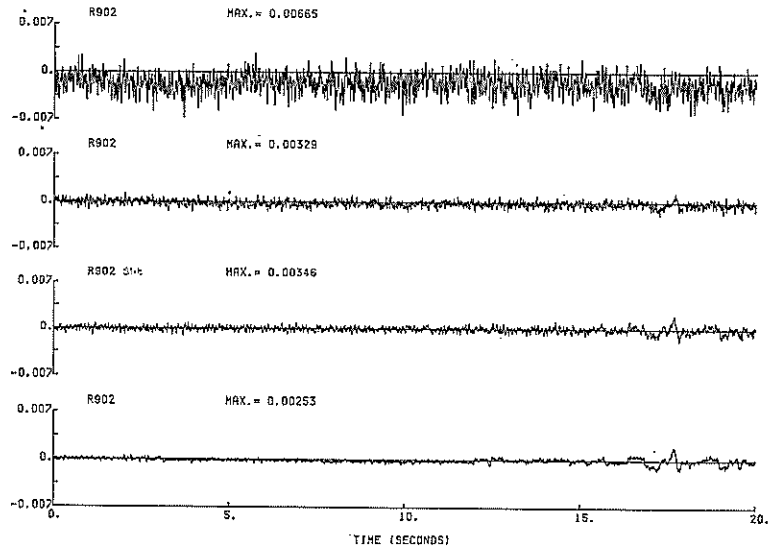
Fig. C1 Time histories of the shear strains at the height of, from the upper most row, 140cm, 100cm 40cm, and 30cm obtained from measured displacements by H11–H15

(to be continued)

(h) Case R—802 (without gravel drain, earthquake input motion, maximum acceleration 105 Gals)

Fig. C1 Time histories of the shear strains at the height of, from the upper most row, 140cm 100cm 40cm, and 30cm obtained from measured displacements by H11–H15

(to be continued)

(i) Case R—902 (with gravel drain a/b=0.3, earthquake input
     motion, maximum acceleration 99 Gals)

Fig. C1 Time histories of the shear strains at the height of,
         from the upper most row, 140cm, 100cm 40cm, and
         30cm obtained from measured displacements by H11–H15

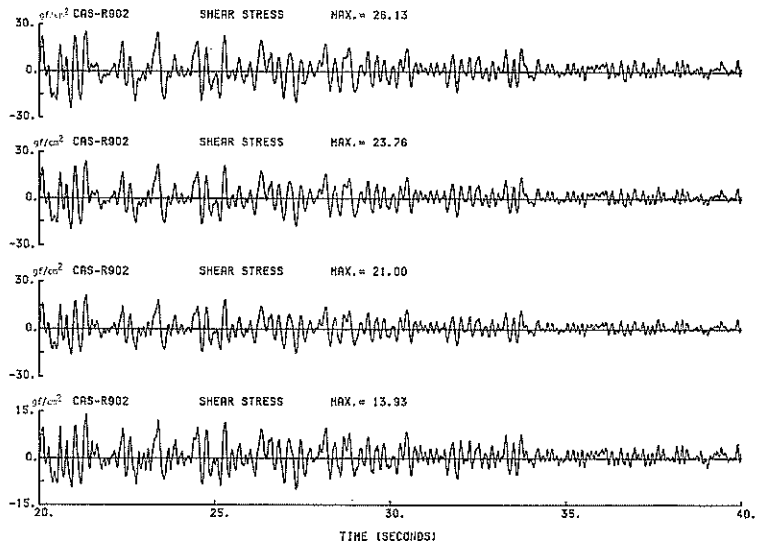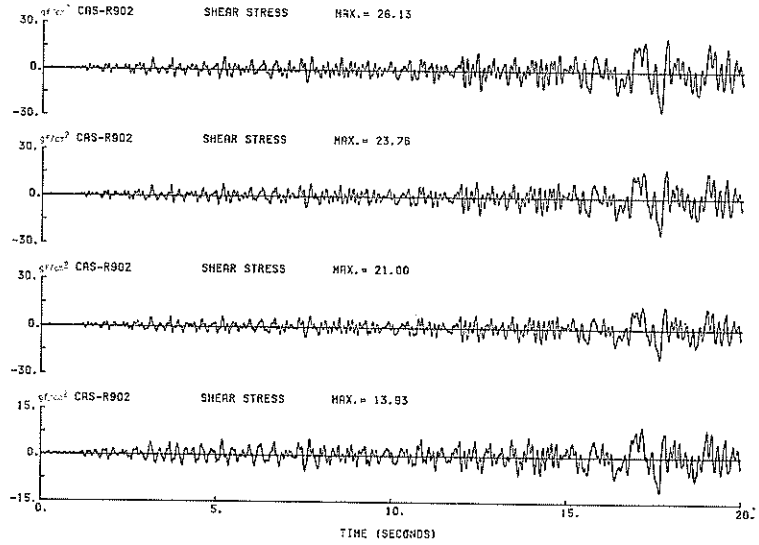## Appendix D   Time histories of the shear stresses

The time histories of the shear stresses were computed from the measured accelerations. The procedure for the computation is presented in 4.2 in the present report. The results are presented in the form of shear stress ratio (shear stress divided by the initial effective vertical stress) in **Fig. D1** for some of the tests and in the form of shear stress in **Fig. D2** for the rest of the tests.
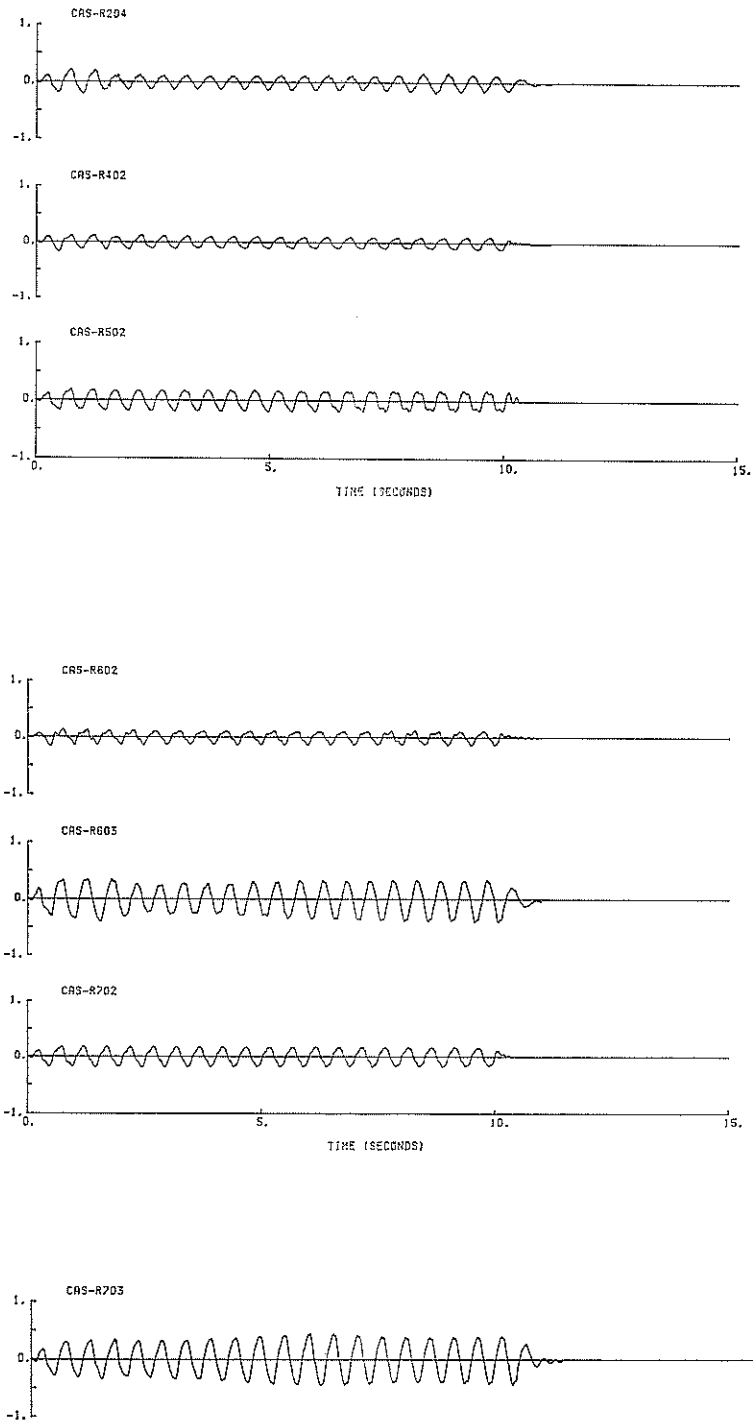
Fig. D1 Time histories of the shear stress ratios at the height of 97.5cm for Cases R—204, R—402, R—502, R—602, R—603, R—702, and R—703

(a) Case R—802

Fig. D2 Time histories of the shear stresses at the height of (from the upper most row in the figures) 37.5cm, 67.5cm, 97.5cm, and 142.5cm (to be continued)

(b) Case R—902

Fig. D2 Time histories of the shear stresses at the height of
(from the upper most row in the figures) 37.5cm,
67.5cm, 97.5cm, and 142.5cm